TAMPEREEN TEKNILLINEN YLIOPISTO
TAMPERE UNIVERSITY OF TECHNOLOGY

ALBERTO BRIHUEGA GARCÍA

CONSTANT ENVELOPE PRECODING FOR LARGE ANTENNA ARRAYS

Master of Science Thesis

Examiner: prof. Mikko Valkama
Examiner and topic approved on 9th August 2017

Abstract

TAMPERE UNIVERSITY OF TECHNOLOGY

Alberto Brihuega García: Constant Envelope Precoding for Large Antenna Arrays

Master of Science Thesis, 77 pages
August 2017
Examiner: Prof. Mikko Valkama

5G, the new generation of mobile communications, is expected to provide huge improvements in spectral efficiency and energy efficiency. Specifically, it has been proven that the adoption of large antenna arrays is an efficient means to improve the system performance in both of these efficiency measures. For these reasons, the deployment of base stations with large amount of antennas has attracted a substantial amount of research interest over the recent years. However, when pure digital beamforming is pursued in large array system context, a large number of transmitter and receiver chains must also be implemented, increasing the complexity and costs of the deployment.

In general, power consumption of the cellular network is recognized as a major concern. Radio transmitters tend to be really power hungry, especially because of the potential energy inefficiency of their power amplifiers. Due to the characteristics of the current and future waveforms utilized in wireless communications, power amplifiers need to work in a relatively linear regime in order not to distort the signal, making the energy efficiency of such highly linear amplifiers to be rather low. If power amplifiers were capable of working in the nonlinear regime without degrading system performance, their energy efficiency could be notably increased, resulting in considerable savings in energy, costs and system complexity.

In this Thesis, the development and evaluation of a constant envelope spatial precoder is being addressed. The precoder is capable of generating a symbol-rate constant envelope signal, which despite pulse-shape filtering yields substantial robustness against the nonlinearities of power amplifiers. This facilitates pushing power amplifiers into heavily nonlinear regime, with the consequent increase in their energy efficiency. At the same time, the precoder is able to perform spatial beamforming

processing in order to mitigate the multi-user interference due to spatial multiplexing. It is assumed that the number of antennas in the base station is much larger than the number of simultaneously scheduled users, implying that large-scale MU-MIMO scenarios are considered, which allows us to exploit the additional degrees of freedom to perform waveform shaping. For the sake of evaluating the proposed precoder performance, different metrics such as PAPR, BER, multi-user interference and beamforming gain are compared to those of currently used precoding techniques.

The obtained results indicate that the studied constant-envelope precoder can facilitate running the PA units of the large-array system in heavily nonlinear region, without inducing substantial nonlinear distortion, while also simultaneously providing good spatial multiplexing and beamforming characteristics. These, in turn, then facilitate larger received SINRs for the scheduled users, and therefore larger system throughputs and a more efficient utilization of the power amplifiers.

Preface

The research work reported in this Master of Science Thesis was financially supported by Tampere University of Technology, Finland, and by the Linz Center of Mechatronics (LCM) in the framework of the Austrian COMET-K2 programme.

I would like to extend my gratitude to Professor Mikko Valkama for all the guidance, help, patience and support during the development of this Master Thesis, and to Dr. Lauri Anttila for his valuable comments and advices. Special thanks to Prof. Markku Renfors for everything he has taught me during this year.

I would also like to thank for the PhD research opportunity I have been granted at the research group. I will make most of it for sure.

Prefacio

Con este Trabajo Fin de Master pongo el broche final a una etapa muy importante de mi vida, la cual me ha permitido formarme como persona mientras disfrutaba estudiando lo que desde siempre me ha apasionado. Han sido 6 años difíciles que han marcado mi forma de pensar y de entender el mundo, pero sobre todo ha sido una etapa divertida, amena y feliz, gracias a las personas que han estado conmigo a lo largo de estos años, que no han sido pocas, y que con mucha gratitud quisiera dedicarles unas palabras que sin duda se merecen.

Gracias en primer lugar a mi madre, mi padre, mi hermana y mis abuelos, por su incodincional apoyo, por aguantar mis nervios y mis malos humos durante estos años de carrera, por haber hecho de mi la persona que ahora soy y haberme permitido llegar hasta aquí.

Gracias a Carlos e Irene, mis *senpais*, por su constante ayuda durante esas duras tardes de estudio en la biblioteca, por aguantar la irremediable tontería que tengo, por todas las *Goikochuco pool parties* que tan bien venían para desconectar y que tanto hemos disfrutado, por ser fieles companeros en la ardua búsqueda de mesa en la cafetería (esto último más bien Irene sólo), y por las largas charlas en Trastornados, porque ante todo y sin importar qué suceda: siempre con la calma. Gracias por vuestra valiosa amistad y por ser tan buenas personas, sin duda habéis hecho que estos años sean mucho mas felices, estoy orgulloso de ser vuestro amigo.

Gracias a los apuntes de Irene, que se merecen especial mención, sin ellos hubiera sido imposible salir de la ETSIT.

Gracias a *Mendo-senpai* por su inestimable ayuda durante el desarrollo de mi TFG y durante el tiempo que estuve en el GTIC, por todo lo que me ha transmitido, por haber sido y ser una fuente de inspiración, por haber confiado en mí y haberme dado la oportunidad de iniciarme en el mundo de las comunicaciones móviles. Eres una gran persona, profesor e ingeniero, te admiro. Gracias también a José Manuel Riera por su interés y dedicación, por haber confiado en mí y haberme dado la oportunidad de entrar en el departamento.

Gracias a Ana, por su amistad, por quererme, preocuparse y enorgullecerse de mí, por todas las largas horas que hemos pasado juntos tanto en clase, biblioteca o de

salseo, por todas esas fiestas en *Soti* (ya no os libráis de mí) y por todos los buenos momentos que hemos pasado juntos y que pasaremos. Gracias por ser tan buena persona, siempre estaré orgulloso de ti. Gracias también a toda su familia y a Tomás, por haberme tratado tan bien siempre y haberme hecho sentir uno más.

Gracias a Ru por todos los desvaríos y risas que nos hemos echado juntos, por contagiarme siempre su optimismo y risa. Porque me encanta la jeta que le echas a la vida y la poca verguenza que tienes (en el buen sentido). Gracias por ser como eres y por tu gran amistad.

Gracias a *George*, por dejarme ser su *Goikommander*, por su valiosa amistad, por ese maravilloso acentillo italo-madrileno-andaluz que le levanta el ánimo a cualquiera, por tener el mejor clima de toda Europa, por todos los montajes que has hecho con mi cara, por todas las *Goikochuco pool parties*, tostarricas y seductoras, y por todos los buenos momentos que hemos pasado. Eres un grande.

Gracias a Ros por ser un gran amigo y una persona increíble, por todos los huevos que le echa a la vida y por salir siempre adelante. Ole tú. Eres un ejemplo a seguir.

Gracias a Andrés, mi amigo de toda la vida, por su inestimable amistad y por todos los buenos momentos vividos juntos, por mal influenciarme y hacer que me diera un poco el aire (aunque nos quedásemos jugando al LoL...). Gracias por haber estado y estar siempre ahí, por muy lejos que estemos ahora siempre podremos contar el uno con el otro.

Gracias a *Ferchu*, por tantísimos e inestimables años de amistad, por quererme como soy, por haber estado siempre ahí sin que importara lo que llevásemos sin hablar o sin vernos. Hemos crecido juntos desde los 3 años, y para tu desgracia, ya no te libras mí. Gracias por todo.

Gracias a *Miguelón*, *Jenny* y a *Anamari*, por ser tan buenas personas, por ser grandes amigos, por todas las risas que nos hemos echado (y todas las secuelas que Ana me ha dejado). Gracias por estar conmigo todo este tiempo apoyándome y enorgulleciéndoos de mí.

Gracias a todas las personas que he conocido, han estado y estarán conmigo en Tampere, en especial a Joselito, Carlos, Pablo, Markel, Amir, Jonas, Sergio, Andrea, Bene, Shadi y Elena. Ha sido un ano increíble y una experiencia inólvidable. Somos una pequena gran familia. Siempre nos quedarán Pyynikki y el kyykkä.

También me gustaría agradecer a Mikko y a Markku por habérme dado la oportunidad de trabajar en el departamento y de quedarme en Tampere haciendo cosas que no están al alcance en cualquier sitio.

Para finalizar, me gustaría dedicarle unas palabras de gratitud y cariño a Laura, que aunque ha tardado demasiado tiempo en llegar, este último año no podría entenderse sin ella. Gracias, te quiero.

Table of Contents

List of Figures

List of Tables

List of Acronyms

ACLR	Adjacent Channel Leakage Ratio
AWGN	Additive White Gaussian Noise
BBU	Baseband Unit
BER	Bit Error Rate
BS	Base Station
CBC	Complement Block Coding
CCDF	Complementary Cumulative Distribution Function
CE	Constant Envelope
CSI	Channel State Information
DPD	Digital Predistortion
DRX	Discontinuous Reception
DTX	Discontinuous Transmission
EIRP	Equivalent Isotropically Radiated Power
EVM	Error Vector Magnitude
FIR	Finite Impulse Response
ISI	Intersymbol Interference
LMMSE	Linear Minimum Mean Square Error
LMS	Least-Mean-Squares
LTE	Long Term Evolution
MIMO	Multiple-Input Multiple-Output
MSE	Minimum Mean Square Error
MSE	Mean Square Error
MUI	Multi User Interference
MU-MIMO	Multi-user Multiple-Input Multiple-Output
OFDM	Orthogonal Frequency-Division Multiplexing
OPEX	Operating Expense
PA	Power Amplifier
PAPR	Peak-to-Average Power Ratio

PTS	Partial Transmit Sequence
QAM	Quadrature Amplitude Modulation
QPSK	Quadrature Phase Shift Keying
RAN	Radio Access Network
RF	Radio Frequency
RRC	Root-Raised Cosine
SINR	Signal-to-Interference-plus-Noise Ratio
SIR	Signal-to-Interference Ratio
SVD	Singular Value Decomposition

List of Symbols

$A(t)$	signal amplitude
C	channel capacity
$C(.)$	cost function
$\mathbb{C}$	complex field
$d(n)$	samples of the desired signal
$e(n)$	error signal
e_m	error at the m-th iteration
$\mathbb{E}\{.\}$	expectation operator
$FT\{.\}$	Fourier transform
$g(t)$	RRC filter impulse response
$G(f)$	Fourier transform of $g(t)$
$\mathbf{h}_{LS}$	least-squares estimation of the channel vector.
$h_{k,n}$	channel coefficient between the n-th transmit antenna and the k-th user
$\mathbf{H}$	channel matrix
$H(Z)$	Z-transform of the channel impulse response
$\mathbf{I}$	identity matrix
k, n, m	indexes
K	number of users
$max(.)$	maximum value operator
$min(.)$	minimum value operator
mui	global multi-user interference
mui_k	k-th user multi-user interference
$\mathbf{n}$	noise vector
$\hat{n}$	filtered noise vector and all sources of interference
n_k	noise at the k-th user
N_t	number of transmit antennas
$\mathbf{R}_x$	autocorrelation matrix of $\mathbf{x}$

$\mathbf{R}_{yx}$	crosscorrelation matrix of $\mathbf{y}$ and $\mathbf{x}$
$\mathbf{s}$	information symbols vector
s_k	k-th user information symbol
$\hat{s}$	scaled information symbols vector
T	sampling period
$trace\{.\}$	trace of a matrix
$\mathbf{U}$	matrix containing the left singular vectors of $\mathbf{H}$
$\mathbf{V}$	matrix containing the right singular vectors of $\mathbf{H}$
$v(n)$	filter input samples
$\mathbf{W}_{RX}$	general RX spatial filter
$\mathbf{W}_{TX}$	general TX spatial precoder
$\mathbf{W}_{RX}^{I}$	identity matrix spatial filter
$\mathbf{W}_{TX}^{I}$	identity matrix spatial precoder
$\mathbf{W}_{RX}^{SVD}$	SVD spatial filter
$\mathbf{W}_{TX}^{SVD}$	SVD spatial precoder
$\mathbf{W}_{RX}^{ZF}$	ZF spatial filter
$\mathbf{W}_{TX}^{ZF}$	ZF spatial precoder
$w(n)$	wiener filter
$W(Z)$	Z-transform of the Wiener filter
$\mathbf{x}$	precoded signal vector
$\mathbf{x_{opt}}$	constant envelope optimum precoded signal vector
$x_{BB}(t)$	baseband equivalent of $x(t)$
x_n	n-th antenna precoded signal
$X(f)$	Fourier transform of $x(t)$
$\mathbf{y}$	received signal vector
$\hat{\mathbf{y}}$	filtered received signal vector
$y(n)$	estimation samples
$Y(f)$	Fourier transform of $y(t)$
$\mathbf{0}$	vector containing zeros
α	RRC roll-off factor and beamforming gain
β	maximum tolerable multi-user interference
Δ	diagonal matrix with the square roots of the eigenvalues of $\mathbf{H}$
η	energy efficiency
λ	step-size in adaptive algorithms
λ_k	k-th eigenvalue of $\mathbf{H}$
∇	gradient of a vector

σ	standard deviation
$\theta_{LMS,m}$	LMS-based constant envelope adaptation phase
θ_n	n-th transmit antenna constant envelope phase component
θ_{opt}	constant envelope optimum phase component
$\mathbf{\Theta}$	constant envelope phase vector
$\|.\|$	module of a vector
$\|\|.\|\|$	norm of a vector
$(.)^T$	transpose of a matrix or vector
$(.)^{-1}$	inverse of a matrix
$(.)^H$	hermitian of a matrix

Chapter 1

Introduction

1.1 Motivation and background

Very demanding requirements have been set up for the next generation of mobile communications commonly referred to as 5G. Such 5G networks should be able to provide 100 times higher data rates, allow 1000 times more connected devices, reduce the energy consumption by 90% and reduce the OPEX of the network by 80% among many other targets [1].

Massive MIMO has emerged as a very important concept enabling the chance of meeting some of the previously stated requirements. Equipping base stations with a very large number of antennas is expected to allow energy and spectral efficiencies to improve in several orders of magnitude [2]. Spatial multiplexing allows to increase, ideally at least, the spectral efficiency of the radio interface linearly proportional to the number of antennas, but it requires to implement a large amount of antennas and radio frequency (RF) chains at the base station (BS) as well as at the user equipment (UE) side. Due to the reduced size of the UEs, focus has shifted to a more practical multi-user MIMO, which allows to exploit the benefits of spatial multiplexing relieving the UE from having big antenna arrays.

Energy consumption is a major concern for future mobile communication networks [3]. 5G is targeting to reduce the system energy consumption by a factor of ten despite the network densification and the increase in the number of devices and radio-frequency chains. It has been proven that the transmit power (for a given bit-rate) of each single-antenna user can be scaled down proportionally to the number of antennas at the base station with perfect channel state information, or to the square root of the number of antennas with imperfect CSI [4], allowing to improve the energy efficiency. Base stations are responsible for 80% of the operator's power consumption, of which, power amplifiers (PA) are responsible for some 40%-50% [5].

There is room for significant improvements in base stations energy consumption, especially in power amplifiers.

Utilized radio access waveforms in wireless communications suffer from having an elevated peak-to-average power ratio (PAPR) [6], so that, power amplifiers need to work in relatively linear regime in order not to distort the signal, however, ensuring this linearity turns to be really power inefficient. There exists an approximate inverse relationship between energy efficiency and linearity. The distortions produced by the nonlinearities of the power amplifiers are very harmful: they produce spectral regrowth which results in adjacent channel interference as well as interference within the signal bandwidth degrading the signal-to-interference ratio (SIR), and thus, the bit error rate (BER).

There are several methods to cope with the distortion produced by the power amplifiers, such as: clipping and digital predistortion techniques. Clipping techniques are based on intentionally clipping the signal before amplification. Clipping allows to reduce the PAPR, but it is a nonlinear process on its own which can produce in-band and out-band interference, furthermore, it can also destroy the orthogonality in multicarrier waveforms [7]. Digital predistortion techniques attempt to realize a distortion function which approximates the inverse of that of the power amplifier, resulting in an overall linear transfer function with relatively low distortion and enabling thus a significant gain in energy efficiency [8]. The predistorter generally creates an expanding nonlinearity, since that of the power amplifier is compressive. Power amplifiers can be modeled either as memoryless devices, which means that the current output is only dependent on the current input, or as memory devices, in which the current output does not only depend on the current input but also on the L previous ones.

In [9–11], a novel method to cope with the PAPR problem was introduced, and this is the reference method which this Master Thesis is based on. Thanks to the additional degrees of freedom provided by large antenna arrays, it is possible to perform waveform shaping in such a way that a discrete-time constant envelope (CE) signal is obtained, while simultaneously being able to perform spatial multiplexing allowing also to increase the spectral efficiency of the system. By using this approach, it is possible to significantly reduce the PAPR of the resulting signal, despite the pulse-shape filtering, which allows to push the PA closer to the nonlinear region, and thus also allowing to improve the energy efficiency of the power amplifiers in a notable way. This approach is known as constant envelope precoding in the literature. Precoding techniques which seek to reduce the PAPR work beautifully together with digital predistortion allowing to achieve better results, which might become a joint approach to cope with the PAPR problem.

In general, one of the most common techniques for spatial multiplexing processing is the zero-forcing (ZF) precoder, however, it introduces very high peak-to-average ratios, therefore, special care needs to be taken to avoid harmful signal distortion. In this Master Thesis the ZF precoder is utilized as a reference method in order to evaluate and compare the performance of the considered CE precoder.

This Master Thesis is based on the studies carried out in [9–11]. A constant envelope precoder for large scale antenna systems has been developed and evaluated. The precoder is capable of performing spatial multiplexing just like ZF does, while reducing the PAPR of the signal with the aim of improving the energy efficiency of power amplifiers, which simultaneously addresses two of the most important targets of 5G, i.e., spectral efficiency and energy efficiency.

1.2 Scope and Outline of the Thesis

In this Master Thesis, the performance of the symbol-rate constant envelope precoder is evaluated and compared to that of ZF. The constant envelope precoder allows to achieve a discrete-time constant envelope signal while providing a trade-off between interference mitigation and beamforming gain. As it has been commentated above, the CE precoder is capable of performing spatial multiplexing allowing the transmission of multiple parallel data streams, within the same physical resources, to increase link and system capacities. At the same time, it is capable of generating a symbol-rate constant envelope signal which enables the improvement of the energy efficiency of base stations, which is a key target for future mobile communication systems. The main performance indicators used to quantify the viability and performance of the spatial precoder are: the resulting PAPR, the bit error rate, the beamforming gain and the multi-user interference supression.

The Master Thesis is organized as follows. In chapter 2, the basics of MIMO techniques, adaptive systems, precoding techniques, waveforms and PAPR mitigation methods are introduced to present a general view of the problem which is addressed. In chapter 3, the mathematical model and the algorithms used to get the precoder coefficients are explained in detail. The different setups that have been utilized in every simulation are explained in chapter 4 together with the obtained results and their analysis. To conclude, final remarks are given in chapter 5.

Chapter 2

Theoretical Framework and Fundamentals

Advanced wireless communication systems are capable of supporting high data rates to a large number of users in a very flexible way. Throughout the years, many different techniques and technologies have been developed in order to meet the requirements of data hungry users and new services. Modern wireless communication systems use high order modulations in order to provide higher spectral efficiency, however, these modulations have high signal-to-interference-plus-noise ratio (SINR) requirements, exhibit increasing peak-to-average power ratios and they are very sensitive to RF imperfections. Multiantenna techniques have become an important technology that enables the improvement of link performance and link capacity. For future mobile communications systems, huge amounts of antennas are expected to be implemented at the base stations which will provide many opportunities not only regarding energy and spectral efficiencies. Adaptive systems are a very key feature in wireless communication systems for adapting the transmission to the time-varying channel or to equalize the effect of the channel among many other regards. Adaptive systems offer a superior performance compared to fixed systems. Furthermore, due to the channel characteristics, different waveforms have been designed in order to cope with the time and frequency selectivities of the channel, as well as to provide a flexible and efficient use of the spectrum. These waveforms typically present very elevated PAPR which makes them really sensitive to nonlinearities, especially to those of power amplifiers. In current wireless communications, highly linear or linearized power amplifiers need to be used in order to avoid harmful distortion of the signal. Many different techniques have been studied in order to linearize the power amplifier response or to reduce the peak-to-average ratio of the signals in order to improve their power efficiency.

In this chapter, the topics commentated above are introduced in more details to make the reader aware of the problem we are addressing.

2.1 Spatial Multiplexing Techniques

Spatial multiplexing benefits from having multiple antennas at the transmitter and receiver sides. By applying signal processing, it is possible to transmit multiple parallel orthogonal (ideally free of interference) data streams over the same time-frequency resources, resulting in important gains in spectral efficiency by exploiting the spatial domain. In fact, the spectral efficiency is increased linearly proportional to the number of antennas, as it is shown in Equation (2.8).

In the following, we will consider narrowband single carrier transmission. Thus, the channel between the k-th receiving antenna and the n-th transmit antenna can be modeled as a complex coefficient (assuming flat fading within the carrier bandwidth). The mathematical model of a MIMO scheme can be typically expressed in the following way:

$$\mathbf{y} = \begin{pmatrix} h_{1,1} & h_{1,2} & \dots & h_{1,n_t} \\ h_{2,1} & h_{2,2} & \dots & h_{2,n_t} \\ \vdots & \vdots & \ddots & \vdots \\ h_{n_r,1} & h_{n_r,2} & \dots & h_{n_r,n_t} \end{pmatrix} \begin{pmatrix} x_1 \\ x_2 \\ \vdots \\ x_{n_t} \end{pmatrix} + \begin{pmatrix} n_1 \\ n_2 \\ \vdots \\ n_{n_r} \end{pmatrix} = \mathbf{Hx} + \mathbf{n} \tag{2.1}$$

where $\mathbf{H} \in \mathbb{C}^{n_r \times n_t}$ denotes the channel matrix, $\mathbf{x}$ is the $\mathrm{n}_t \times 1$ transmitted symbols vector, and $n_k \sim \mathcal{CN}(0, \sigma^2)$ is the additive white Gaussian noise (AWGN) at the k-th receiving antenna . If the channel matrix $\mathbf{H}$ is known at the transmitter and receiver sides, it is possible to perform spatial precoding and spatial filtering based on the so-called singular value decomposition (SVD) of the channel matrix: $\mathbf{H} = \mathbf{U}\mathbf{\Delta}\mathbf{V}^H$, where $\mathbf{U}$ and $\mathbf{V}$ are orthogonal matrices of dimensions $n_r \times n_r$ and $n_t \times n_t$ formed by the left and right singular vectors of $\mathbf{H}$ respectively, while $\mathbf{\Delta}$ is a $n_r \times n_t$ non-negative diagonal matrix, whose values are the square roots of the non-zero eigenvalues of $\mathbf{H}$.

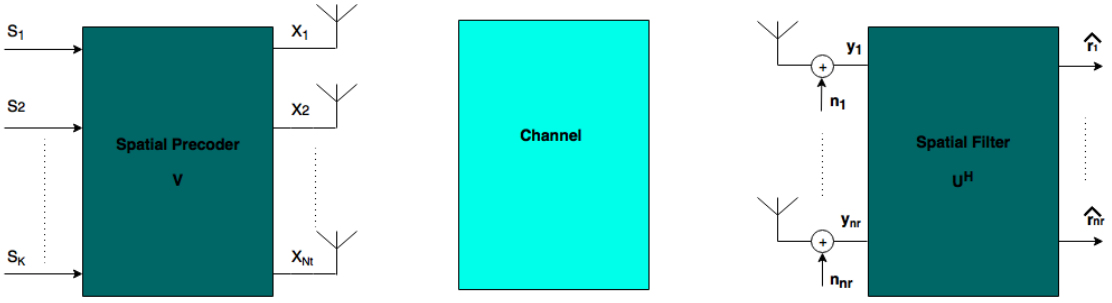

Figure 2.1: Spatial multiplexing based on SVD

Based on the singular value decomposition of the channel matrix, Equation (2.1) can be expressed as:

$$\mathbf{y} = \mathbf{U}\boldsymbol{\Delta}\mathbf{V}^H\mathbf{x} + \mathbf{n} \tag{2.2}$$

Then, if we apply $\mathbf{W}_{TX}^{SVD} = \mathbf{V}$ and $\mathbf{W}_{RX}^{SVD} = \mathbf{U}^{\mathbf{H}}$ as spatial precoder and spatial filter respectively, we have:

$$\mathbf{x} = \mathbf{V}\mathbf{s} \tag{2.3}$$

where $\mathbf{s}$ denotes the information symbols vector.

$$\mathbf{r} = \mathbf{U}^H\mathbf{y} \tag{2.4}$$

therefore, Equation (2.2) results in:

$$\mathbf{r} = \left(\mathbf{U}^H\mathbf{U}\right)\boldsymbol{\Delta}\left(\mathbf{V}^H\mathbf{V}\right)\mathbf{s} + \mathbf{U}^H\mathbf{n} \tag{2.5}$$

which is represented in Figure (2.1), where $\mathbf{r} = \mathbf{U}^H\mathbf{y}$ is the filtered received signal and $\hat{\mathbf{n}} = \mathbf{U}^H\mathbf{n}$ is the filtered noise. Therefore, Equation (2.5) can be rewritten in the following way:

$$\mathbf{r} = \boldsymbol{\Delta}\mathbf{s} + \hat{\mathbf{n}}$$

$$r_k = \lambda_k s_k + \hat{n}_k, \;\; where\, k \in [1, min\{n_t, n_r\}] \tag{2.6}$$

where r_k and s_k denote the filtered received signal at the k-th antenna branch and the intended information symbol for the k-th antenna branch respectively, while λ_k are the square roots of the eigenvalues of $\mathbf{H}$, which translates into beamforming gain. Notice that it has been possible to separate all data streams without them interfering to one another. It can be demonstrated that the ergodic capacity of the SVD-based transmission scheme can be expressed as follows:

$$C = \max_{Tr(R_x)=P} \mathbb{E}\left\{\log_2 det\left(\mathbf{I} + \frac{SNR}{N_t}\mathbf{H}\mathbf{R}_{\mathbf{x}}\mathbf{H}^H\right)\right\} \tag{2.7}$$

where $\mathbf{R}_{\mathbf{x}}$ is the autocorrelation matrix of the transmitted symbols: $\mathbf{R}_{\mathbf{x}} = \mathbb{E}\{\mathbf{x}\mathbf{x}^{\mathbf{H}}\}$ with a constraint in the total transmit power. If we assume that optimal power allocation is not performed at the transmitter side, $\mathbf{R}_{\mathbf{x}}$ is chosen such that $\mathbf{R}_{\mathbf{x}} = \mathbf{I}$, if we express $\mathbf{H}$ in terms of its SVD decomposition, (2.7) can be rewritten as:

$$C = \mathbb{E}\left\{\sum_{k=1}^{min(N_t,N_r)} \log_2\left(1 + \frac{SNR}{N_t}\lambda_k^2\right)\right\} \tag{2.8}$$

where λ_k^2 are the eigenvalues of $\mathbf{H}\mathbf{H}^H$. The expectation operator takes over λ_i which typically follows a Gaussian/Rayleigh/Rice distribution, so that, λ_i^2 is chi-square distributed.

As it can been seen in Equation (2.8), the capacity is linearly proportional to the number of antennas. Massive MIMO will try to exploit this feature by means of the implementation of large antenna arrays. Notice that the number of parallel data stream is given by $min\{Nt, Nr\}$, which means that a sufficiently large amount of antennas needs to be also implemented at the receiver side, whose size is rather reduced when considering mobile devices. This leads us to a more practical concept of spatial multiplexing, the so-called multi-user MIMO (MU-MIMO).

2.1.1 Multi-user MIMO

Multi-user MIMO follows the same principle than that of the previous technique, however, the receiver antennas are not located within the same device, but they belong to different users with different spatial locations. Hence, the spatial multiplexing gain can be shared among many users and there is no need for the user devices to implement lots of antennas, which may be unfeasible. Furthermore, since the data streams are intended for different users, better diversity performance can be achieved, and there is no need to have such a rich scattering environment like in a point-to-point single-user MIMO. MU-MIMO eliminates the problem of unfavorable propagation environment, but it introduces some extra complexity when considering user allocation and scheduling, it suffers from co-scheduled users interference and it requires channel state information from all users. MU-MIMO presents more interest from a practical point of view since typically a single user does not require such a big amount of parallel streams.

The mathematical model for MU-MIMO follows the same form of Equation (2.1), but this time, the data streams are intended for different users, and the channel coefficients define the different users' channels. An example of MU-MIMO transmission scheme where a base station with 8 antennas simultaneously serves a set of 2 antennas users is shown in the Figure (2.2) below, which is equivalent to a 8x8 single-user MIMO scheme.

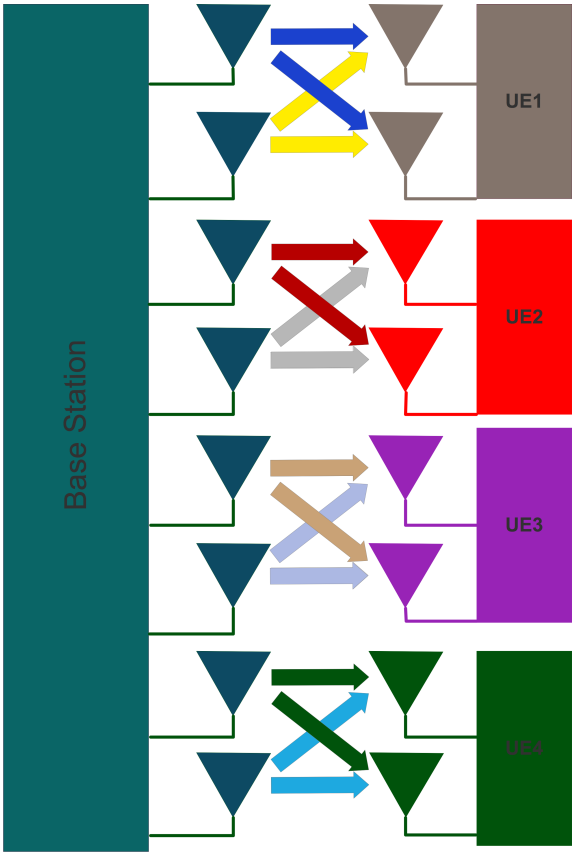

Figure 2.2: MU-MIMO spatial multiplexing

2.2 Zero-Forcing

Conventional spatial linear processing can also be utilized in order to perform spatial multiplexing. ZF and MMSE can be used either at the receiver or transmitter sides. When used at the transmitter side, channel state information (CSI) feedback is needed, while when used at the receiver side there is no need for CSI feedback, however, they may enhance the noise level, specially when deep fading occurs. In the following, it is assumed perfect channel state information.

2.2.1 Zero-Forcing Precoder

Zero-forcing principle is a well-known and basic method for cancelling the channel effect and thus, it allows to eliminate the inter-stream interference. The precoder weights are given by the right pseudo-inverse of the channel matrix:

$$\mathbf{W}_{TX}^{ZF} = \mathbf{H}^H \left(\mathbf{H}\mathbf{H}^H\right)^{-1} \tag{2.9}$$

for computing the pseudo-inverse it has been considered that the number of transmit antennas is larger than the number of antennas at the receiver side. The precoded

data symbols are obtained in the following way: $\mathbf{x} = \mathbf{W}_{TX}^{ZF}\mathbf{s}$, and thus, the received signal is given by the following expression:

$$\mathbf{y} = \mathbf{H}\mathbf{W}_{TX}^{ZF}\mathbf{s} + \mathbf{n} = \mathbf{s} + \mathbf{n} \tag{2.10}$$

which ideally cancels the effect of the channel. In this particular case, the RX spatial filter is given by the identity matrix $\mathbf{W}_{RX}^{I} = \mathbf{I}$, and thus:

$$\mathbf{r} = \mathbf{W}_{RX}^{I}\mathbf{y} = \mathbf{s} + \mathbf{n} \tag{2.11}$$

This technique is rather simple and provides perfect spatial equalization (assuming ideal channel state information knowledge), however, as it will be shown further below, the ZF precoder is responsible for a huge increase in the PAPR of the signal, which may be prohibitive.

2.2.2 Zero-Forcing Detection

This time, the zero-forcing processing will be implemented at the receiver side, and thus, no channel state information needs to be reported to the transmitter. However, as it can be observed in Equation (2.14), the performance may be worse compared to that of the precoder case due to a potential noise enhancement. The precoder matrix in this particular case is given by the identity matrix: $\mathbf{W}_{TX}^{I} = \mathbf{I}$, and thus, $\mathbf{x} = \mathbf{I}\mathbf{s}$

The received signal can be expressed as:

$$\mathbf{y} = \mathbf{H}\mathbf{W}_{TX}^{I}\mathbf{s} + \mathbf{n} = \mathbf{H}\mathbf{s} + \mathbf{n} \tag{2.12}$$

The ZF spatial filter is given by the left pseudo-inverse of the channel matrix:

$$\mathbf{W}_{RX}^{ZF} = \left(\mathbf{H}^{H}\mathbf{H}\right)^{-1}\mathbf{H}^{H} \tag{2.13}$$

and thus, the received filtered signal can be expressed in the following way:

$$\mathbf{W}_{RX}^{ZF}\,\mathbf{y} = \mathbf{r} = \left(\mathbf{H}^{H}\mathbf{H}\right)^{-1}\mathbf{H}^{H}\mathbf{H}\mathbf{I}\mathbf{s} + \left(\mathbf{H}^{H}\mathbf{H}\right)^{-1}\mathbf{H}^{H}\mathbf{n} \tag{2.14}$$

which can be rewritten as:

$$\mathbf{r} = \mathbf{s} + \hat{\mathbf{n}} \tag{2.15}$$

where $\hat{\mathbf{n}} = \left(\mathbf{H}^{H}\mathbf{H}\right)^{-1}\mathbf{H}^{H}\mathbf{n}$ represents the filtered noise. The channel inversion may enhance the effect of noise when deep fading occurs, resulting in a worse performance compared to that of the ZF precoder.

2.3 Adaptive Filtering

In wireless communication systems, the effect of the channel needs to be compensated since it may introduce frequency and time selectivity, which really degrades system performance. Typically, the channel is time-varying, which means that methods that are capable of following channel variations need to be implemented because fixed filters are inadequate for this purpose. Channel impulse response can be approximated by a filter whose coefficients automatically adapt themselves in order to follow these variations. Furthermore, channel information is very important not only for equalizing the channel effect at the receiver, but also for the transmitter to carry out signal precoding to provide beamforming gain, spatial equalization or to do resource allocations based on time-frequency dependent user scheduling . Also, adaptive filtering can be used for interference cancellation, when there is specific knowledge of other users' transmissions. In this section, the fundamentals of adaptive filtering are introduced [12][1] [13][2].

Adaptive filtering is based on two processes:

- Filtering: through which the filtered output signal is generated
- Adaptive process: through which the variable parameters are adjusted

which are illustrated in the Figure (2.3) below.

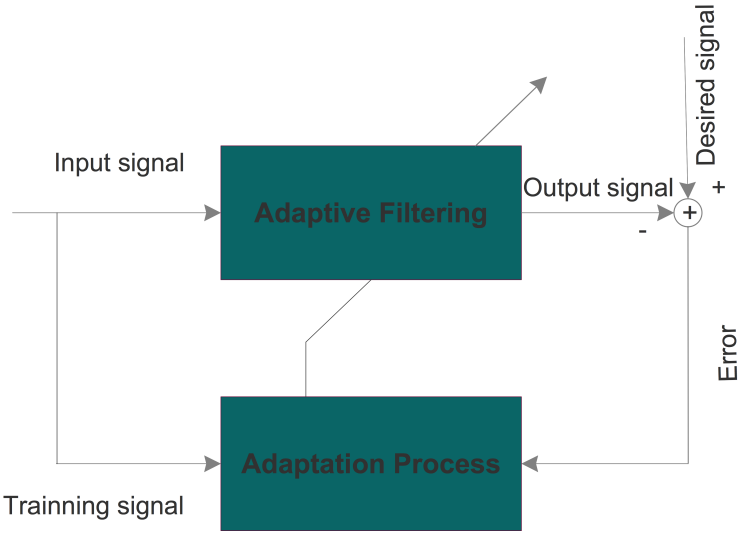

Figure 2.3: Adaptive filtering

[1]The following contents regarding adaptive filtering are based on the lecture notes of Mikko Valkama, *"Advanced Course in Digital Transmission", Tampere University of Technology.*

[2]The following contents of adaptive filtering are based on the lecture notes of Mariano García, Santiago Zazo, Miguel Ángel García, *"Signal Analysis for Communications" Escuela Técnica Superior de Ingenieros de Telecomunicación, Universidad Politécnica de Madrid.*

The target is to minimize the error between the output signal and the target one. Although the filtering process is linear itself, the adaptation algorithm does not necessarily need to be linear, in case it is not, the whole process would be nonlinear. The idea is that given a set of observations of the signal of interest, we want to build the system which allows to optimally approximate these observations. The filtering process can be carried out either by finite impulse response (FIR) or infinite impulse response (IIR) filters. The adaptation algorithm can use statistical information of the signals involved or just follow a deterministic approach. Signal statistics are not typically known, however, they can be estimated by means of the instantaneous observed samples.

2.3.1 Linear Minimum Mean Square Error Estimator

There are different methods to measure or quantify how good the adaptive system is. The common way to do so is by measuring the error between the desired signal and the filter output signal. The so-called mean-squared error (MSE) is a very extended method in which the following cost function is to be minimized, resulting in the so-called minimum mean square error (MMSE):

$$C\left(y,\hat{y}\right)=\mathbb{E}\{|y-\hat{y}|^2\} \tag{2.16}$$

where y and $\hat{y}$ are the desired and the estimated signals respectively. The basics of bayesian estimation, where a random variable is trying to be estimated by means of a set of observable data, consist of defining a positive cost function such that defined in Equation (2.16). It can be demonstrated that the cost function is a random variable and thus, it can be expressed as a function of an expectation, the so-called bayesian risk, which depends on the so-called conditional risk. Hence, the objective is to minimize this latter function. It can be demonstrated that the conditional risk can be expressed as follows:

$$\mathcal{R}'\left(x\right)=\int_{\infty}^{\infty}C\left[y,g(x)\right]f_y\left(y\mid x\right)dy \tag{2.17}$$

where $f_y\left(y\mid x\right)$ is the conditional probability of y given the observation x. By substituting Equation (2.16) in Equation (2.17), the conditional risk can be expressed as:

$$\mathcal{R}'\left(x\right)=\int_{\infty}^{\infty}\left(|y-\hat{y}|^2\right)f_y\left(y\mid x\right)dy \tag{2.18}$$

$$\begin{gathered}\frac{\partial\mathcal{R}'}{\partial\hat{y}}=0\rightarrow-2\int_{\infty}^{\infty}\left(|y-\hat{y}|\right)f_y\left(y\mid x\right)dy\\ \rightarrow\hat{y}_{MMSE}=g\left(x\right)=\int_{\infty}^{\infty}yf_y\left(y\mid x\right)dy=\mathbb{E}\{Y\mid X=x\}\end{gathered} \tag{2.19}$$

Typically, the estimation of a random variable is a nonlinear function of the observations, which turns to be very difficult to analyze. However, if we restrict the estimator to be jointly Gaussians and linear dependent upon the observations, the estimation of a random variable leads to the concept of optimal linear filter or Wiener filter, whose solution is tightly related to the orthogonality principle, making the derivations straightforward. The orthogonality principle is given by:

$$\mathbb{E}\{(\hat{\mathbf{y}} - \mathbf{y})\,\mathbf{x}^T\} = \mathbf{0} \tag{2.20}$$

where $\hat{\mathbf{y}}$ is a linear estimator dependent upon the observations, hence: $\hat{\mathbf{y}} = \mathbf{A}\mathbf{x}$, thus, Equation (2.20) can be expressed as:

$$\mathbb{E}\{(\mathbf{A}\mathbf{x} - \mathbf{y})\,\mathbf{x}^T\} = \mathbf{0} \tag{2.21}$$

resulting in:

$$\mathbf{A} = \mathbf{R}_{yx}\mathbf{R}_x^{-1} \tag{2.22}$$

where $\mathbf{R}_x = \mathbb{E}\{\mathbf{x}\mathbf{x}^T\}$ and $\mathbf{R}_{yx} = \mathbb{E}\{\mathbf{y}\mathbf{x}^T\}$. Hence, the linear estimator which results in the minimum MMSE, also known as linear minimum mean square error (LMMSE), is fully characterized by the second-order statistics.

2.3.2 Channel Estimation

Based on the results of section 2.3.1, the basics of channel estimation are going to be explained. The structure of the adaptive system for modeling this purpose is shown in the Figure (2.4) below.

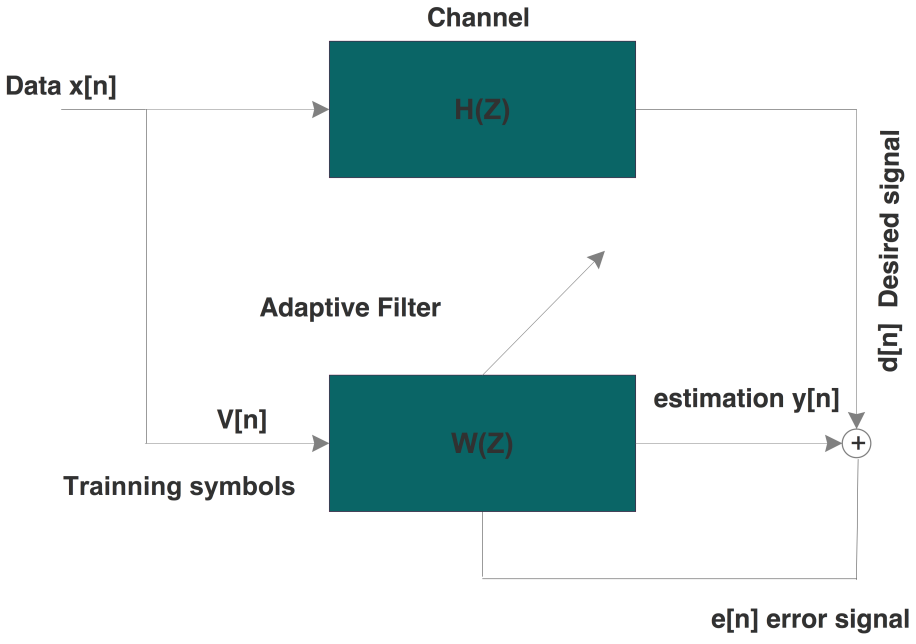

Figure 2.4: Channel estimation

The adaptive filter $W(Z)$ will follow the variations of the channel response $H(Z)$ by dynamically adjusting its coefficients based on:

- The observations $v(n)$, which are typically known as pilots or training sequence.
- The desired signal $d(n)$, which is the received signal.
- The estimation signal $y(n)$, which is obtained by filtering the training sequence with the adaptive filter.
- The error signal $e[n]$.

The filter coefficients will be selected such that y[n] approximates d[n], and hence, w[n] will follow the channel impulse response h[n]. Based on the orthogonality principle, the filter coefficients can be selected as follows:

$$\mathbb{E}\{\Big(d[n] - \mathbf{w}^T[\mathbf{n}]\mathbf{v}[\mathbf{n}]\Big)\,\mathbf{v}^T[\mathbf{n}]\} = \mathbf{0}^T \tag{2.23}$$

thus, the filter coefficients are given by:

$$\mathbf{w} = \mathbf{R}_v^{-1}\mathbf{R}_{dv} \tag{2.24}$$

which is known as the Wiener filter which is the LMMSE optimal solution and it is fully characterized by the second order statistics, where $\mathbf{R}_v = \mathbb{E}\{\mathbf{v}\mathbf{v}^T\}$, and $\mathbf{R}_{dv} = \mathbb{E}\{\mathbf{d}\mathbf{v}^T\}$. It is important that the training symbols used for estimating the channel have low cross-correlation properties to provide good results.

2.3.3 Adaptive Algorithms

The Wiener filter is not adaptive as such, but it is a fixed optimum solution based on the second order statistics, which are not typically known, however they can be estimated by using sample statistics, leading to the well-known least mean squares (LMS) algorithm.

The LMS algorithm is based on steepest-descent method, where the adaptation process follows the opposite direction of that given by the gradient of the error surface, which has the following form for MSE type error:

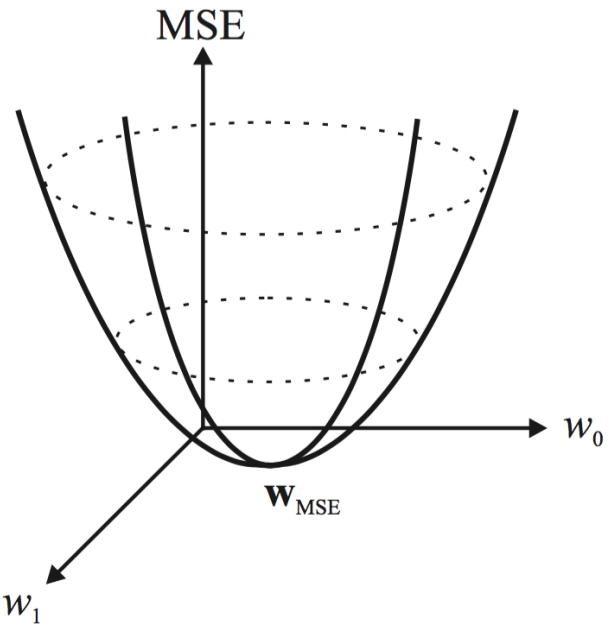

Figure 2.5: MSE error surface [12]

Where the global minimum corresponds to the Wiener solution. The steepest-descent algorithm moves along the error surface a certain "distance" given by the so-called step-size, until it reaches the global minimum or a certain stop condition is met. The bigger the step-size, the faster the algorithm converges, however is more sensitive to oscillations around the Wiener solution. The steepest-descent algorithm can be expressed as follows:

Steepest-Descent Algorithm

$$\mathbf{w}[n+1] = \mathbf{w}[n] - \lambda \nabla e[n] \tag{2.25}$$

Where w[n] and w[n+1] are the filter coefficients for the current and next iterations respectively, λ is the step-size and ∇ is the gradient operator and the error is given by:

$$\begin{aligned} e_{MSE}[n] &= \mathbb{E}\left\{\left(d[n] - \mathbf{w}^T[n]\mathbf{v}[n]\right)\left(d[n] - \mathbf{w}^T[n]\mathbf{v}[n]\right)^T\right\} \\ &= \mathbf{R}_d - \mathbf{R}_{dv}\mathbf{w}[n] + \mathbf{w}^T[n]\mathbf{R}_v\mathbf{w}[n] \end{aligned} \tag{2.26}$$

$$\nabla_w\left(e_{MSE}[n]\right) = 2\mathbf{R}_v\mathbf{w}[n] - \mathbf{R}_{dv} = -\mathbb{E}\{\mathbf{v}[n]\mathbf{e}[n]\} \tag{2.27}$$

as it can be seen from Equation (2.27), the gradient of the error surface depends on the second order statistics, which are typically unknown and thus, they need to be estimated. This is the principle of LMS algorithm.

LMS algorithm

$$\mathbf{w}[n+1] = \mathbf{w}[n] + \lambda \mathbf{v}[n]e[n] \tag{2.28}$$

Where the term $\mathbf{v}[n]\mathbf{e}[n]$ is the instantaneous gradient estimate, as it can be deduced from Equation (2.27). While the steepest-descent algorithm is completely deterministic, the LMS is a random vector.

2.4 Nonlinear Distortion

In this section, the fundamentals of the nonlinearities of radio transmitters are introduced, especially those caused by power amplifiers. Nonlinearities are responsible for harmonic-distortion, spectral regrowth and in-band interference, effects which cause extremely harmful degradation of systems performance [18][3].

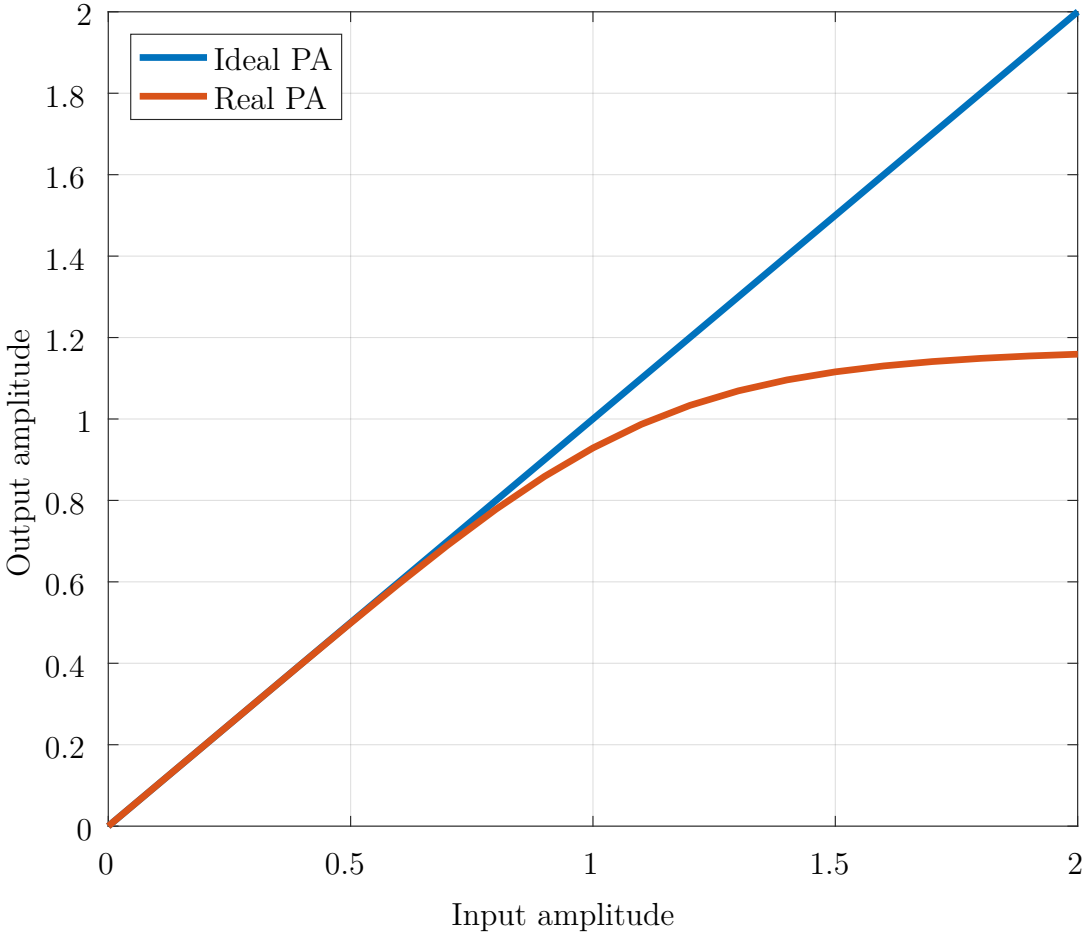

Figure 2.6: Power amplifier saturation

[3]The following contents regarding nonlinear distortion are based on the lecture notes of Mikko Valkama, Markku Renfors *"Radio Architectures and Signal Processing", Tampere University of Technology.*

The saturation behavior of power amplifiers is responsible for the nonlinearity effects on the signal. Such behavior can be described with an instantaneous polynomial model such as:

$$y(t) = b_1 x(t) + b_2 x^2(t) + b_3 x^3(t) + \cdots + b_n x^n(t) \tag{2.29}$$

from which, the frequency domain signal can be obtained:

$$Y(f) = b_1 X(f) + b_2 X(f) * X(f) + b_3 X(f) * X(f) * X(f) + \cdots \tag{2.30}$$

where '$*$' denotes the convolution operator. If we consider W to be the input signal bandwidth, it can be seen from previous equation that new frequencies will appear. E.g., $X(f)*X(f)$ generally has twice the bandwidth of $X(f)$, unless $x(t)$ is a constant envelope signal.

Typically even terms lack of interest for this analysis since they create distortion around baseband and twice the frequency carrier, but not arround the band of interest. However, if the system bandwidth is extremely large, all terms should be taken into account, in other cases, antenna filtering suppresses them. For example, when feeding a nonlinear device with two tones at f_1 and f_2, second order distortion can produce frequency terms at $f_1 + f_2$ or $f_1 - f_2$. On the other hand, odd terms like third-order distortion produce new frequencies (among others) at: $2f_1 - f_2$ or $2f_2 - f_1$, which may lie over the band of interest and cause harmful effects on the signal.

In the figure below, the intermodulation terms produced by a third order nonlinear device are represented.

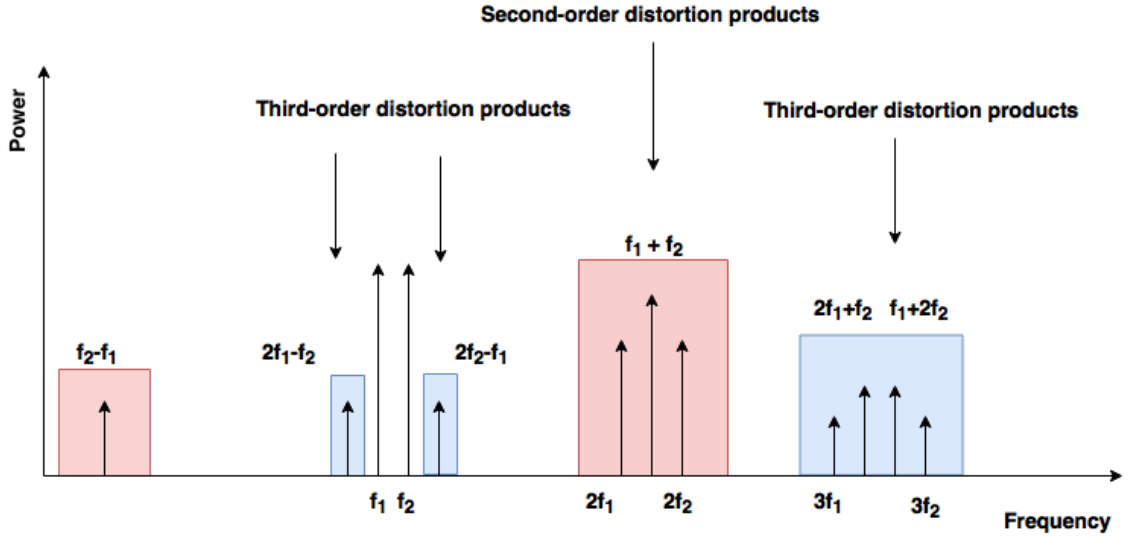

Figure 2.7: Second and third-order intermodulation products

Therefore, as it can be seen in Figure (2.7), the more harmful intermodulation products are $2f_1 - f_2$ and $2f_2 - f_1$, since they will most likely lie over the desired

band. The rest of the new components may become harmful depending on the used radio architecture or system specifications.

2.4.1 Role of the Envelope on the Signal Distortion

The distortion is heavily dependent upon the characteristics of the envelope of the signal that passes through the nonlinear device. Let us assume that we feed a general passband signal of the form: $x(t) = A(t)cos(w_c t + \phi(t))$ to a third-order nonlinearity such that $y(t) = b_1 x(t) + b_3 x^3(t)$, which results in:

$$\begin{aligned} y(t) = &\left(b_1 A(t) + \frac{3}{4} b_3 A^3(t)\right) cos\left(w_c t + \phi(t)\right) \\ &+ \frac{1}{4} b_3 A^3(t) cos(3w_c t + 3\phi(t)) \end{aligned} \tag{2.31}$$

where $A(t)$ and $\phi(t)$ denote the amplitude and phase of the input signal respectively, while w_c denotes the carrier frequency. If we only consider the terms around the main carrier we have:

$$\left(b_1 A(t) + \frac{3}{4} b_3 A^3(t)\right) cos\left(w_c t + \phi(t)\right) \tag{2.32}$$

Thus, the term $\frac{3}{4} b_3 A^3(t) cos\left(w_c t + \phi(t)\right)$, which is caused by the third order distortion term, has an equivalent baseband of the following form:

$$\hat{x}_{BB}(t) = A^3(t) e^{j\phi(t)} \tag{2.33}$$

which is typically written as follows:

$$\hat{x}_{BB}(t) = |A(t)|^2 A(t) e^{j\phi(t)} = |x_{BB}(t)|^2 x_{BB}(t) \tag{2.34}$$

where $x_{BB}(t) = A(t)e^{j\phi(t)}$. Equation (2.34) can be expressed on the frequency domain as:

$$FT\left\{x_{BB}^3(t)\right\} = FT\left\{|x_{BB}(t)|^2\right\} * FT\left\{|x_{BB}(t)| e^{j\phi(t)}\right\} \tag{2.35}$$

where '*' denotes the convolution operator and $FT\{\cdot\}$ denotes the Fourier transform. If we consider $x_{BB}(t)$ to have constant envelope, then, $|A(t)|^2 = |A|^2$, leading to:

$$FT\left\{x_{BB}^3(t)\right\} = |A|^2 \cdot FT\left\{x_{BB}(t)\right\} \tag{2.36}$$

which clearly shows that it does not present any spectral regrowth. However, if $x(t)$ is a non-constant envelope signal, $|x_{BB}(t)|^2 * |x_{BB}(t)|$ occupies three times more bandwidth than $x_{BB}(t)$. With constant envelope signals, we can push the amplifiers really harshly in order to obtain good power efficiency without causing any inband

distortion or spectral regrowth around the band of interest. Of course, it still produces the third-order harmonic $b_3A^3(t)cos(3w_ct + 3\phi(t))$ but it is effectively filtered away by the antenna. In the figure below this idea is intuitively shown:

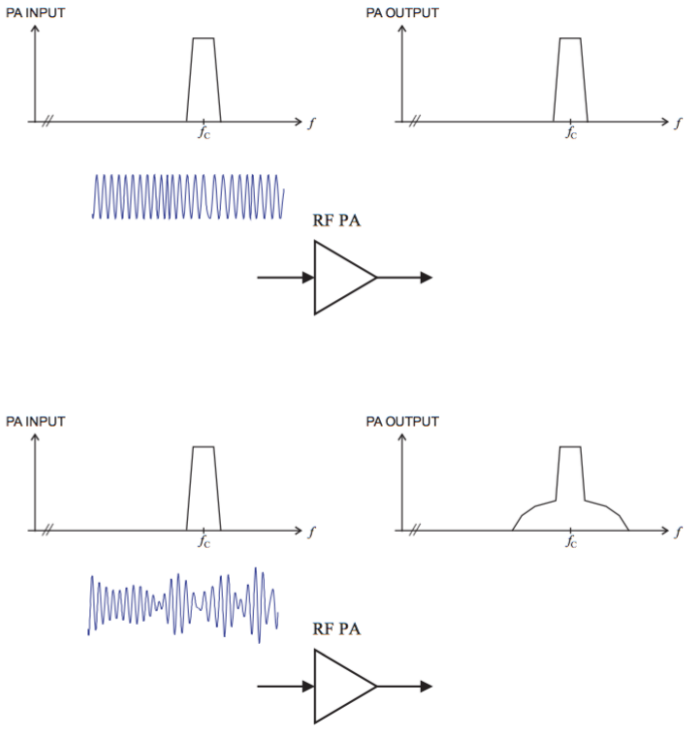

Figure 2.8: Effect of the envelope [18]

2.4.2 Nonlinear Distortion Behavioral Models

In this section, different techniques for modeling power amplifiers are introduced. Correct modeling of power amplifiers is a crucial task since there are different techniques, such as digital predistortion, that try to compensate for these harmful effects by means of applying the inverse function of the measured model. Therefore, their efectivity depends on how accurate the model is. Power amplifiers are modeled by means of mathematical black-box models with reasonable complexity and accuracy. They may take into account nonlinear and memory effects. Typically these models relate the amplitude and phase of input samples to those of the output samples [18], [22]. Distortion can be modeled as memoryless, which means that the current output is only dependent on the current input, or as memory distortion, in which the current output does not only depend on the current input but also on the L previous ones, leading to memory or memoryless approaches.

2.4.3 AM/AM and AM/PM

AM/AM relates the instantaneous output envelope to the input envelope, on the other hand AM/PM relates the instantaneous output phase to the instantaneous input envelope. Let us assume that the AM-AM and AM-PM transformations over the amplitude and phase respectively are represented by the functions: $f_A(\cdot)$ and $f_\theta(\cdot)$. Therefore, if we feed the power amplifier with a baseband signal of the form $x_{BB}(t) = |A(t)| \cdot e^{j\phi(t)}$, the signal at the power amplifier output would be given by (considering memoriless distortion) [18]:

$$y(t) = f_A(|x_{BB}(t)|) \cdot e^{j(\phi(t)+f_\theta(|x_{BB}(t)|))}$$

Rapp Model

Rapp model is a well known and simple approach for modeling the AM-AM memoryless characteristic of the power amplifier:

$$f_A = \frac{A_{output}}{A_{input}} = \frac{1}{\left[1 + \left(\frac{A_{input}}{A_{sat}}\right)^{2p}\right]^{1/2p}} \tag{2.37}$$

where p is the smoothness factor, and A_{sat} is the output saturation level. The following figure represents the Rapp's AM/AM model for a smoothness factor of 2.5:

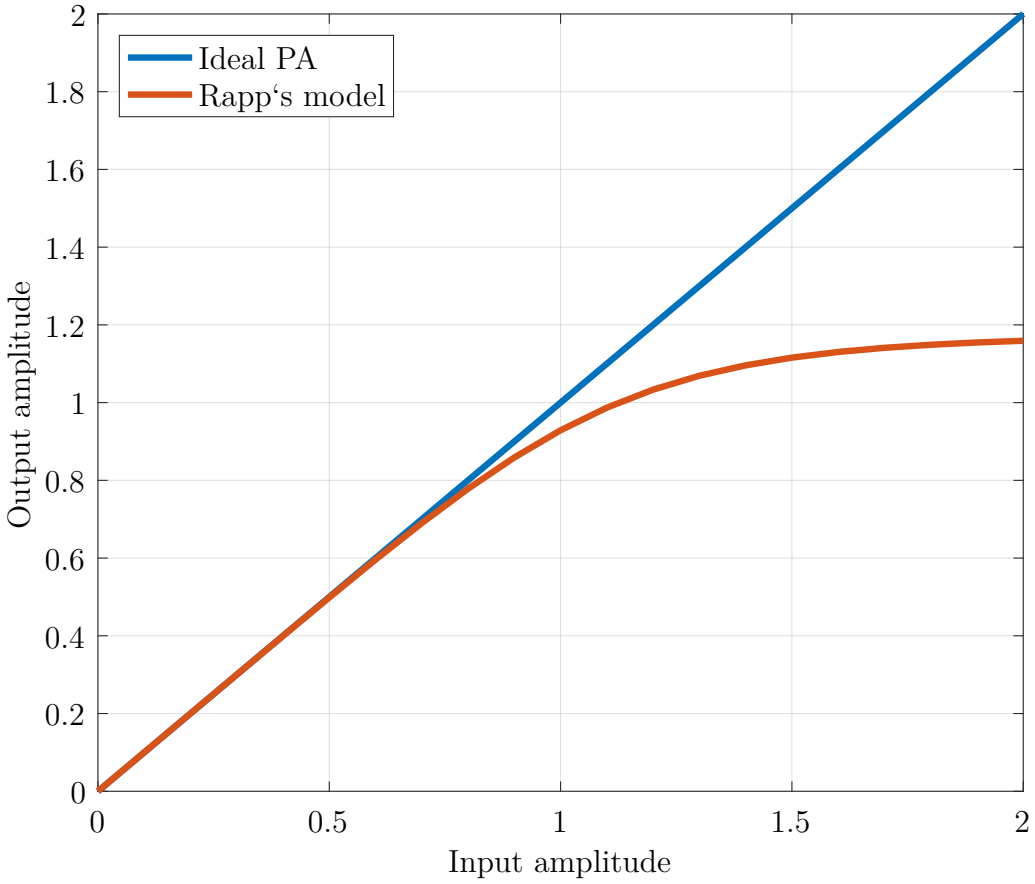

Figure 2.9: Rapp's AM/AM model

Saleh Model

Saleh's model provides both, the AM/AM and AM/PM characteristics for a memoryless power amplifier:

$$f_A = \frac{\alpha_a A_{input}}{1 + \beta_a A_{input}^2} \tag{2.38}$$

where α_a is the small signal gain and β_a defines the saturation voltage such that $A_{sat} = 1/\sqrt{\beta_a}$

$$f_\theta = \frac{\alpha_\theta A_{input}}{1 + \beta_\theta A_{input}^2} \tag{2.39}$$

where β_{theta} defines the saturation phase such that $\phi_{sat} = 1/\sqrt{\beta_\theta}$.

Instantaneous complex polynomial models, like the one shown in Equation (3.12), are also widely used. However, all these models are memoryless, which basically means that they are frequency independent, making them to be only valid for narrowband systems. Due to the increasing necessity of utilizing wider bandwidth, memoryless models turned to be insufficient.

2.4.4 Memory-based Models

When system bandwidth increases, frequency selectivity of the nonlinear device needs to be taken into account when modeling its behavior. Typically, memory effects are modeled with FIR filters. Wiener, Hammerstein and Volterra methods are widely used. They are different approaches:

- Cascading a FIR filter either before or after an instantaneous nonlinearity model e.g., a polynomial-based model.
- Cascading a FIR filter before and after an instantaneous nonlinearity
- Memory polynomial model, where parallel branches, corresponding to the odd terms of a polynomial model followed by a FIR filter, are combined.

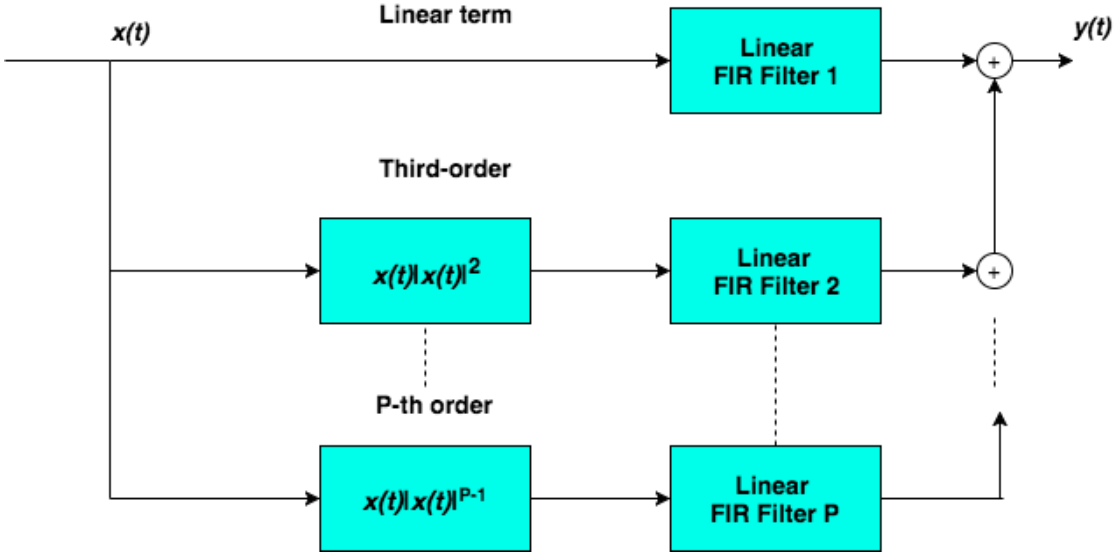

Figure 2.10: Memory polynomial model

2.5 Energy Consumption and the PAPR Problem

The total energy consumption of the mobile network is targeted to be reduced a 90% [1]. Being able to do so while providing 1000 times more capacity is not trivial whatsoever. Due to the densification of the network, the increase in energy consumption may be unacceptable. High energy performance for reducing network consumption is needed and it is critical since it means ≈ 15-25% of the network OPEX [14]. Reducing base stations energy consumption would really facilitate off-grid network deployment with renewable energies [15], allowing to deploy sites in places where it is not possible to connect to the electrical grid. *Green Mobile Networks* is emerging as a key concept to reduce the greenhouse gas fingerprint.

There are different approaches to reduce the power consumption. As it is explained in [15], nowadays the system load has little effect on the network energy consumption. Mobile networks are designed to be always on in order to provide continuous and highly reliable operation, however, it is mainly affected by the signals used to access the network like the broadcast channel and synchronization signals in LTE. To cope with this issue they introduce the concept of always available which does not necessarily mean always on, although, signals to access the network need to be always active anyway, but for example, increased discontinuous transmission (DTX) and discontinuous reception (DRX) times are introduced. Also cloudification and virtualization of the network can provide important energy savings. Cloud-RAN is a novel network architecture where the baseband processing is centralized and shared among many sites in the so-called virtualized baseband units (BBU) pool. This will allow to decrease the cost of the network, since energy consumption is reduced compared to the traditional radio access network (RAN) architectures [17], where more BBU are required. Manufacturers focus on new base stations with improved hardware and software efficiency, most of the total energy budget is actually consumed by the coolers and RF components [16]. Base stations are responsible for the 80% of the operator's power consumption, of which, the power amplifiers are responsible for the 40%-50% [5].

Hence, one major approach to reduce energy consumption is to improve power amplifiers energy efficiency, fact that is being approached in this Master Thesis.

2.5.1 The PAPR Problem

The efficiency of power amplifiers is directly related to the PAPR. The PAPR is the ratio between the peak power and the average power of the transmit signal:

$$PAPR\left[x\left(t\right)\right]_{dB} = 10 * log_{10}\left(\frac{max\left\{\left|x(t)\right|^2\right\}}{\mathbb{E}\left\{\left|x(t)\right|^2\right\}}\right),\ t \in T \tag{2.40}$$

it is also important to notice that the PAPR of the RF-modulated signal is 3 dB higher than that of the baseband signal. In the following, it will only be considered the PAPR of the baseband signal. For constant envelope signals, the value of their PAPR is 0 dB, for non-constant envelope signals, the PAPR depends on the specific signal waveform and it can be arbitrarily large. In the figure below, a non-constant envelope signal is represented.

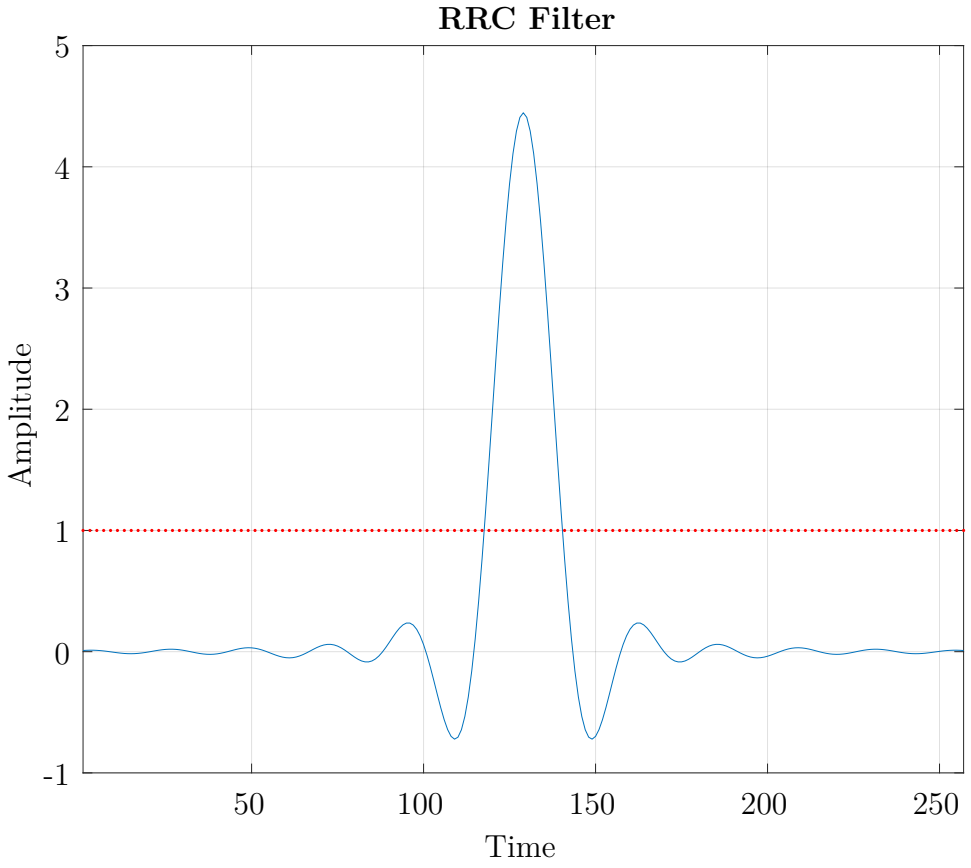

Figure 2.11: Peak-to-average power ratio

The dotted red line represents the mean amplitude (in this case the mean amplitude corresponds to the mean power as well), which turns to be 1, while the peak value of the amplitude rises up to a value of 4.44, resulting in a PAPR of 12.94 dB. The PAPR is typically interpreted as a random variable, for example, in multicarrier waveforms like orthogonal frequency division multiplexing (OFDM), many subcarriers are coherently or incoherently added causing constructive or destructive summations which have an effect on the signal waveform and thus, in its PAPR. The nature of the summation depends on the different subcarrier symbols which are random, as well as on the IFFT weights. Therefore, it is interpreted as a random variable and typically represented by means of its complementary cumulative distribution function (CCDF) as it is shown in the figure below:

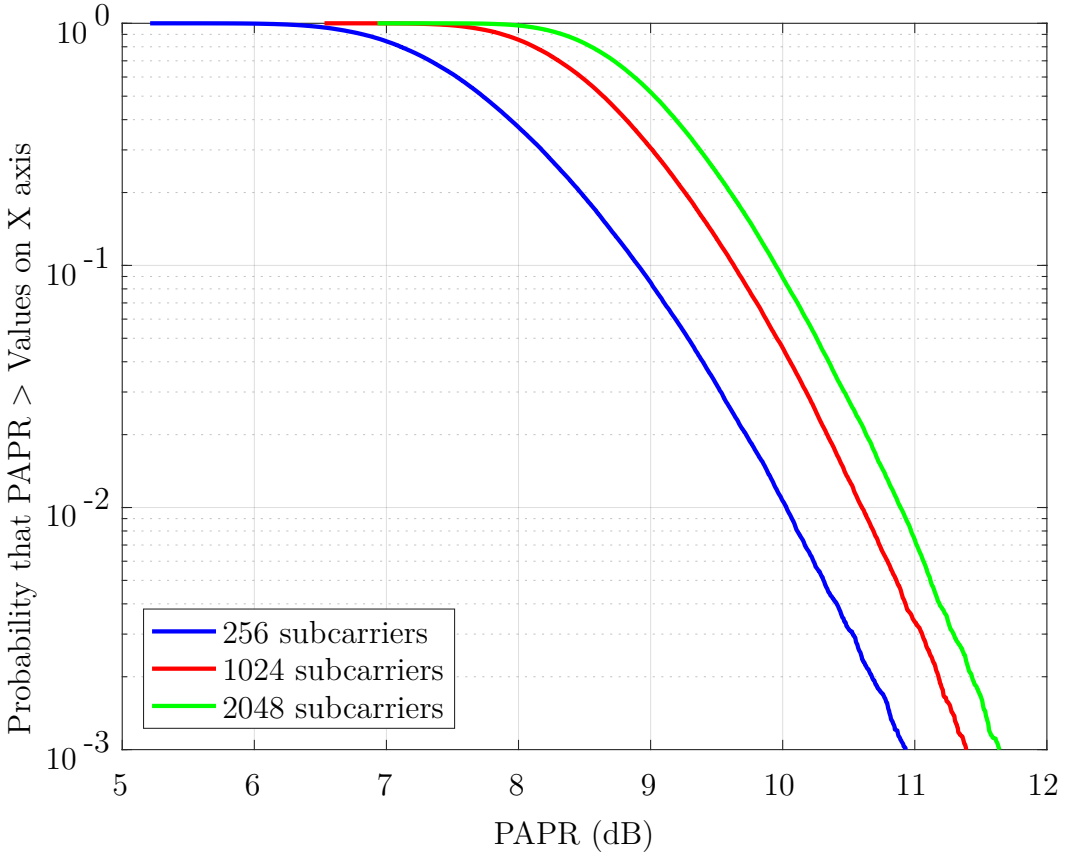

Figure 2.12: PAPR of the OFDM signal for different number of subcarriers

Non-constant envelope signals, like the one shown in Figure (2.11), are very sensitive to nonlinearities. Nonlinearities produce spectral regrowth which results in adjacent channel interference, as well as interference within signal bandwidth degrading BER performance (they also produces harmonic distortion, however, this effect can be overcome rather easily) as it has been previously mentioned. Both effects are really harmful and need to be considered in the system specifications by means of different figures of merit such as: PAPR, Adjacent Channel Leakage Ratio (ACLR) or Error Vector Magnitude (EVM) in order to ensure a correct system performance.

If we want to avoid significant signal distortion due to the nonlinearities of the power amplifier, it is required to ensure a linear operation range over PAPR times the average power. Hence, power amplifiers operation point is very far away from its saturation point in order to provide such linear behavior. This means that most of the DC power supply is wasted, leading to a low energy efficiency and higher operation costs for the operators. This fact can be observed in the figure below.

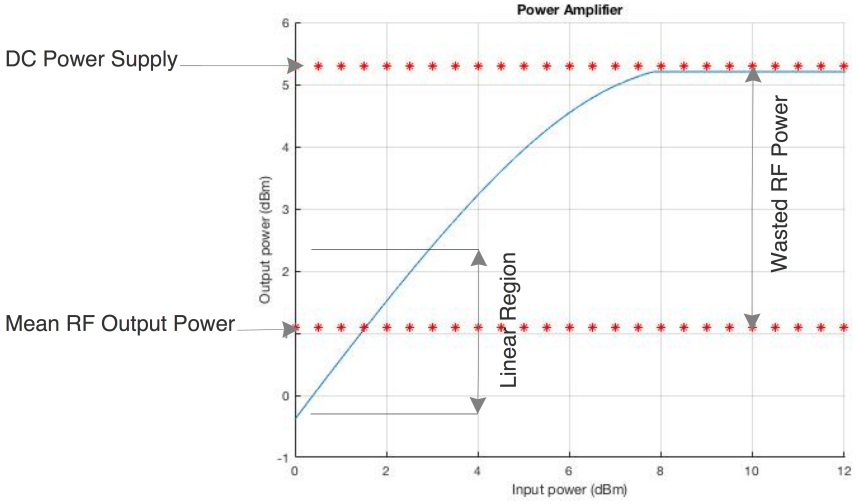

Figure 2.13: Power amplifier model

The saturation power is given by the DC power supply, which is the maximum output power of the power amplifier. To ensure the linear behavior it is necessary to have a certain back-off , the higher the back-off, the more linear behavior we will have, however power efficiency degrades. The back-off is typically defined as how many dB's below the 1 dB compression point the power amplifier is operating, where the 1 dB compression point is the input signal value which causes the gain to drop 1 dB from its small signal value. In Figure (2.13), it has been considered that the mean power output of the signal is given by the dotted line, a sufficiently big back-off has been chosen such that the operation range is linear enough. That is how current systems like LTE (Long Term Evolution), which uses an OFDM signal with elevated PAPR, define their power amplifiers operation point.

The efficiency of a power amplifier can be defined as:

$$\eta = \frac{Average\ Output\ Power}{DC\ Power\ Supply} \tag{2.41}$$

which is dependent on the PAPR as stated below [20]:

$$\eta = \frac{0.5}{PAPR} \tag{2.42}$$

where it has been assumed that the power amplifier is fully linear, the 0.5 in the numerator assumes a modulated RF signal. Notice that the PAPR of an OFDM signal is easily above 10 dB, which would result in a very poor energy efficiency.

There are several methods such as: digital predistortion (DPD), envelope tracking or clipping techniques [19] that allow to cope with this issue. These techniques are brievely introduced in the following section.

2.5.2 PAPR Mitigation

Currently used waveforms, such as OFDM, provide elevated spectral efficiency, tolerate the multipath propagation in a very acceptable way and they show good immunity to frequency selectivity, however they suffer from having a really high PAPR. Techniques for improving power amplifiers efficiency have drawn researchers attention throughout the years. There are different techniques which provide fairly good results and they are widely used in current wireless communication systems. Some of these techniques are: envelope tracking, clipping, partial transmit sequences, coding schemes and tone reservation [20].

Clipping Techniques

A simple way to reduce the PAPR consists on clipping the signal amplitude when it is above a certain level. If the OFDM symbol $\mathbf{s}$ is clipped at a level A, the clipped signal is given by [7]:

$$\hat{\mathbf{s}} = \begin{cases} s, & |\mathbf{s}| \leq A \\ A, & |\mathbf{s}| > A \end{cases} \tag{2.43}$$

The clipping is carried out at the transmitter, so that the receiver needs to estimate the clipping to compensate it. Clipping introduces abrupt changes on the envelope of the signal causing in-band and out-band distortions.

Partial Transmit Sequences

With partial transmit sequences (PTS) approach, the input data is divided into M subblocks. One of the block is fixed as the reference one, and then relative phase shifts of $k \cdot 90^o$ are applied to the M-1 subblocks. The combination with lowest PAPR is selected. The are 4^{M-1} alternative cases to be tested.

Coding Schemes

When N signals are coherently added, they produce a peak power which is N times its average power. The maximum PAPR of a multicarrier signal is given by:

$$Max_{PAPR} = N \cdot max\left\{|A_m|\right\} \tag{2.44}$$

where N is the number of active subcarriers and $\{A_m\}$ is the symbol alphabet. Of course, this happens with extremely low probability and not all codewords result in a bad PAPR. The coding schemes attempt to reduce the occurrence probability

of coherently adding all the subcarriers [20]. Complement Block Coding (CBC) and Modified Complement Block Coding (MCBC) are the most attractive coding schemes for this regard. They are based on complementary bits that are added to the original information bits, techniques that have proven their ability to effectively reduce the PAPR. CBC and MCBC are more flexible when choosing the coding rate, the frame size and they have lower implementation complexity than other coding techniques [20].

2.5.3 Digital Predistortion

Another approach to improve power amplifiers efficiency is to linearize their transfer function. Digital Predistortion is a highly cost-effective method for this regard, which also allows to mitigate the nonlinear distortion effects like spectral regrowth or spurious emissions. After modeling the power amplifier characteristic by means of the methods stated in section 2.4.2, the inverse function of this model is used in order to predistort the signal before passing through the power amplifier, and thus, a higher linear response is obtained.

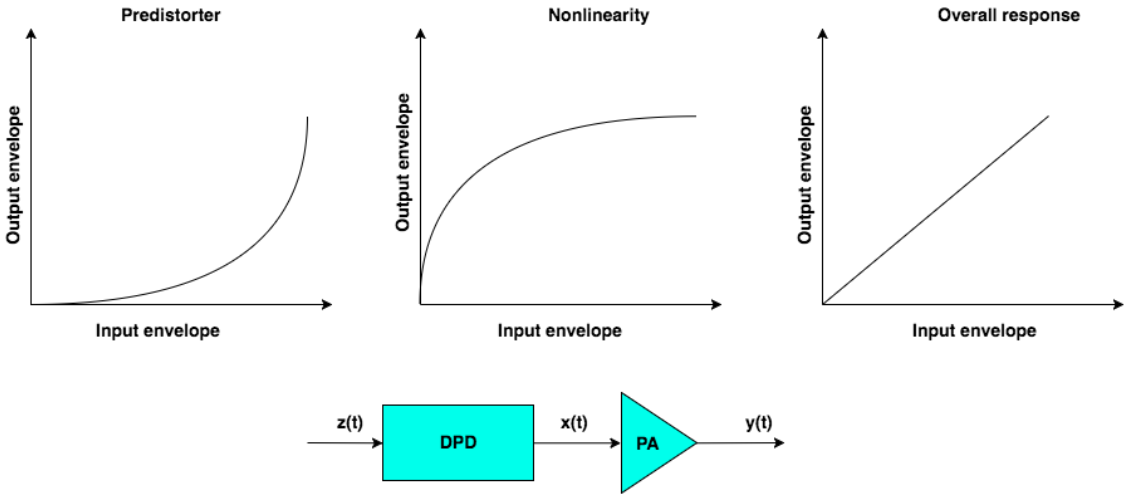

Figure 2.14: Digital predistortion scheme

The performance of DPD depends basically on how accurate the power amplifier model is. A fact that needs to be considered when implementing DPD is that it may enhance the PAPR of the PA input signal, therefore, an extra back-off should be considered. It also typically requires a 5-10x oversampling factor. Since models do not exactly reproduce power amplifiers behavior, there will be still nonlinear distortion on the signal, however, these effects are milder.

Direct-based and indirect-based approaches for DPD implementation are shortly introduced below:

Direct learning

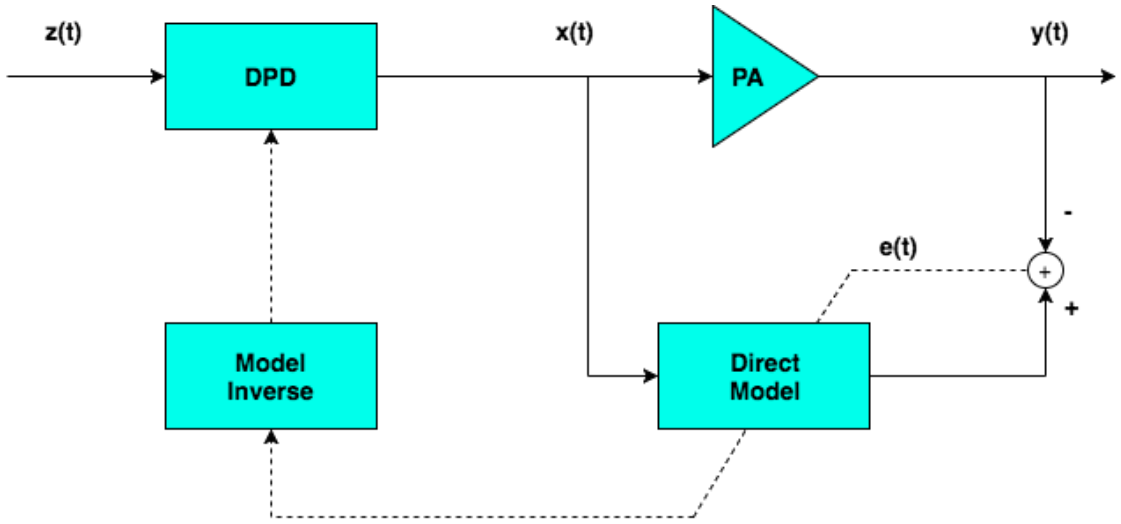

Figure 2.15: Direct learning approach

Direct learning attempts to obtain the transfer characteristic of the power amplifier (it follows the same basics than that of channel estimation) to feedback then its inverse to the DPD block. For memoryless models is a really straightforward approach.

Indirect learning

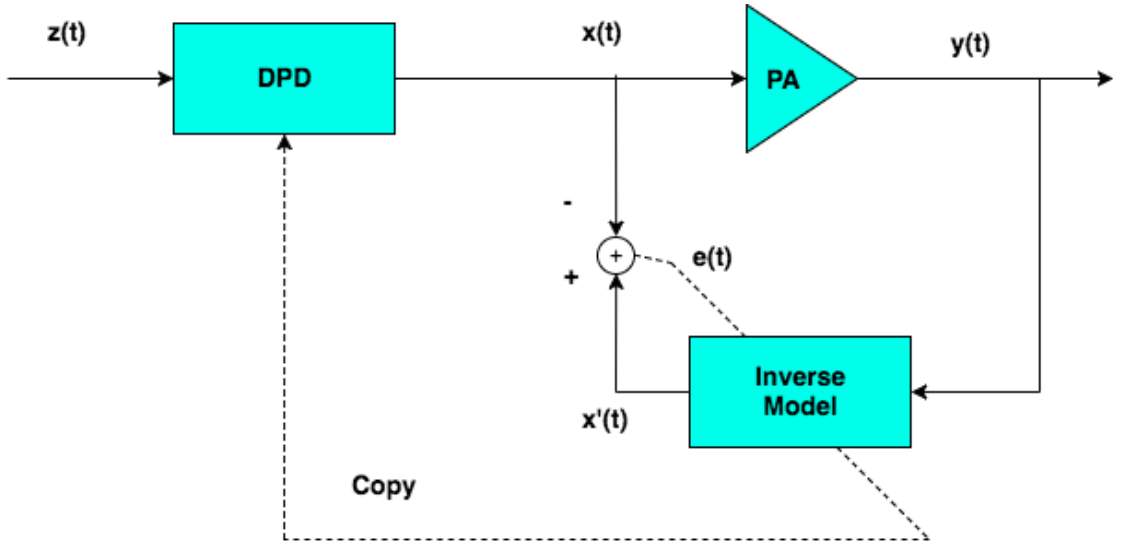

Figure 2.16: Indirect learning approach

In indirect learning, we directly attempt to obtain the inverse response of the PA by minimizing the error between the power amplifier input and the output of the

inverse model. It follows the same basics of channel equalization techniques or inverse filtering.

Chapter 3

Constant Envelope Precoder

In this chapter, the fundamentals of constant envelope (CE) precoding are introduced. Large antenna arrays have lots of benefits such as the ability to spatially multiplex many parallel links or to provide very narrow beams by means of beamforming techniques. Massive MIMO has become a very important enabler for 5G mobile networks enabling the opportunity of meeting the data rate and link reliability requirements. As it has been addressed in the earlier chapters, power consumption is a big concern for future mobile systems, and base station consumption has plenty of room for improvement. Constant envelope precoding attempts to simultaneously address the energy consumption problem and the need of higher data rates.

In [9–11], *Saif Khan Mohammed and Erik G. Larsson* introduced the concept of constant envelope precoding. This kind of precoder is capable of achieving a discrete-time constant envelope signal while providing spatial precoding. The objectives of the precoder are: improving the PAPR characteristics of the signal for efficient power amplifiers utilization, the spectral efficiency and the link performance. We will consider a large-scale MU-MIMO scenario where the number of transmit antennas is larger than the number of co-scheduled users. Thus, thanks to the additional degrees of freedom available, it is possible to perform waveform shaping such that a constant envelope signal is ideally achieved. This would provide another way to address the problem of the PAPR, based on precoding techniques, and it could be jointly used with other techniques like digital predistortion.

3.1 Discrete-Time System Model

Let us assume a large-scale MU-MIMO scenario where K denotes the number of single-antenna co-scheduled users, and N_t denotes the number of transmit antennas at the base station, where $N_t >> K$. It will be assumed that there is a total power constraint P_t. Let $\mathcal{S}$ denote the information alphabet and $\mathbf{s} = (s_1, s_2, \cdots, s_K)^T$

denote the vector of information symbols to be transmitted per time instant, where $s_k \in \mathcal{S}$ denotes the information symbol intended for the k-th user.

Let $\mathbf{W}_{TX} \in \mathbb{C}^{N_t \times K}$ denote the precoding matrix:

$$\mathbf{W}_{TX} = \begin{pmatrix} w_{1,1} & w_{1,2} & \dots & w_{1,K} \\ w_{2,1} & w_{2,2} & \dots & w_{2,K} \\ \vdots & \vdots & \ddots & \vdots \\ w_{N_t,1} & w_{N_t,2} & \dots & w_{N_t,K} \end{pmatrix} \tag{3.1}$$

the precoded data symbols denoted by $\mathbf{x} = (x_1, x_2, \cdots, x_{N_t})^T$ are obtained as follows:

$$\begin{pmatrix} x_1 \\ x_2 \\ \vdots \\ x_{N_t} \end{pmatrix} = \begin{pmatrix} w_{1,1} & w_{1,2} & \dots & w_{1,K} \\ w_{2,1} & w_{2,2} & \dots & w_{2,K} \\ \vdots & \vdots & \ddots & \vdots \\ w_{N_t,1} & w_{N_t,2} & \dots & w_{N_t,K} \end{pmatrix} \begin{pmatrix} s_1 \\ s_2 \\ \vdots \\ s_K \end{pmatrix} \tag{3.2}$$

which are constrained to have constant envelope such that: $|x_n| = \sqrt{P_t/N_t}$. Note that the amplitude of the signal is the same in every antenna branch and in every time instant. The precoder will thus map the K data streams into the N_t antenna branches.

The precoder outputs x_n are of the form:

$$x_n = \sqrt{\frac{P_t}{N_t}} e^{j\theta_n} \quad , \quad n = 1, \cdots, N_t \tag{3.3}$$

the precoder will generate a constant amplitude signal in every antenna branch, each of them with a certain phase. Those phases will be selected in such a way that the multi-user interference produced by the spatial multiplexing transmission is minimized, or in such a way that the information symbols can be properly scaled to provide beamforming gain.

In the following we will consider narrowband single carrier transmission. Thus, the channel between the k-th user and the n-th antenna can be modeled as a complex coefficient (assuming flat fading within the carrier bandwidth). Let $\mathbf{H} \in \mathbb{C}^{K \times N_t}$ denote the channel matrix:

$$\mathbf{H} = \begin{pmatrix} h_{1,1} & h_{1,2} & \dots & h_{1,N_t} \\ h_{2,1} & h_{2,2} & \dots & h_{2,N_t} \\ \vdots & \vdots & \ddots & \vdots \\ h_{K,1} & h_{K,2} & \dots & h_{K,N_t} \end{pmatrix}$$

where $h_{k,n}$ denotes the complex weight of the zero-mean-unit-variance flat-fading Rayleigh channel between the k-th user and the n-th transmit antenna.

The vector of received symbols $\mathbf{y} = (y_1, y_2, \cdots, y_K)^T$ is given by:

$$\begin{pmatrix} y_1 \\ y_2 \\ \vdots \\ y_K \end{pmatrix} = \begin{pmatrix} h_{1,1} & h_{1,2} & \dots & h_{1,N_t} \\ h_{2,1} & h_{2,2} & \dots & h_{2,N_t} \\ \vdots & \vdots & \ddots & \vdots \\ h_{K,1} & h_{K,2} & \dots & h_{K,N_t} \end{pmatrix} \begin{pmatrix} x_1 \\ x_2 \\ \vdots \\ x_{N_t} \end{pmatrix} + \begin{pmatrix} n_1 \\ n_2 \\ \vdots \\ n_K \end{pmatrix} \tag{3.4}$$

where $n_k \sim \mathcal{CN}(0, \sigma^2)$ is the AWGN at the k-th user, while y_k denotes the received symbol by the k-th user and can be expressed as:

$$y_k = \sqrt{\frac{P_t}{N_t}} \sum_{n=1}^{Nt} h_{k,n} e^{j\theta_n} + n_k \ , \quad k = 1, \cdots, K \tag{3.5}$$

The constant envelope scheme can be seen in the figure below:

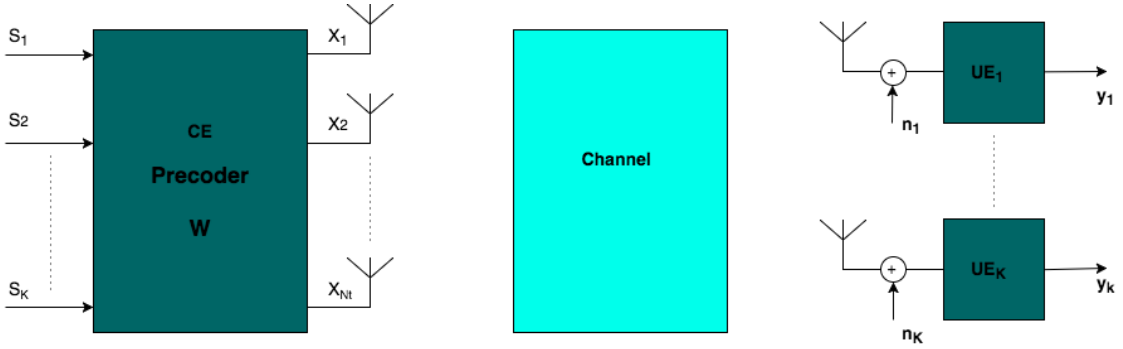

Figure 3.1: Discrete-time system model

Let $\mathbf{\Theta} = (\theta_1, \cdots, \theta_{N_t})^T$ denote the phases of the transmitted per-antenna constant envelope signals, θ_n is selected such that the global multi-user interference power is minimized. The spatial multiplexing interference seen by the k-th user is given by:

$$mui_k = \sqrt{\frac{P_t}{N_t}} \sum_{n=1}^{Nt} h_{k,n} e^{j\theta_n} - s_k \tag{3.6}$$

the interference is calculated as the difference between the noise-free received symbol and the actual information symbol intended for the k-th user, therefore, $\mathbf{\Theta}$ is selected such that:

$$mui = \sum_{k=1}^{K} \left| \left(\sqrt{\frac{P_t}{N_t}} \sum_{n=1}^{Nt} h_{k,n} e^{j\theta_n} - s_k \right) \right|^2 \tag{3.7}$$

is minimized. The parameter mui takes into account the interference seen by every user. The adaptation process needs to be based on the global interference in order to optimize the performance of every single user.

In the following, it will be assumed that the multi-user interference is Gaussian distributed and that it is uncorrelated with the noise and with the desired signal. Equation (3.5) can be rewritten as follows:

$$y_k = s_k + mui_k + n_k = s_k + \hat{n}_k \tag{3.8}$$

where $\hat{n}_k$ takes into account the effect of the multi-user interference term plus the white Gaussian noise. Further below, $\hat{n}_k$ will also take into account the effect of more interference sources, which will be also modeled as independent Gaussian sources. The calculation of $\hat{n}_k$ will be crucial for evaluating the SINR in a proper manner.

The problem at hand can be interpreted as an optimization problem with constraints in the total transmit power and in the signal amplitude:

$$\begin{aligned} \Theta = (\theta_1, \theta_2, \cdots, \theta_{N_t}) &= \arg \min_{\theta_n \in [-\pi,\pi), n=1,\ldots,N_t} f(\Theta, \mathbf{s}) \\ f(\Theta, \mathbf{s}) &= \sum_{k=1}^{K} \left| \left(\sqrt{\frac{P_t}{N_t}} \sum_{n=1}^{Nt} h_{k,n} e^{j\theta_n} - s_k \right) \right|^2 \\ s.t. \quad & ||\mathbf{x}||^2 = P_t \\ & |x_n| = \sqrt{\frac{P_t}{N_t}} \end{aligned} \tag{3.9}$$

which turns to be a nonlinear least squares optimization problem, which is unfortunately non-convex. Therefore, the objective function $f(\Theta, \mathbf{s})$ might have multiple local minima, making gradient descent algorithms non suitable for this purpose. However, as it is stated in [9], when the ratio between the number of antennas and the number of co-scheduled users is big enough, thanks to the additional degrees of freedom available, the values of the local minima tend to the value of the global minimum, enabling the utilization of gradient descent algorithms.

In the following, the gradient descent-based algorithm is explained. The algorithm consists of $N_t \times M$ iterations, where M is a certain prefixed integer value. Let the index $n \in [1, \cdots, i, \cdots, N_t]$ denote the iteration for the n-th antenna and $m \in [1, \cdots, j, \cdots, M]$ denote the m-th sub-iteration. First, a vector $\mathbf{x}$ of $N_t \times 1$ components is generated such that $\mathbf{x} = (\sqrt{\frac{P_t}{N_t}} e^{j\theta_1}, \cdots, \sqrt{\frac{P_t}{N_t}} e^{j\theta_{N_t}})$ (recall that $\mathbf{x}$ denotes the precoder output). In every n-th iteration, the phase of the symbol at the n-th antenna branch is adapted following M sub-iterations of the gradient descent algorithm, while the phases of the rest of the antenna branches remain fixed. The precoder output at the m-th sub-iteration will be denoted by $\mathbf{x_m} = (\sqrt{\frac{P_t}{N_t}} e^{j\theta_{1,m}}, \cdots, \sqrt{\frac{P_t}{N_t}} e^{j\theta_{N_t,m}})$, the phase components of $\mathbf{x}$ are initialized to zero: $\mathbf{\Theta_1} = (\theta_{1,1}, \cdots, \theta_{i,1}, \cdots, \theta_{N_t,1})^T = (0, 0, \cdots, 0)^T$. After the M sub-iterations, the phase of the m-th sub-iteration which resulted in the lowest multi-user interference (which will be denoted by θ_{opt}) is selected and the phase of the n-th antenna

branch is set to that value. Then, the algorithm moves to the $(n+1)$-th antenna branch and proceeds the same way. It is assumed that perfect channel state information is available at the transmitter side, therefore the channel coefficients $h_{k,n}$ are known.

Algorithm 1 LMS-based optimization

$\mathbf{\Theta_1} = (0, 0, \cdots, 0)^T$
for $n = 1$ to N_t **do**
  for $m = 1$ to M **do**
    $e_m = \sum_{k=1}^{K} \left| \left(\sqrt{\frac{P_t}{N_t}} \sum_{n=1}^{Nt} h_{k,n} e^{j\theta_{n,m}} - s_k \right) \right|^2$
    $\theta_{n,m+1} = \theta_{n,m} + \theta_{LMS,m}(e_m)$
    if $e_m < threshold$ **then**
      $threshold = e_m$
      $\theta_{opt,n} = \theta_{n,m}$
    end if
  end for
  $\theta_n = \theta_{opt,n}$
end for
return $\mathbf{x}_{opt} = \left(\sqrt{\frac{P_t}{N_t}} e^{j\theta_{1,opt}}, \cdots, \sqrt{\frac{P_t}{N_t}} e^{j\theta_{N_t,opt}} \right)$

After a certain number of subiterations, it has been observed that running the algorithm more times does not provide any substantial gain, thus M has been chosen experimentally to prevent this to happen. LMS-based approach is inexpensive computationally and easy to implement. However, it is possible to find methods with faster convergence speed, but it lacks of interest for the purpose of the Thesis.

The discrete-time model will be used to:

- Characterize the BER performance of the constant envelope precoder considering the effects of AWGN and multi-user interference (MUI) in the calculation.
- Characterize the MUI as a function of the number of transmit antennas and the number of co-scheduled users.
- Characterize the achievable beamforming gain for a fixed level of MUI.

3.2 Continuous-Time System Model

In the previous section, the discrete-time model has been described. With an eye to modeling the effects of the constant envelope precoding on the PAPR of the signal and on the power amplifier distortion, the continuous-time system model will be now introduced.

In order to generate the single carrier waveform, the precoder outputs will be followed by a root-raised-cosine (RRC) filter to perform pulse shaping, and by a nonlinear power amplifier. Due to the finite discrete implementation of the RRC filters, some intersymbol interference (ISI) will take place. On the other hand, feeding a power amplifier with a non-constant envelope signal will introduce in-band interference, effects that will have an impact on the system performance.

The continuous-time system scheme is shown in the figure below:

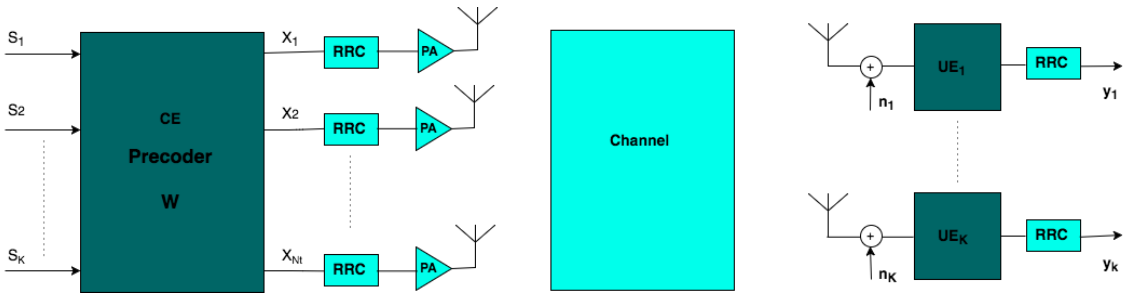

Figure 3.2: Continuous-time scheme

The continuous-time system model will be used for the following purposes:

- Characterization of the PAPR behavior of the constant envelope precoder after pulse shaping.
- Characterization of the BER performance of the constant envelope precoder considering the effects of AWGN, MUI, power amplifier distortion and the ISI introduced by the FIR RRC filters in the calculation.
- Characterization of the BER performance of the constant envelope precoder considering the effects of AWGN, MUI, ideal power amplifier and the ISI introduced by the FIR RRC filters in the calculation, with an eye to comparing the achievable BER when no-distortion takes place in the power amplifier.

In the following, we will detail the implementation of the RRC and PA blocks.

3.2.1 RRC filtering

Given a discrete symbol sequence s, the transmitter filter generates a continuous-time signal, process which has been traditionally known as pulse shaping. The filtered signal must meet some requirements regarding its time and frequency domains characteristics.

- The resulting waveform must be band-limited.
- The filter must be realizable.

- The ISI introduced by the filtering process should be as low as possible. Ideally zero ISI is achieved when Nyquist criterion is met.

However, there are practical limitations when approaching the design of the filter. In order to achieve the band-limited waveform, the best choice would be an ideal low-pass filter in frequency domain (no transition band). However, its impulse response is a sinc, which is non-casual and introduces infinite delay, it is not realizable and it is extremely difficult to approximate, in case it was attainable, it would present very strict synchronization demands. In practice, a trade-off among those requirements is achieved by the so-called root-raised-cosine filter. RRC filters are an implementation of a low-pass Nyquist filter, which means it is free of ISI, it provides a band-limited waveform whose excess bandwidth can be adjusted by the so-called roll-off factor, which defines the steepness of the transition band. Its frequency response is given by:

$$G(f) = \begin{cases} T & 0 \leq f < (1-\alpha)\,T/2 \\ \frac{T}{2}\left[1 - \sin\left(\frac{\pi T}{\alpha}\left(|f| - \frac{1}{2T}\right)\right)\right] & (1-\alpha)\,T/2 \leq f \leq (1+\alpha)\,T/2 \\ 0 & f > (1+\alpha)\,T/2 \end{cases} \tag{3.10}$$

where T denotes the sampling period.

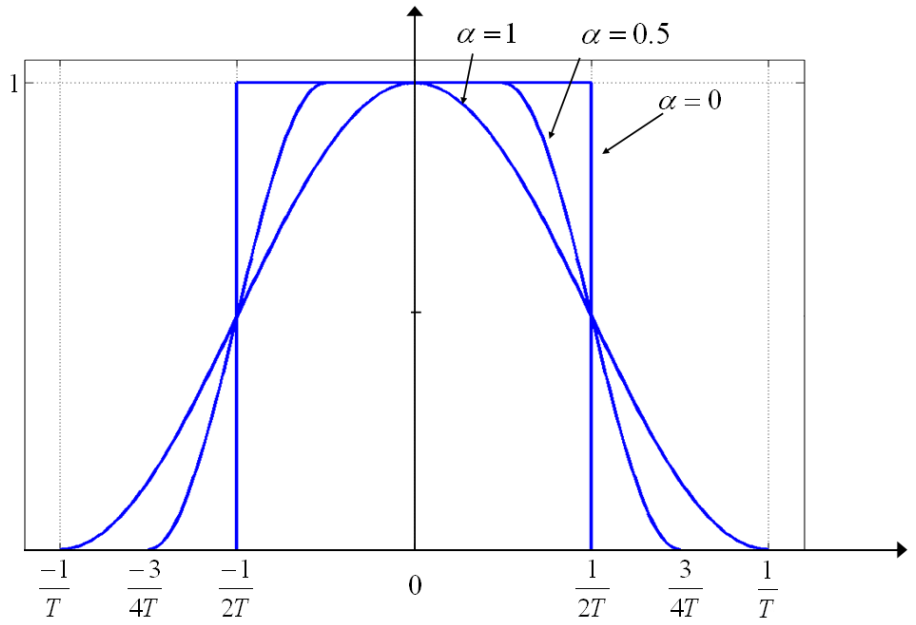

Figure 3.3: RRC frequency response [23]

On the other hand, the impulse response can be shown to be a sinc function of the form:

$$g(t) = \frac{sin(\pi t/T)}{\pi t/T}\frac{cos(\alpha\pi t/T)}{1-(2\alpha t/T)^2} \tag{3.11}$$

The role of the roll-off factor is crucial for the filter characteristics. The smaller the roll-off, the lower the excess bandwidth, the larger the PAPR and the smaller the attenuation of the stop band. In order to implement the RRC filter, a finite number of samples should be used, thus, the filter is no longer a fully RRC filter (only an approximation) and therefore, some ISI will take place. Trade-off between filter complexity and ISI.

Regarding the implementation, an eight symbols RRC filter with an 4x oversampling factor and a roll-off factor of 0.4 has been utilized for the simulations, hence, the filter order turns to be 32 + 1. The implemented filter can be seen in the figure below:

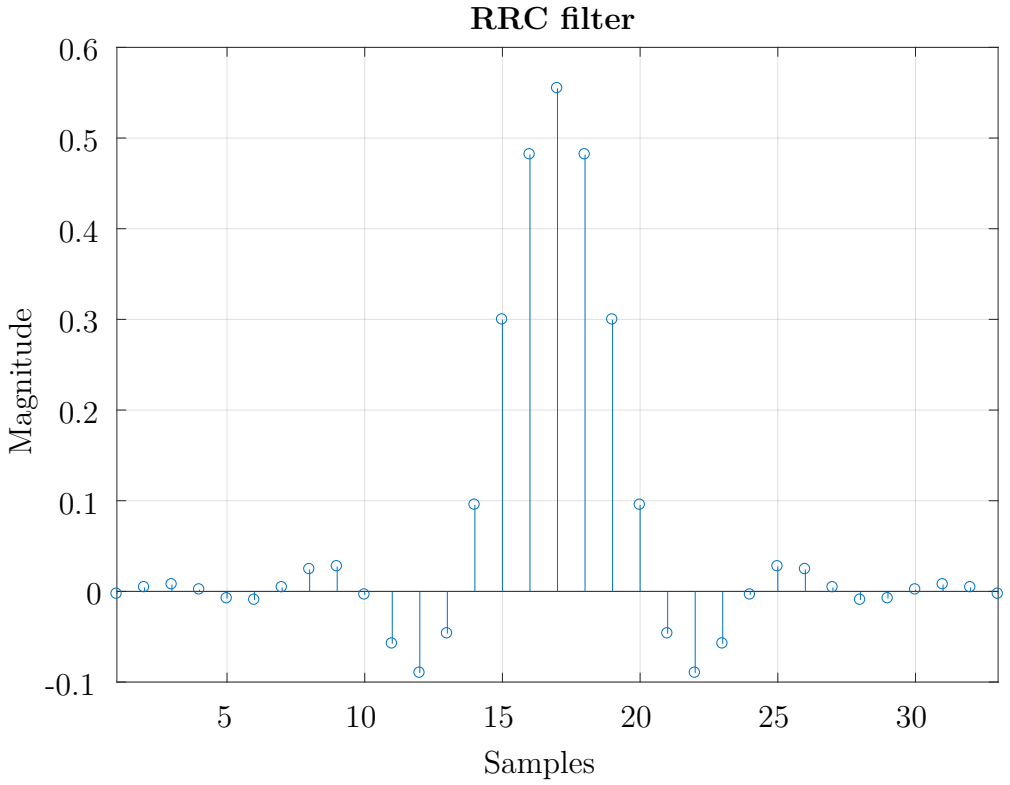

Figure 3.4: RRC filter with 0.4 roll-off factor and x4 oversampling

3.2.2 Nonlinear power amplifier

As it has been already mentioned in the previous chapter, nonlinear power amplifiers introduces in-band distortion and spectral regrowth. In the following, we will focus on the in-band distortion effect, since it is the one responsible for degrading the signal-to-interference ratio of the transmitted signal, and thus, the bit error rate, which is one of the performance indicators utilized for comparing ZF and CE precoders.

With the purpose of modeling the power amplifier transfer function, memoryless polynomial models have been utilized. Since the system to be modeled requires a large amount of antenna branches, and thus, the same number of power amplifiers, 100 power amplifier models have been used for the simulations.

The power amplifiers have been modeled by means of 9-th order polynomials of the following form:

$$y(t) = b_1 x(t) + b_3 x^3(t) + b_5 x^5(t) + b_7 x^7(t) + b_9 x^9(t) \tag{3.12}$$

whose baseband equivalent form is given by:

$$\begin{aligned} y(t) = b_{1_{BB}} x_{BB}(t) + b_{3_{BB}} x_{BB}(t) \left|x_{BB}(t)\right|^2 + b_{5_{BB}} x_{BB}(t) \left|x_{BB}(t)\right|^4 + \\ + b_{7_{BB}} x_{BB}(t) \left|x_{BB}(t)\right|^6 + b_{9_{BB}} x_{BB}(t) \left|x_{BB}(t)\right|^8 \end{aligned} \tag{3.13}$$

The utilized polynomial models behave expansively when pushed too harshly, this can be observed in the figure below.

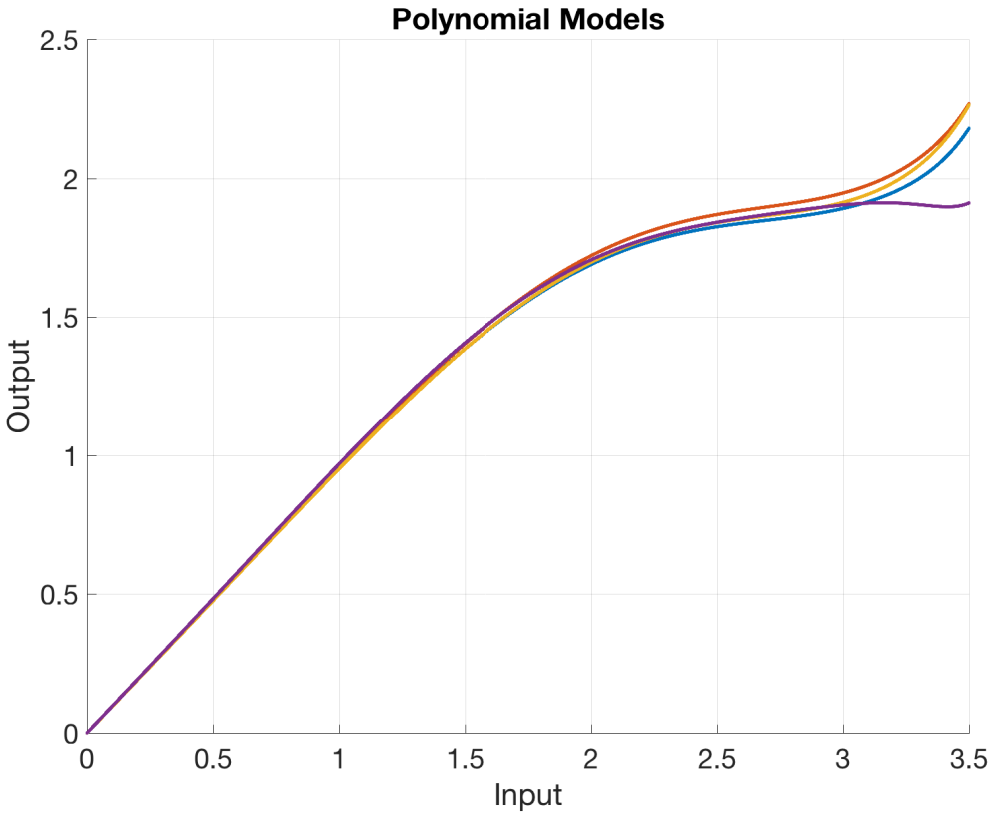

Figure 3.5: Power amplifier polynomial models

In practice, this phenomenon does not take place: power amplifiers present compressing nonlinearities (saturation behavior), so that, the polynomial models have been properly clipped allowing a certain degree of nonlinear compressing behavior as it can be seen in the figure below.

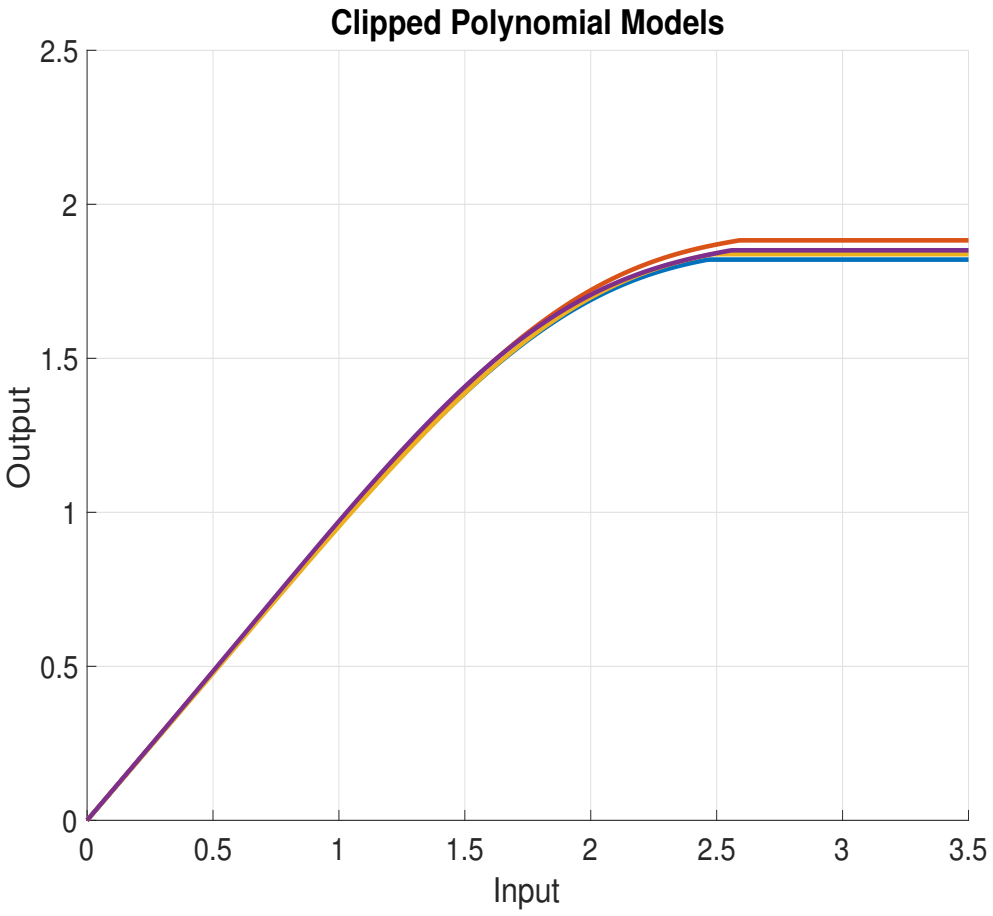

Figure 3.6: Clipped polynomial models

The reason behind utilizing a different power amplifier model for every antenna branch is to illustrate a more practical simulation, since in real systems all power amplifiers differ from one another.

With an eye to better understanding the power amplifier distortion effect on the BER performance, also ideal amplifier with unit linear gain (no distortion introduced) will be utilized.

3.3 Beamforming gain

Traditional MIMO precoders, such as ZF, provide beamforming gain when the number of transmit antennas increases (with a fixed number of co-scheduled users) [24]. This means that besides performing the spatial multiplexing processing, the total transmit power required to obtain a certain data rate is lower compared to the single antenna case. The actual achievable beamforming gain is linear dependent upon the number of antennas.

Constant envelope precoder also allows to achieve linear beamforming gain with increasing number of transmit antennas. However, in order to do so, a different approach needs to be considered. The strategy is basically the same than that for the cases explained above, however a new constraint needs to be fixed: the assumable global multi-user interference. By setting the multi-user interference constraint, the precoder will try to select the phase weights in such a way that the interference remains below that level, while providing beamforming gain. Since the phases are not specifically selected to minimize the multi-user interference, the minimum achievable interference will be lower than that of the non-beamforing case (the available number of degrees of freedom are utilized to meet both purposes). The system model follows the same principle than the one in section 3.1 with small modifications.

Let $\mathcal{S}$ denote the information alphabet, and $\hat{\mathbf{s}} = (s_1/\sqrt{\alpha}, s_2/\sqrt{\alpha}, \cdots, s_K/\sqrt{\alpha})^T$ denote the scaled vector of information symbols to be transmitted per time instant, where $s_k \in \mathcal{S}$ denotes the information symbol intended for the k-th user and α denotes the beamforming power gain.

Let $\mathbf{W}_{TX} \in \mathbf{C}^{N_t \times K}$ denote the precoding matrix:

$$\mathbf{W}_{TX} = \begin{pmatrix} w_{1,1} & w_{1,2} & \dots & w_{1,K} \\ w_{2,1} & w_{2,2} & \dots & w_{2,K} \\ \vdots & \vdots & \ddots & \vdots \\ w_{N_t,1} & w_{N_t,2} & \dots & w_{N_t,K} \end{pmatrix} \tag{3.14}$$

the precoded, denoted by $\mathbf{x} = (x_1, x_2, \cdots, x_{N_t})^T$, are obtained as follows:

$$\begin{aligned} \begin{pmatrix} x_1 \\ x_2 \\ \vdots \\ x_{N_t} \end{pmatrix} &= \begin{pmatrix} w_{1,1} & w_{1,2} & \dots & w_{1,K} \\ w_{2,1} & w_{2,2} & \dots & w_{2,K} \\ \vdots & \vdots & \ddots & \vdots \\ w_{N_t,1} & w_{N_t,2} & \dots & w_{N_t,K} \end{pmatrix} \begin{pmatrix} \hat{s}_1 \\ \hat{s}_2 \\ \vdots \\ \hat{s}_K \end{pmatrix} \\ &= \begin{pmatrix} w_{1,1} & w_{1,2} & \dots & w_{1,K} \\ w_{2,1} & w_{2,2} & \dots & w_{2,K} \\ \vdots & \vdots & \ddots & \vdots \\ w_{N_t,1} & w_{N_t,2} & \dots & w_{N_t,K} \end{pmatrix} \begin{pmatrix} s_1 \\ s_2 \\ \vdots \\ s_K \end{pmatrix} /\sqrt{\alpha} \end{aligned} \tag{3.15}$$

The amplitude of the signal in every antenna branch has been reduced $\sqrt{\alpha}$ times as a result of the beamforming processing. The precoder outputs x_n are of the form:

$$x_n = \sqrt{\frac{P_t}{\alpha N_t}} e^{j\theta_n} \quad , \quad n = 1, \cdots, N_t \tag{3.16}$$

and k-th user's received signal can be expressed as follows:

$$y_k = \sqrt{\frac{P_t}{\alpha N_t}} \sum_{n=1}^{Nt} h_{k,n} e^{j\theta_n} + n_k \ , \quad k = 1, \cdots, K \tag{3.17}$$

For the k-user to receive the unscaled symbol s_k, phase vector Θ must be chosen such that the multi-user interference with regards to the scaled information symbol is minimized:

$$mui = \sum_{k=1}^{K} \left| \left(\sqrt{\frac{P_t}{\alpha N_t}} \sum_{n=1}^{Nt} h_{k,n} e^{j\theta_n} - \sqrt{\alpha} s_k \right) \right|^2 \tag{3.18}$$

this way, the phase vector will try to produce information symbols of the form $\sqrt{\alpha} s_k$ at the receiver side, cancelling the $\sqrt{\alpha}$ amplitude scaling of every antenna branch. This is how the beamforming gain is achieved.

$$y_k = \sqrt{\frac{P_t}{\alpha N_t}} \sum_{n=1}^{Nt} h_{k,n} e^{j\theta_n} = \sqrt{\frac{P_t}{\alpha N_t}} \sqrt{\frac{\alpha N_t}{P_t}} s_k = s_k \tag{3.19}$$

The optimization problem can be stated in the following form:

$$\Theta = (\theta_1, \theta_2, \cdots, \theta_{N_t}) = \arg \min_{\theta_n \in [-\pi, \pi), n=1,\ldots,N_t} f(\Theta, \mathbf{s})$$

$$f(\Theta, \mathbf{s}) = \sum_{k=1}^{K} \left| \left(\sqrt{\frac{P_t}{\alpha N_t}} \sum_{n=1}^{Nt} h_{k,n} e^{j\theta_n} - \sqrt{\alpha} s_k \right) \right|^2$$

$$\begin{aligned} s.t. \qquad & ||\mathbf{x}||^2 = P_t/\alpha \\ & |x_n| = \sqrt{\frac{P_t}{\alpha N_t}} \\ & \sum_{k=1}^{K} \left| \left(\sqrt{\frac{P_t}{\alpha N_t}} \sum_{n=1}^{Nt} h_{k,n} e^{j\theta_n} - \sqrt{\alpha} s_k \right) \right|^2 \leq \beta \end{aligned} \tag{3.20}$$

where β denotes the maximum multi-user interference allowed in the system. It is very important to note that the algorithm is dependent upon the parameter α. The maximum achievable beamforming gain (α) depends on the antenna configuration as well as on the targeted β. This value of α is not known beforehand, therefore it needs to be calculated on the go or it can been stored in look-up tables or predefined curves,

The pseudocode of the beamforming adaptation process is detailed below:

Algorithm 2 LMS-based optimization for beamforming gain

$\mathbf{\Theta_1} = (0, 0, \cdots, 0)^T$
$\alpha = 1$
while $e_m(\alpha) < \beta$ **do**
  for $n = 1$ to N_t **do**
    for $m = 1$ to M **do**
      $e_m(\alpha) = \sum_{k=1}^{K} \left| \left(\sqrt{\frac{P_t}{\alpha N_t}} \sum_{n=1}^{Nt} h_{k,n} e^{j\theta_{n,m}} - \sqrt{\alpha} s_k \right) \right|^2$
      $\theta_{n,m+1} = \theta_{n,m} + \theta_{LMS,m}(e_m(\alpha))$
      if $e_m < threshold$ **and** $\leq \beta$ **then**
        $threshold = e_m(\alpha)$
        $\theta_{opt,n} = \theta_{n,m}$
      end if
    end for
    $\theta_n = \theta_{opt,n}$
  end for
  $\alpha = \alpha + stepsize$
end while
return $\mathbf{x}_{opt} = \left(\sqrt{\frac{P_t}{N_t}} e^{j\theta_{1,opt}}, \cdots, \sqrt{\frac{P_t}{N_t}} e^{j\theta_{N_t,opt}} \right)$

One always desires to provide the maximum achievable beamforming gain for a given value of β. However, this is an unknown value that depends on the antenna configuration and on the desired multi-user interference cancellation. α is obtained by a searching procedure. The algorithm is run repeatedly for increasing values of α, the higher the value of the parameter *stepsize*, the faster the solution is achieved, however, the error is higher. The algorithm runs until the highest value of α that allows to meet all the constraints is found. The maximum achievable gain α for a certain configuration could be stored in a look-up table or in predefined curves to speed-up the process.

3.4 Comparing zero-forcing and constant envelope precoders

For the sake of a better understanding of the performance of the constant envelope precoder, the same continuous-time and discrete-time schemes have been implemented with a zero forcing precoder.

Zero forcing precoder mitigates the multi-user interference with ideal channel state information, so no MUI will take place, however, due to the characteristics of the ZF precoded waveform, more severe power amplifier distortion will occur for a given

mean transmit power when compared to that of the constant envelope precoded signal.

In order to properly compare both transmission schemes, some facts need to be carefully considered.

- Both precoders must have the same total transmit power.
- SINR at the receiver side must be calculated in a proper manner.
- Power amplifier input signal must lay on the model range.

On the normalization of the output sum-power

In order to perform a fair comparison of both precoders, the total transmitted power must be the same in both cases. This is of course a trivial consideration, however, it is not that simple since both precoders provide different beamforming gains, and thus, the total radiated power may vary from one to another. In order to ensure the same total radiated power we will proceed as follows:

Let us assume a precoding model as the ones we have been utilizing so far: $\mathbf{x} = \mathbf{W}_{TX}\mathbf{s}$, where $\mathbf{x}$ is the precoder output signal, $\mathbf{W}_{TX}$ is the precoding matrix and $\mathbf{s}$ is the data vector. In order to guarantee the same total radiated power, we will fix the output-sum-power, or what it is the same, the trace of the covariance of $\mathbf{x}$:

$$cov(\mathbf{x}) = \mathbb{E}\left\{\mathbf{x}\mathbf{x}^H\right\} = \mathbf{W}_{TX}\mathbb{E}\left\{\mathbf{s}\mathbf{s}^H\right\}\mathbf{W}_{TX}^H = \sigma^2\mathbf{W}_{TX}\mathbf{W}_{TX}^H \tag{3.21}$$

where it has been assumed that the data streams are independent from one another and have a power of σ^2. Thus, the total output power is given by:

$$\mathbb{E}\left\{||\mathbf{x}||^2\right\} = trace\left\{cov(\mathbf{x})\right\} = \sigma^2 trace\left\{\mathbf{W}_{TX}\mathbf{W}_{TX}^H\right\} \tag{3.22}$$

Since the data streams of both precoders will be the same, if one wants to get the same output sum-power, he or she would need to normalize the trace of $\mathbf{W}_{TX}\mathbf{W}_{TX}^H$:

$$\begin{aligned} \alpha^2 trace\left\{\mathbf{W}_{TX}\mathbf{W}_{TX}^H\right\} &= 1 \\ \rightarrow \alpha &= \frac{1}{\sqrt{trace\left\{\mathbf{W}_{TX}\mathbf{W}_{TX}^H\right\}}} \end{aligned} \tag{3.23}$$

α is a normalization factor which basically represents the beamforming gain. The normalized precoder output would eventually be:

$$\mathbf{x} = \alpha\mathbf{W}_{TX}\mathbf{s} \tag{3.24}$$

Note that with the approach stated above, one ensures the mean sum-output power to be the same, but not the instantaneous sum-power. It is also important to have in

mind that the individual antenna powers run arbitrarily. In the case of the constant envelope precoder, the instantaneous antenna power is the same in every antenna branch and at every time instant, however this does not occur with the zero-forcing precoder, the mean power output power will be normalized, however the amplitude variations at the individual antenna branches can be huge. This will constitute a drawback for the zero-forcing precoder as it will be shown further below.

On the estimation of the SINR

Bit error rate curves are typically represented as a function of the SINR. Due to the effect of the power amplifier distortion, it turns to be a difficult task, because not all the transmit power transforms into *useful power* but also into nonlinear distortion, therefore, the received SINR must be properly estimated for both schemes. The interference of each precoder has different sources, for the constant envelope precoder the sources of interference are:

- Multi-user interference.
- Power amplifier distortion.
- ISI due to FIR filtering.
- AWGN.

on the other hand, for the zero-forcing precoder we only have:

- Power amplifier distortion.
- ISI due to FIR filtering.
- AWGN.

recall that zero-forcing precoder is capable of completely eliminating the multi-user interference since perfect CSI knowledge is assumed. However, due to the PAPR characteristics of ZF waveform, it is expected to be more harmfully affected by the power amplifier nonlinearities.

Note that the estimation of the SINR is also tightly ligated to the normalization of the output sum-power, so both of them need to be properly calculated, otherwise the comparison will be meaningless. Due to the precoders have different beamforming gains, different transmit powers could lead to same received SINR, thus, to carry out a fair comparison, both precoders must utilize the same transmit power.

In order to estimate the SINR at the receiver side, we will follow a least-squares-based approach, under the following assumptions: all interference sources are Gaussian distributed and uncorrelated with the desired signal and with one another.

Let $\hat{n}$ denote all sources of interference, thus: $\mathbb{E}\{|\hat{n}|^2\} = \sigma^2_{noise} + \sigma^2_{MUI} + \sigma^2_{distortion} + \sigma^2_{ISI}$. Let y denote the received signal at the k-th user, the channel vector will be denoted by $\mathbf{h}$, while the precoded data symbols are represented by $\mathbf{x} = (x_1, \cdots, x_{N_t})$ (note that $\mathbf{x}$ is free of interference). The system model is as follows:

$$y = \mathbf{h}^T\mathbf{x} + \hat{n} \tag{3.25}$$

we will assume that there exists a linear transformation $\mathbf{y}_{LS} = \mathbf{A}\mathbf{h}_{LS}$ such that it minimizes the following cost function:

$$||\mathbf{A}\mathbf{h}_{LS} - \mathbf{y}||^2 \tag{3.26}$$

where $\mathbf{A}$ is the precoded symbols matrix and $\mathbf{y}$ denotes the vector containing the set of samples of the desired signal . The solution is given by the orthogonality principle:

$$\mathbf{h_{LS}} = \left(\mathbf{A}^H\mathbf{A}\right)^{-1}\mathbf{A}^H\mathbf{y} \tag{3.27}$$

therefore, $\hat{n}$ can be estimated in the following way:

$$\hat{n} = y - \mathbf{h}^T_{LS}\mathbf{x} \tag{3.28}$$

and finally, the SINR can be calculated as:

$$\widehat{SINR} = \frac{|\mathbf{h}^T_{LS}\mathbf{x}|^2}{|\hat{n}|^2} \tag{3.29}$$

Chapter 4

Evaluation Environment and Obtained Results

In this chapter, the results obtained for the zero-forcing and constant envelope precoders will be detailed. Simulations have been carried out with MATLAB_R2016b. The results will be presented in the following order:

- PAPR behavior.
- CE precoder multi-user interference as a function of the number of antennas and co-scheduled users.
- Bit error rate for multi-user interference limited scenarios.
- CE and ZF beamforming gains.
- CE and ZF bit error rate performances for the continuous-time model implementation.

4.1 PAPR Behavior

The peak-to-average power ratio results will be used to measure the sensitivity of the generated waveform to the power amplifier nonlinearities, and to predict the behavior of the system when the power amplifier is included in the simulations. The PAPR, as it has been explained, is defined as the ratio between the peak power and the average power of the given waveform over a certain observation period. The higher the PAPR, the more likely it will be for the signal amplitude to range out of the linear zone, and therefore, to occur nonlinear distortion.

The setup for this simulation is as follows:

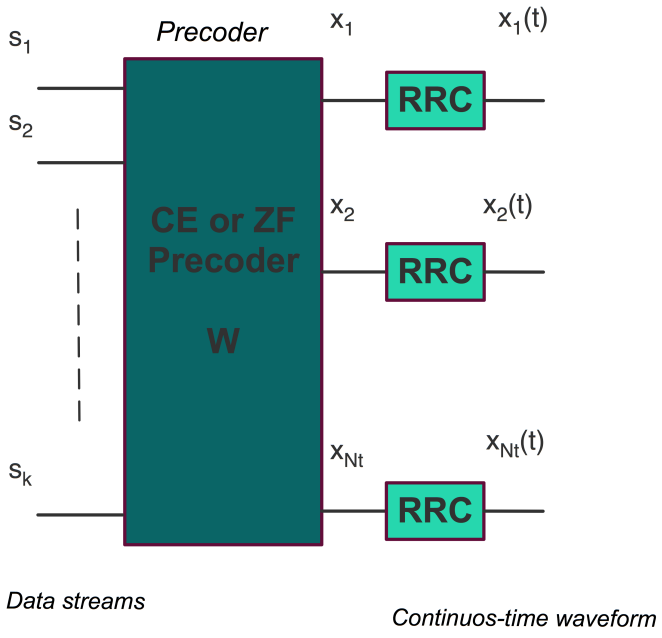

Figure 4.1: PAPR simulation setup

For the constant envelope precoder, the coded symbols $\mathbf{x}$ are of the form $x_n = \sqrt{\frac{P_t}{N_t}}e^{j\theta_n}$ which results in a PAPR of 0 dB, however due to the effect of the RRC filtering, the resulting continuos-time waveform will not have constant envelope anymore. The PAPR of the symbols constellation has no effect on the resulting PAPR, since, regardless of the used constellation, the precoder will always generate symbols of the form $x_n = \sqrt{\frac{P_t}{N_t}}e^{j\theta_n}$.

In the case of zero-forcing precoder, the resulting PAPR depends on the RRC filtering as well as on the PAPR of the symbols constelation, for the simulations, the information bits have been mapped to 16-QAM symbols. Furthermore, since the precoder inverts the channel response, in every antenna branch and in every time instant, a different weight will be applied, which really deteriorates the PAPR of the resulting waveform.

The PAPR results for the constant envelope and zero-forcing precoders are shown in the figures below. The simulation setup is as follows:

- Number of transmit antennas: 24
- Number of simultaneously scheduled users: 4
- Roll-off factor: 0.4
- Modulation: QPSK, 16-QAM and 64-QAM

- Baseband signals, for the RF-modulated signal the PAPR is 3 dB higher.

With an eye to seeing how the precoder influences the resulting waveform PAPR, the PAPR distribution of RRC filtered information symbols is shown below:

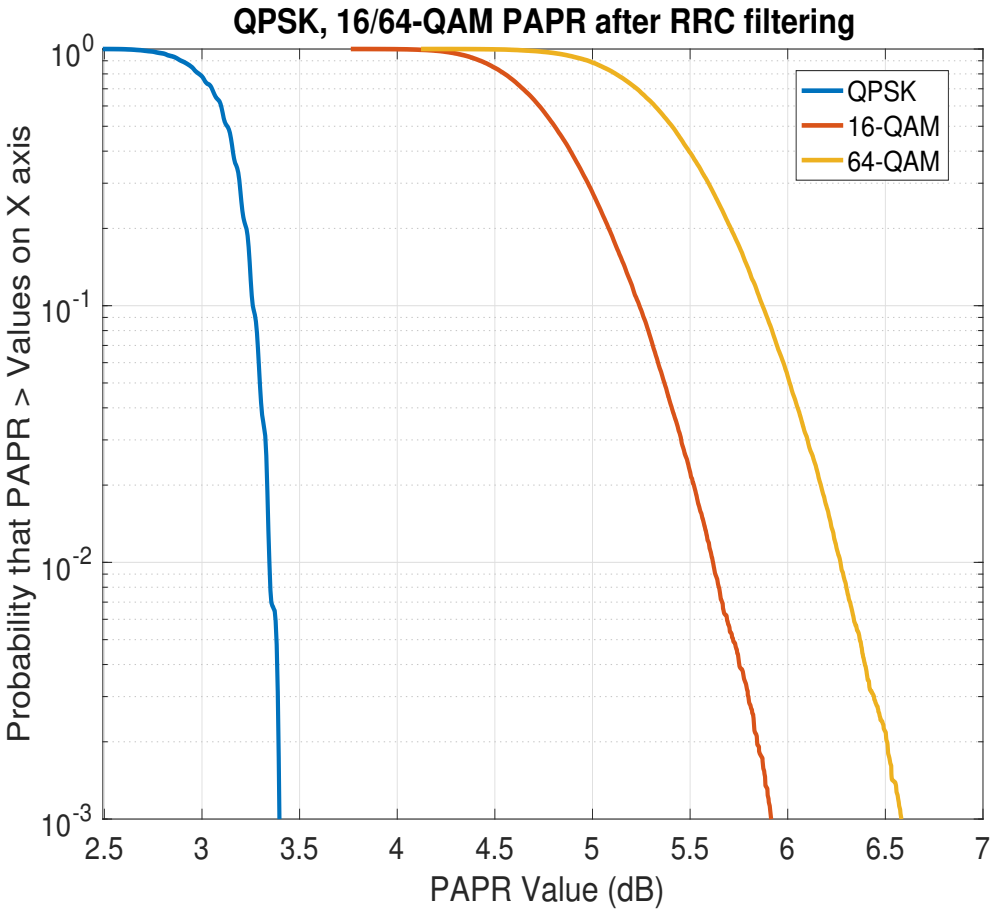

Figure 4.2: PAPR of the information symbols after RRC filtering

As it can be observed in the figure above, the modulation order affects the PAPR of the resulting waveform: the higher the PAPR of the used constellation, the higher the PAPR of the waveform. 16-QAM modulation has been utilized in the results shown further below.

Zero-Forcing PAPR

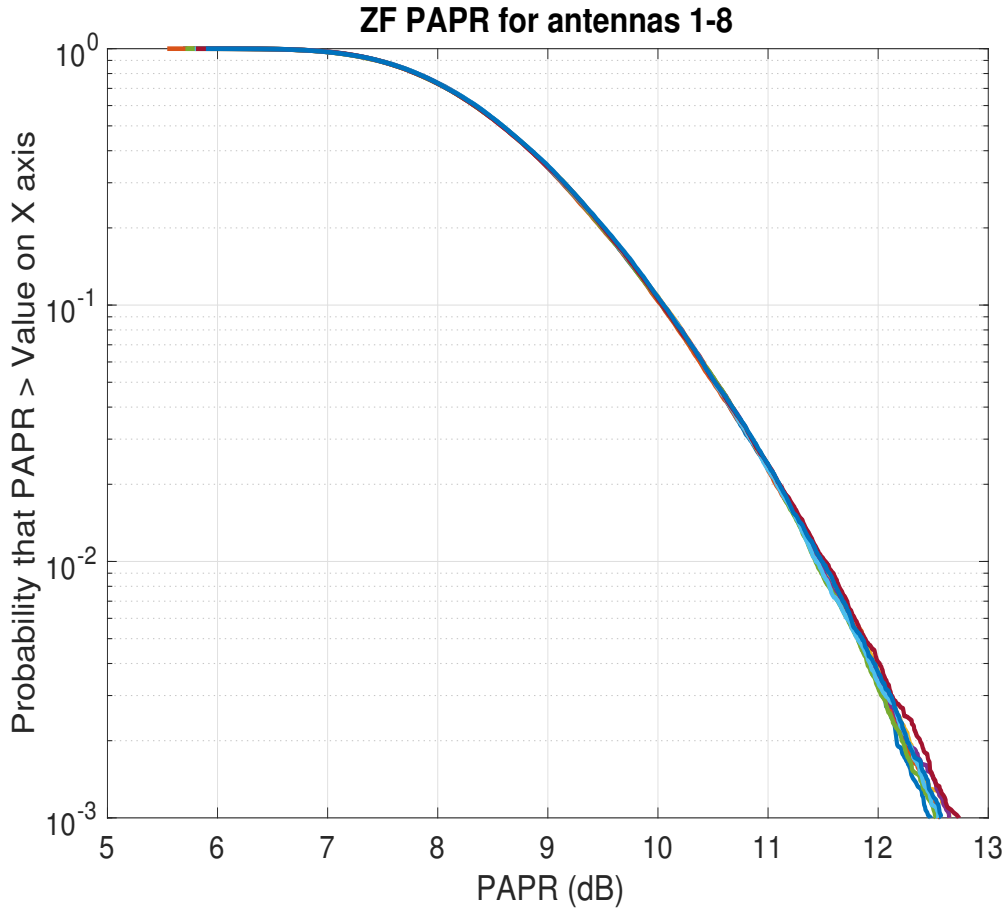

Figure 4.3: ZF PAPR (16-QAM)

The resulting PAPR for the zero-forcing precoder turns to be really large, being able to rise up to a value of 13 dB with a probability of 10^{-3}. Note that in every antenna branch the PAPR behavior is basically the same. In order to avoid harmful distortion, a sufficiently big back-off needs to be applied, which would lead to a very inefficient power utilization. This is the main drawback of utilizing the zero-forcing approach as precoder. With perfect channel state information, the spatial precoding allows to completely remove the multi-user interference without enhancing the noise level as it may happen when zero-forcing is used as spatial filter at the receiver side. However, the variations on the signal amplitude are huge, fact that leads to a very inefficient use of the power amplifier if a certain linear operation wants to be ensured. By using equation (2.42), the resulting energy efficiency if the results shown in Figure (4.3) are considered is:

$$\eta = \frac{0.5}{10^{(12.5+3)/10}} = 0.014 = 1.4\% \tag{4.1}$$

where it has been assumed that the power amplifier input is RF-modulated, therefore, its PAPR is 3 dB higher than the baseband waveform. The resulting energy

efficiency is extremely low, roughly 1%, in practice, PAPR reduction techniques together with DPD, allow to significantly improve power amplifier efficiency.

The constellation order also affects the resulting PAPR for the zero-forcing precoded signal, as it can be observed in the Figure (4.4) below.

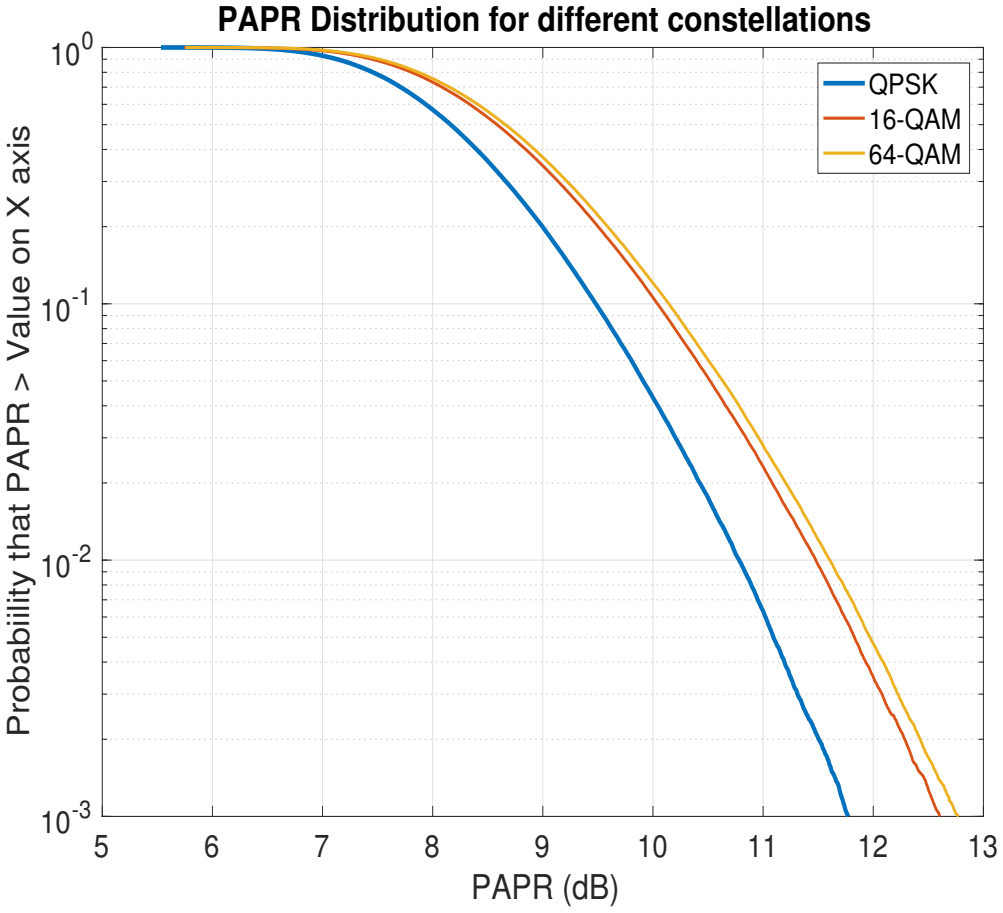

Figure 4.4: ZF PAPR for different constellations

The curves in Figure (4.4) represent the PAPR distribution resulting after averaging the PAPR distributions of the 8 antennas in Figure (4.3). The PAPR depends on the modulation order, although not very significantly, the PAPR is mainly dictated by the effect of the precoder.

CE precoder PAPR

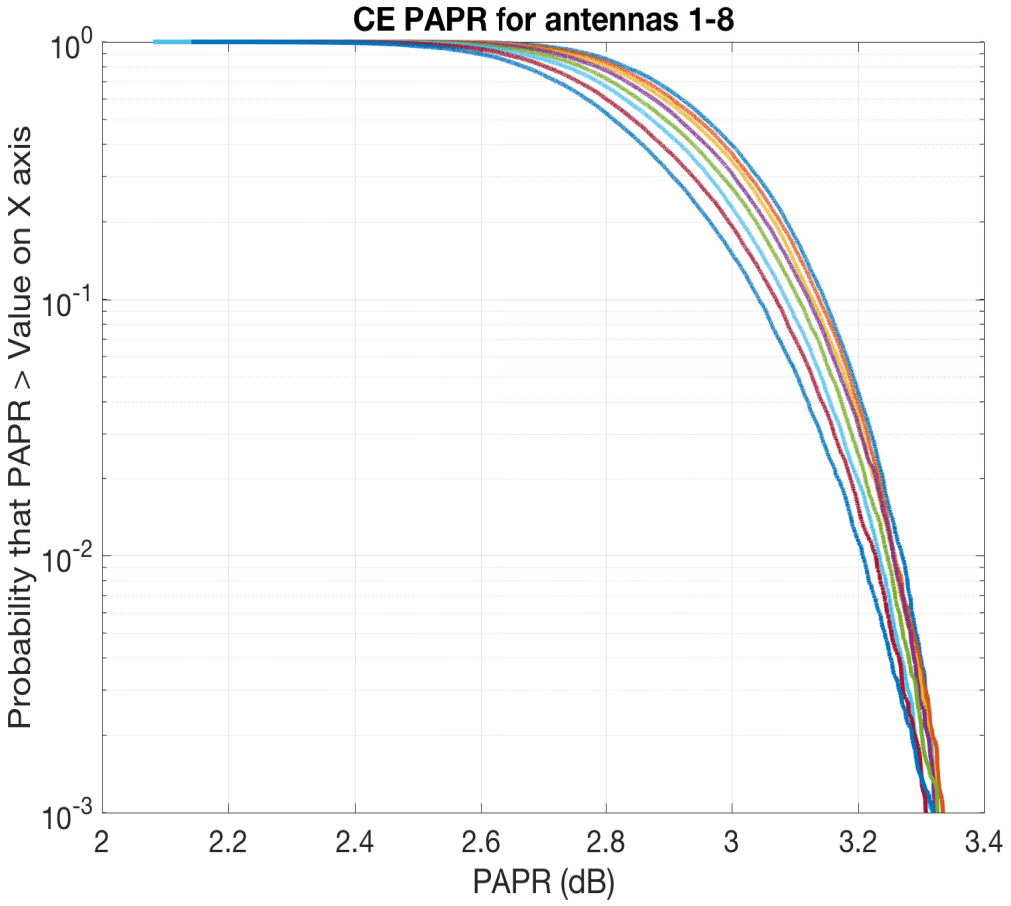

Figure 4.5: CE PAPR

The resulting PAPR distribution for the constant envelope precoder is limited to a very small range: from 2.6 to nearly 3.4 dB. The improvement with regards to the uncoded information symbols as well as to the zero-forcing precoded symbols is very significant. The constant envelope precoder allows to perform spatial precoding while reducing the PAPR of the resulting waveform. This will enable the utilization of spatial precoders while ensuring a better power utilization of PA, which simultaneously addresses the need of higher data rates and energy efficiency. The resulting energy efficiency for the constant envelope case shown in Figure (4.5) is:

$$\eta = \frac{0.5}{10^{(3.3+3)/10}} = 0.11 = 11\% \tag{4.2}$$

thus, the energy efficiency is 8 times higher than that of the zero-forcing precoder, which is a significant improve. In the figure below, the PAPR distributions of both precoders are jointly shown.

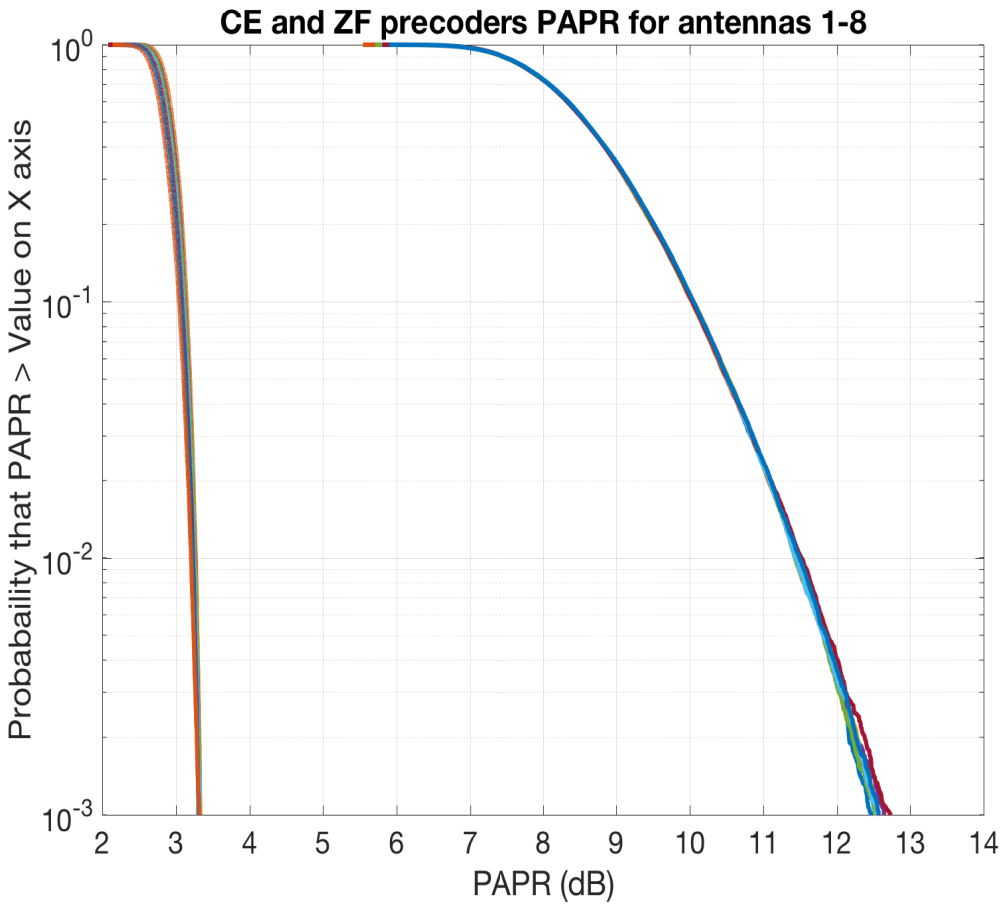

Figure 4.6: CE and ZF PAPR

4.2 Multi-user Interference for Constant Envelope Precoder

In the following, we will show how the maximum achievable signal-to-interference ratio, when only multi-user interference is taken into account, is dependent on the number of transmit antennas and number of co-scheduled users.

Intuitively, one can expect that as the ratio N_t/K increases, a better interference cancellation can be achieved due to the extra degrees of freedom available, which in fact happens. In the next figures, it will be shown how the multi-user interference reduces with increasing number of transmit antennas and fixed number of users. For evaluating the multi-user interference, the discrete-time system model of Figure (3.1) will be used, thus, the interference term $\hat{n}_k$ will only take into account the effect of the multi-user interference (considering a noise-free received signal). The algorithm for the simulation follows the same approach that algorithm 1, which is run repeatedly for different antenna configurations, and then, the power of the

per-user multi-user interference is calculated for each configuration in the following manner:

$$|mui_k|^2 = \left| \sqrt{\frac{P_t}{N_t}} \sum_{n=1}^{Nt} h_{k,n} e^{j\theta_n} - s_k \right|^2 \tag{4.3}$$

in the figures below, only the multi-user interference power for the k-th user will be represented due to it is equal for every user.

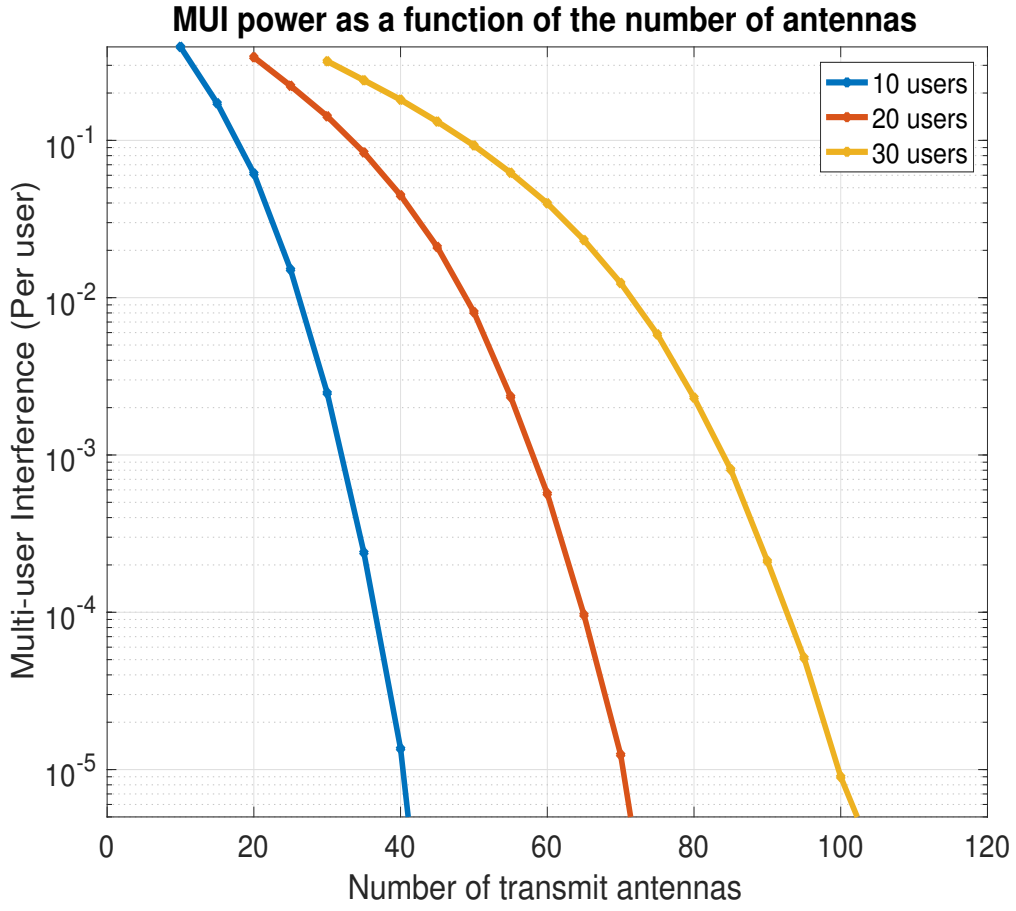

Figure 4.7: Multi-user interference power

As it was expected, the multi-user interference decreases with increasing number of antennas and decreases for increasing number of users. From Figure 4.7 it can be observed that:

- For a N_t/K ratio ranging from 1 to 2, the improvement in the MUI is basically linear.
- For a N_t/K ratio above 2, the improvement becomes exponential.

a N_t/K ratio of 4 is sufficiently large to make multi-user interference nearly negligible, since link capacity will be most likely noise-limited. Thus, a reasonable amount of antennas would need to be deployed in order to ensure good performance. The

amount of antennas allocated to a set of users could be optimized based on channel state information reports, e.g., allocating the minimum amount of antennas such that the multi-user interference would not deteriorate system performance, although extra antennas would be able to provide beamforming gain if needed.

The multi-user interference can be made arbitrarily small when the ratio N_t/K is sufficiently large as it can be shown in the figure below:

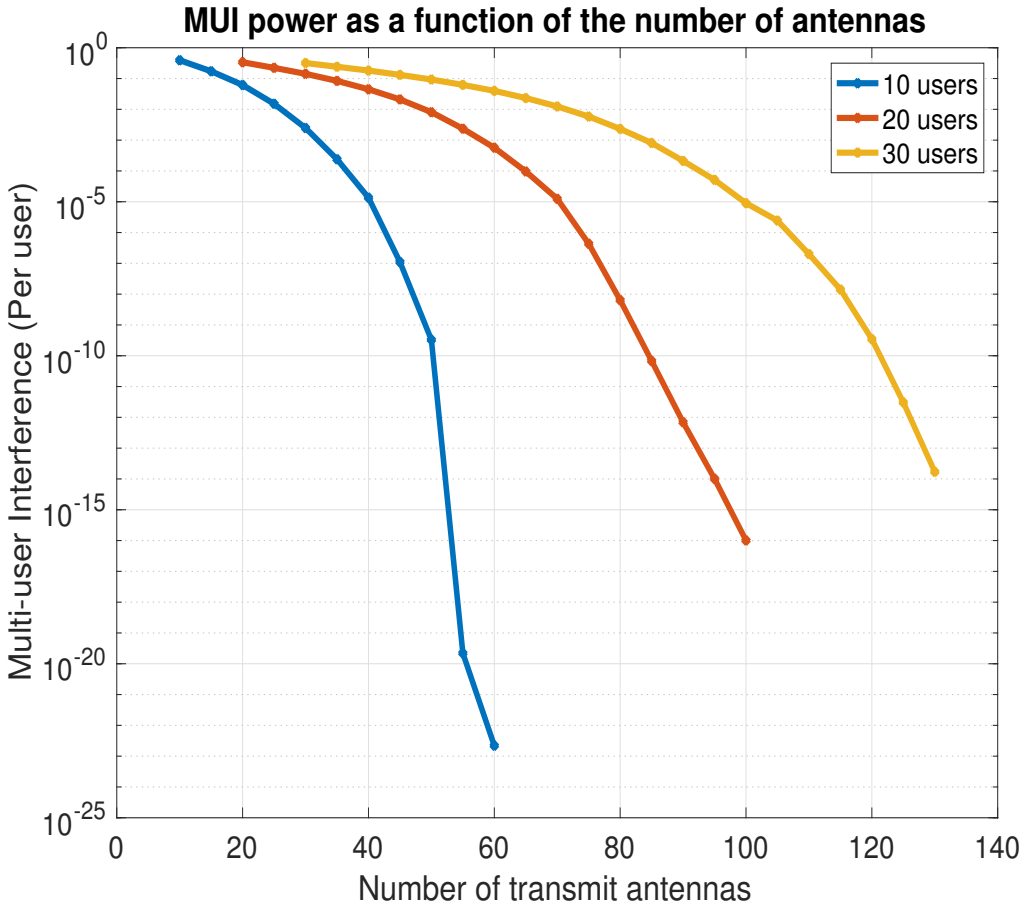

Figure 4.8: MUI power with large N_t/K ratio

For a certain antenna configuration, it is possible to calculate the k-th user signal-to-interference ratio due to the effect of MUI in the following way.

$$SIR_k = \frac{\mathbb{E}\{||\mathbf{x}||^2\}}{\mathbb{E}\{||\mathbf{mui}_k||^2\}} \tag{4.4}$$

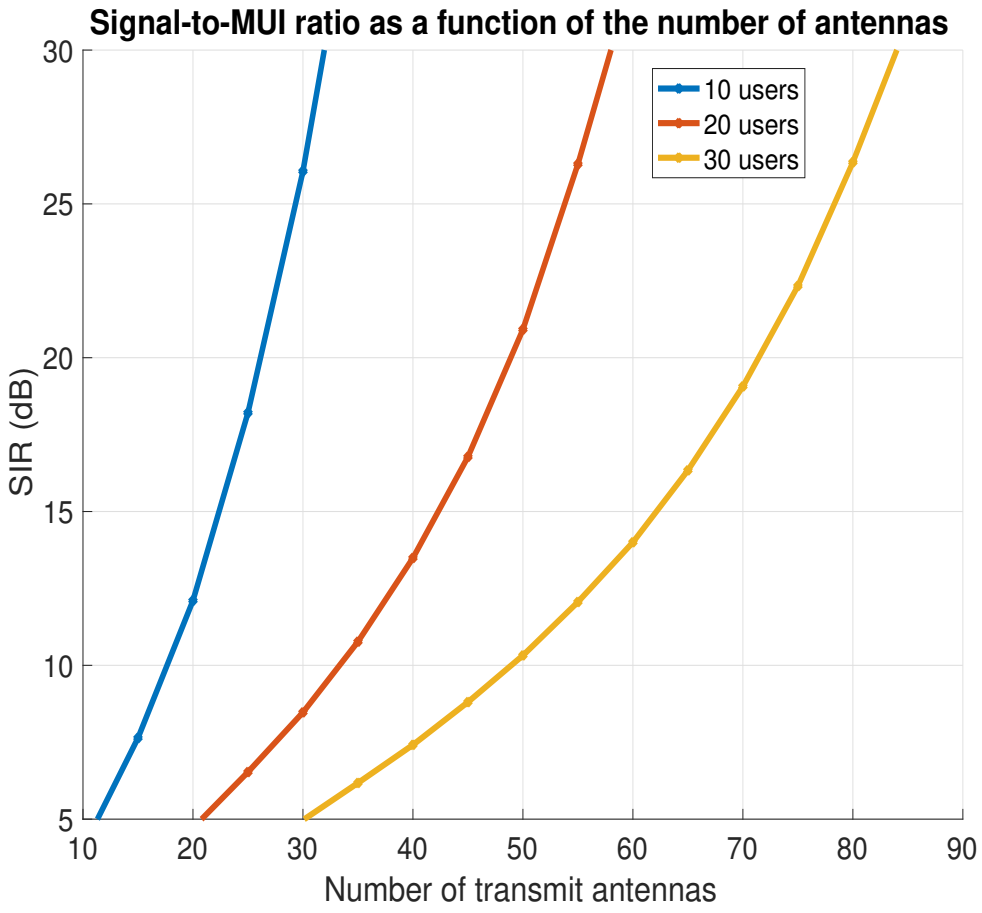

Figure 4.9: Signal-to-MUI power ratio

In the tables below, some values of interest of the signal-to-multi-user interference for a given N_t/K ratio are shown:

Tabla 4.1: Achievable SIR for $K = 10$

K = 10				
N_t/K	**1**	**2**	**3**	**4**
SIR (dB)	3.99	12.1	26.06	48.67

Tabla 4.2: Achievable SIR for $K = 20$

K = 20				
N_t/K	**1**	**2**	**3**	**4**
SIR (dB)	4.7	13.49	32.46	81.94

Tabla 4.3: Achievable SIR for $K = 30$

K = 30				
$\mathbf{N_t/K}$	**1**	**2**	**3**	**4**
SIR (dB)	5	14	36.75	94.59

We can conclude that utilizing 1 antenna per user is insufficient to provide good performance since noise level is most of the times way below those values. Utilizing 2 antennas per user would be sufficient for many scenarios, while using between 3 and 4 antennas per user would ensure an interference level below noise floor. It can also be observed that same N_t/K ratios, for different antenna configurations, do not provide the same interference cancellation. Although, the ratio is the same, more degrees of freedom $(N_t - K)$ are available for increasing number of users. For a N_t/K ratio of 4, for the 10 users configuration we have $40 - 10 = 30$ degrees of freedom, while for the 30 users configuration we have $120 - 30 = 90$, which is significantly higher.

4.3 Beamforming Gain

With increasing number of antennas, the required transmit power to obtain a certain capacity decreases linearly proportional to the number of antennas. This is known as beamforming gain. In this section, the beamforming gains of both precoders are compared. To calculate the beamforming gain of zero-forcing precoder, the method explained in section 3.4 has been utilized, on the other hand, to calculate the beamforming gain for the constant envelope precoder, a searching procedure based on algorithm 2 has been used.

Constant Envelope Precoder Beamforming Gain

In order to obtain a certain spectral efficiency, the required transmit power of traditional precoders such as zero-forcing or maximum ratio transmission can be scaled down linearly proportional to the number of antennas. In the figures below, it will be shown how this fact also takes places in the case of constant envelope precoder. However, as it was previously commentated in section (3.3), the maximum achievable gain also depends on the targeted multi-user interference. In the following figures, its dependency upon the number of antennas and the targeted MUI will be shown.

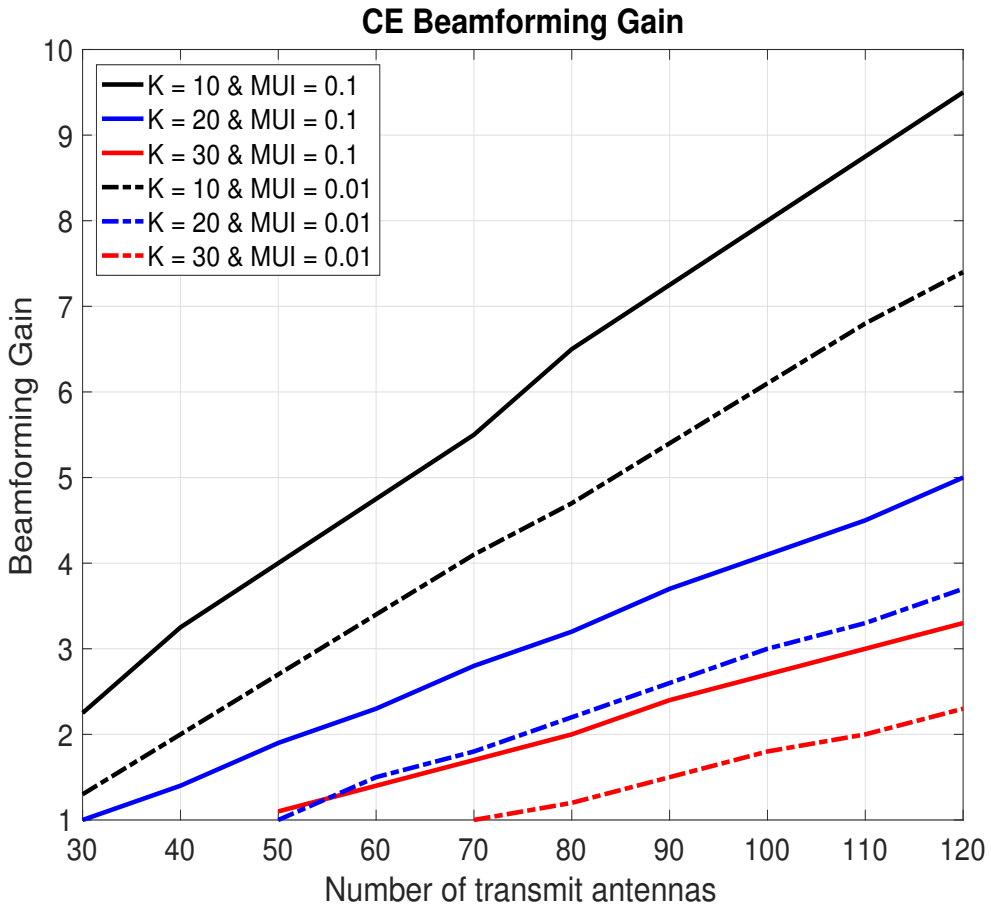

Figure 4.10: CE beamforming gain in linear units

As it can be observed, the beamforming gain is linear dependent upon the number of transmit antennas as well as traditional precoders. Depending on the targeted multi-user interference, different beamforming gains can be achieved. It can be seen that the stricter the multi-user interference constraint is, the lower beamforming gain can be provided (for a fixed K), this fact takes place since the available degrees of freedom are utilized to find the phase vector that simultaneously meets the MUI constraint while scaling the information symbols. In the next figure, the beamforming gain is expressed in logarithmic units:

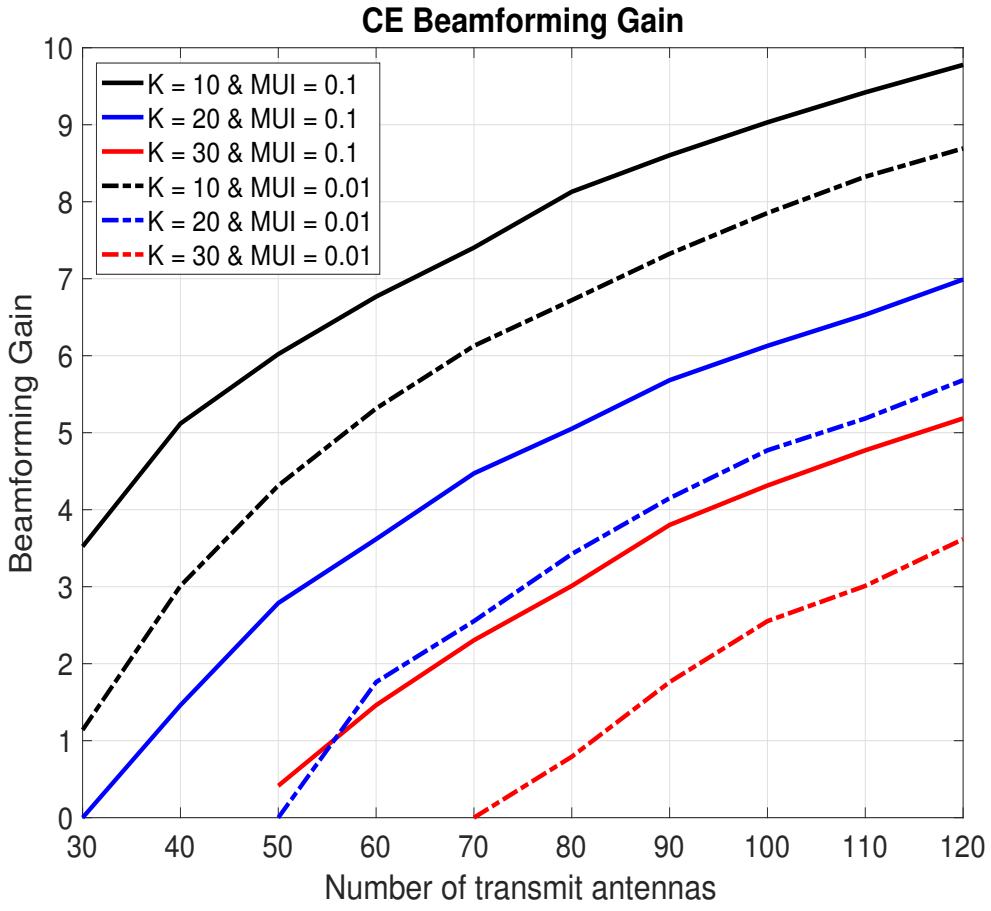

Figure 4.11: CE beamforming gain (dB)

In the tables below some values of interest are indicated:

Tabla 4.4: CE beamforming gain for K=10 and MUI = 0.1

K = 10 and MUI = 0.1						
N_t/K	**3**	**4**	**5**	**6**	**9**	**12**
Beamforming gain (dB)	3.5	5.12	6.02	6.76	8.6	9.78

Tabla 4.5: CE beamforming gain for K=10 and MUI = 0.01

K = 10 and MUI = 0.01						
N_t/K	**3**	**4**	**5**	**6**	**9**	**12**
Beamforming gain (dB)	1.14	3.01	4.31	5.32	7.32	8.69

Tabla 4.6: CE beamforming gain for K=20 and MUI = 0.1

K = 20 and MUI = 0.1				
N_t/K	**3**	**4**	**5**	**6**
Beamforming gain (dB)	3.62	5.05	6.13	6.99

Tabla 4.7: CE beamforming gain for K=20 and MUI = 0.01

K = 20 and MUI = 0.01				
N_t/K	**3**	**4**	**5**	**6**
Beamforming gain (dB)	1.77	3.424	4.77	5.68

Tabla 4.8: CE beamforming gain for K=30 and MUI = 0.1

K = 30 and MUI = 0.1			
N_t/K	**2**	**3**	**4**
Beamforming gain (dB)	1.46	3.80	5.18

Tabla 4.9: CE beamforming gain for K=30 and MUI = 0.01

K = 30 and MUI = 0.01			
N_t/K	**2**	**3**	**4**
Beamforming gain (dB)	0	1.76	3.62

By setting up a 10 dB more restrictive MUI constraint, the beamforming gain drops around 2 dB for the lowest N_t/K ratio, however, when the number of degrees of freedom increases, this difference reduces. For a better understanding, it is interesting to take a look to the beamforming gain in Figure (4.11) together with Figure (4.9). Since the signal power is constrained to be unit, the MUI values map into SIR as: $SIR = -MUI$ (in dB units). For example, for $K = 10$, in order to get 10 dB of SIR, it is necessary to utilize at least 18 antennas, on the other hand, to achieve 20 dB of SIR, 27 antennas are needed, which means that 9 more antennas are required. For increasing number of antennas, the number of degrees of freedom available for beamforming is nearly the same for $MUI = 0.1$ and $MUI = 0.01$, that is why the the beamforming gain for both constraints tend to converge to the same value. On the other hand, for the configuration $MUI = 0.01$ & $K = 30$, in order to achieve a SIR of 20 dB it is required to have at least 72 antennas, that is why, for a N_t/K ratio of 2 (60 antennas), no beamforming gain (0 dB) can be provided.

Zero Forcing Precoder Beamforming Gain

This time, the beamforming gains of the zero-forcing precoder (for the same users/antenna configuration than that of CE precoder) are shown.

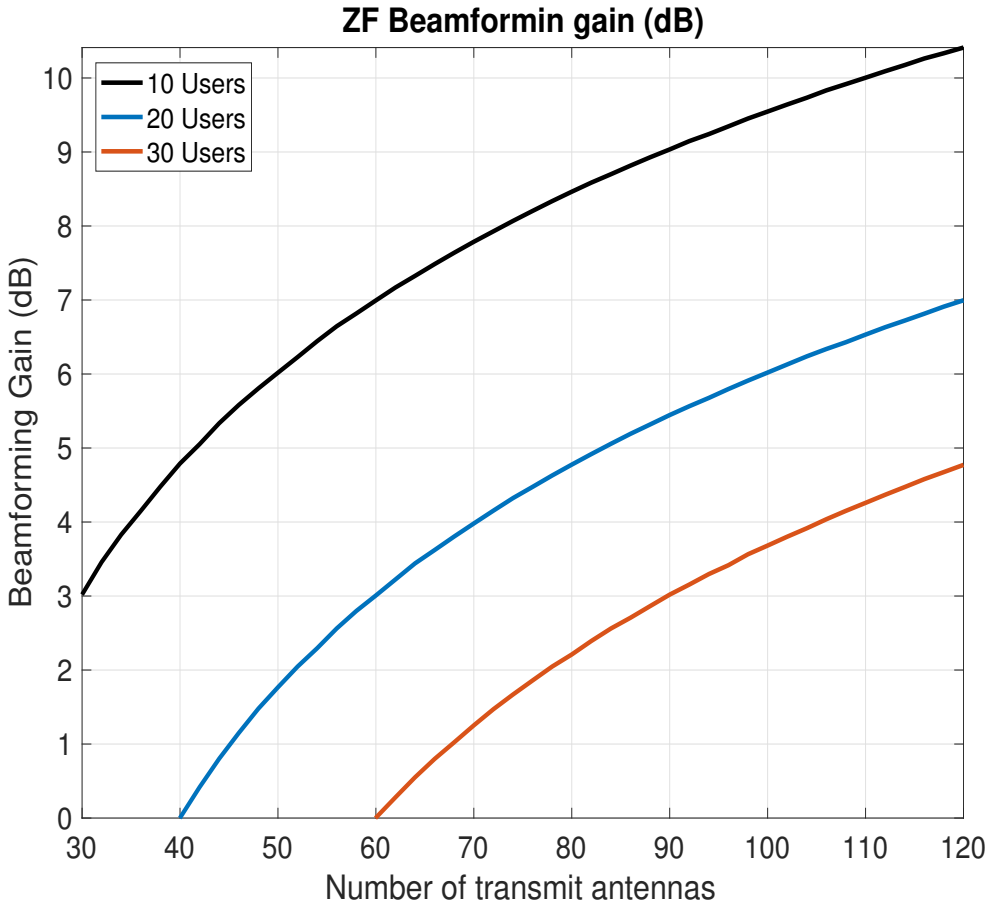

Figure 4.12: ZF beamforming gain (dB)

The zero forcing precoder is obtained as the pseudoinverse of the channel matrix, whose coefficients are independent samples of zero-mean and unit-variance Gaussian distributions, thus, when the number of transmit antennas goes to infinity while the number of receive antennas is constant, the row vectors of $\mathbf{H}$ are asymptotically orthogonal, and hence we have:

$$\frac{\mathbf{H}\mathbf{H}^{\mathbf{H}}}{N_t} \approx \mathbf{I}_{Nr} \tag{4.5}$$

when computing $\left(\mathbf{H}\mathbf{H}^{\mathbf{H}}\right)^{-1}$, the resulting coefficients of the ZF precoder tend to be smaller, which translates into beamforming gain.

In the tables below some values of interest are indicated:

Tabla 4.10: ZF beamforming gain for K=10

K = 10						
N_t/K	**3**	**4**	**5**	**6**	**9**	**12**
Beamforming gain (dB)	3.02	4.76	6.02	6.99	9.03	10.41

Tabla 4.11: ZF beamforming gain for K=20

K = 20				
N_t/K	**3**	**4**	**5**	**6**
Beamforming gain (dB)	3.00	4.78	6.02	6.99

Tabla 4.12: ZF beamforming gain for K=30

K = 30				
N_t/K	**3**	**4**	**5**	**6**
Beamforming gain (dB)	3.02	4.77	6.02	6.99

note that same N_t/K ratios lead to same beamforming gains. In Figure 4.12, the beamforming gain of ZF is represented in linear units

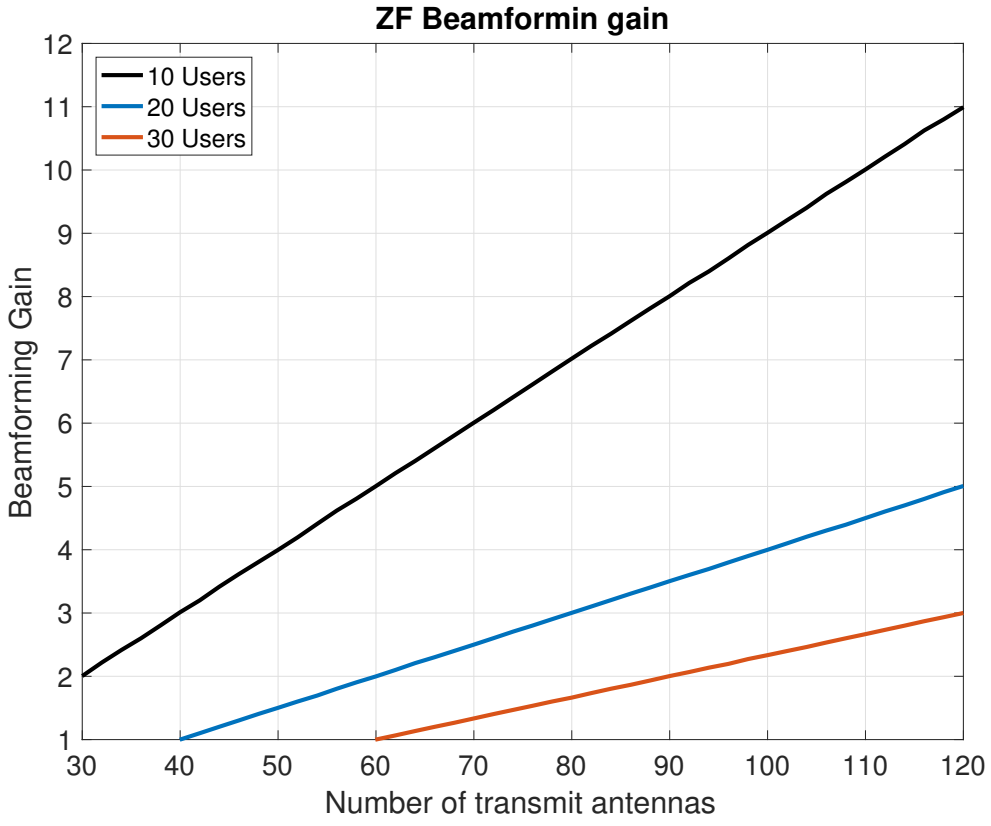

Figure 4.13: ZF beamforming gain in linear units

Beamforming Gain Comparison

After having analyzed the beamforming gains of both precoders, it is time to compare them. In the figure below, the results for ZF and CE, for the different MUI constraints, are shown:

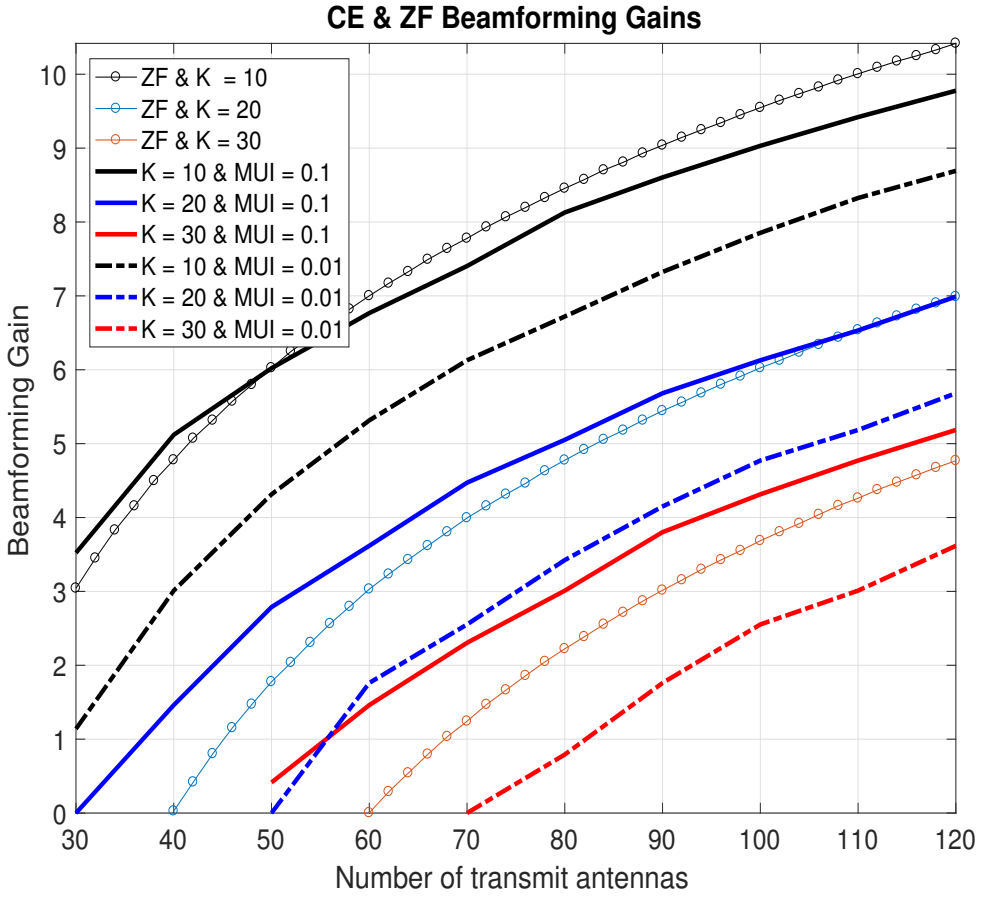

Figure 4.14: ZF vs CE beamforming gains (dB)

Zero forcing is capable of completely suppressing the MUI interference, it is interesting to see that for mild MUI constraints, CE is capable of providing more beamforming gain than ZF precoder. However, if we want the MUI to be reduced more significantly, the ZF precoder provides better results.

Tabla 4.13: ZF and CE beamforming gains for K=10

K = 10				
$\mathbf{N_t}$	**30**	**60**	**90**	**120**
ZF	3.02	6.99	9.03	10.41
CE (MUI = 0.1)	3.5	6.76	8.6	9.78
CE (MUI = 0.01)	1.14	5.32	7.32	8.69

Tabla 4.14: ZF and CE beamforming gains for K=20

K = 20				
$\mathbf{N_t}$	**60**	**80**	**100**	**120**
ZF	3.00	4.78	6.02	6.99
CE (MUI = 0.1)	3.62	5.05	6.13	6.99
CE (MUI = 0.01)	1.77	3.42	4.77	5.68

4.4 Link Performance

Lastly, the performance of the whole link is going to be evaluated and compared to that of ZF precoder. In the following, the setup shown in Figure (3.2) is going to be utilized. The performance is going to be evaluated by means of the bit error rate. The algorithms are run repeatedly for increasing transmit power (noise level at receiver side is fixed), which has multiple impacts on the resulting SINR: when transmit power is increased, the signal level at the receiver side increases, which enhances the SINR, however, when the transmit power is sufficiently large to push the power amplifiers too harshly, nonlinear distortion will take place at the power amplifier. Thus, the power amplifier output signal will be constituted by useful signal plus distortion, and therefore, the useful signal power at the receiver does not anymore increase linearly, while the interference will increase, degrading the SINR and therefore, the BER. When the power amplifiers are sufficiently pushed, the inband distortion will be large enough to limit the link performance, so BER will saturate and will start to worsen.

In order to properly compare both precoders, which is a non trivial task, the bit error rate is going to be represented as a function of the relative transmit power. At the same time, the equivalent back-off for that relative transmit power is represented together with the BER curve. BER curves are typically represented as a function of the SINR or E_B/N_0, however, increasing transmit power does not necessarily map into increasing SINR in the problem at hand. Furthermore, same transmit powers do not map into the same received SINR due to different nonlinear distortion and different beamforming gains. Separately, the SINR at the receiver side will be represented as a function of the relative transmit power. For low transmit powers, the SINR is expected to increase the same way as the transmit power does, since nearly all transmit power will turn into useful signal plus negligible distortion. It is in this operation regime where ZF is expected to perform slightly better due to the higher beamforming gain. However, as the transmit power increases, the link performance of the constant envelope precoder should outperform that of ZF, since significant lower distortion will occur.

With an eye to better understanding the effect of the power amplifier on the link performance, the same scheme has been implemented with ideal (unit linear gain) power amplifiers. Due to those power amplifiers are fully linear, they will be seamless to the input signal, since they offer the same response regardless of the input power and thus, no distortion will take place.

Two scenarios are going to be examined: in the first one, it will be considered that both schemes present the same equivalent isotropically radiated power (EIRP), while in the second one, both precoders will have the same transmit power, but not the same EIRP due to the different beamforming gains. Clarification: in the same EIRP configuration, the EIRP of the ZF precoder has been made equal to that of the CE precoder, which means that the transmit power of the ZF precoder has been reduced to match that value.

In the following, a multi-user interference suppression of 20 dB (for the CE precoder) has been set up in every simulation. The noise floor at the receiver side is around 20 dB above the multi-user interference, and thus, the noise is the main source of interference together with the nonlinear distortion. For low transmit powers, we will find the system operating in a noise-limited scenario, on the other hand, as the transmit power increases the nonlinear distortion becomes more significant until it turns to be the main source of interference.

Same EIRP

In the figure below the resulting BER for the constant envelope precoder is shown.

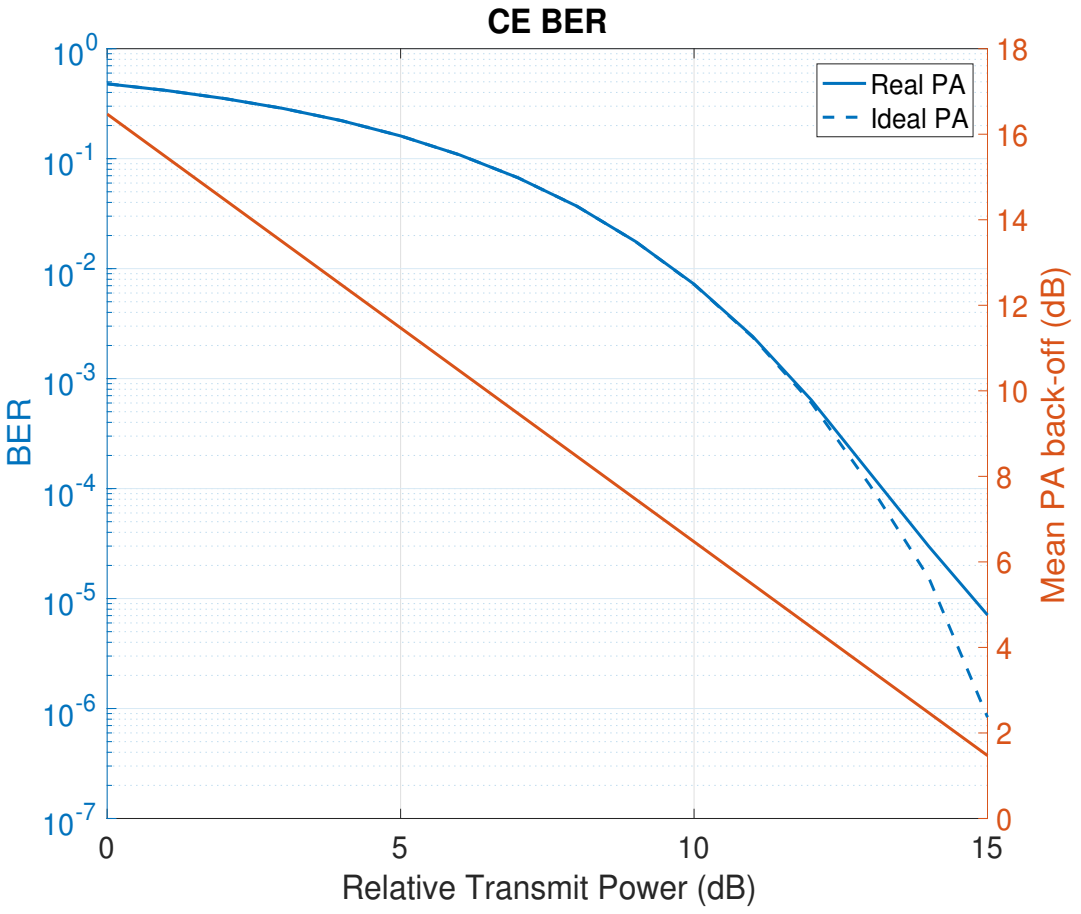

Figure 4.15: CE BER and mean back-off value of the power amplifiers

Since power amplifier models are normalized, the mean amplitude of its input signal is scaled such that it properly fits in the polynomial models (this scaling is undone at the power amplifier output). This is done in such a way that there is sufficient back-off, and thus, enough room for increasing the transmit power over a wide range. The noise floor of the receiver has been set-up to a constant value, the resulting SNR ranges between -1 dB and 14 dB for the considered range of relative transmit power.

The relative transmit power ranges from 0 to 15 dB, while the equivalent power amplifier back-off ranges between 16.5 and 1.5 dB respectively. For low transmission powers, we find ourselves in a very linear operation regime, in which nonlinear distortion is negligible, and thus this corresponds to the noise-limited region. As it will be seen, increasing the transmit power corresponds to an increase (of the same amount) of the SINR.

In dashed line, the link performance when ideal power amplifiers are utilized is represented, while the solid one shows the performance when the polynomial models are used. As it can be observed, both configurations have the same performance when sufficient back-off is applied (negligible nonlinear distortion). When transmit power is sufficiently increased, nonlinear distortion starts to be significant compared

to the noise floor. This takes place for a back-off of 3.5 dB, which is close to the PAPR of the CE continuous-time waveform. As it can be observed, the BER does not fully saturate for the utilized power range, the SINR keeps improving as the transmit power increases, but to a lesser extent.

Thanks to the LS-based estimation of the received SINR, it is possible to know how the relative transmit powers map into their corresponding SINRs. BER is represented together with the estimated SINR, instead of with the back-off value.

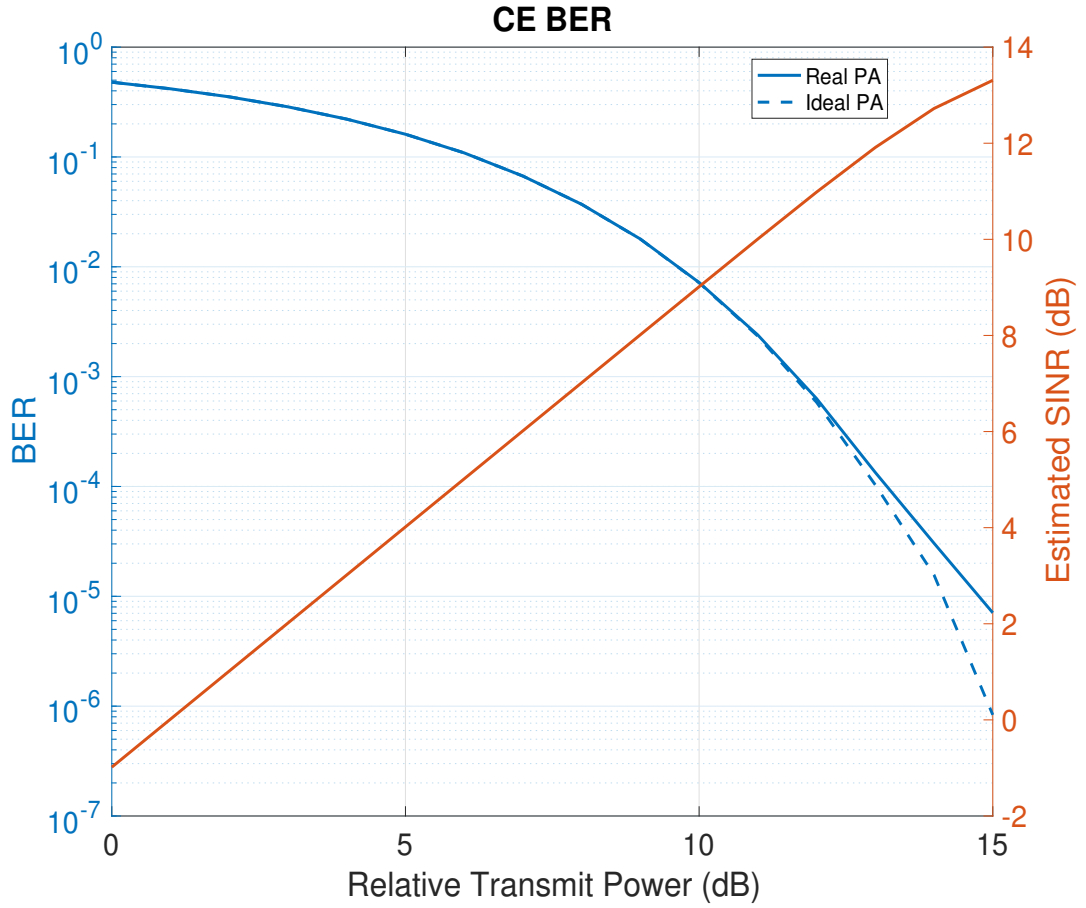

Figure 4.16: CE BER and estimated SINR

The SINR increases linearly (1 dB stepwise) for most of the relative transmit powers due to the nonlinear distortion is nearly negligible. Note that for the highest transmission power, the SINR increases to a lesser extent. For the ZF precoder, it is expected that the achievable SINR will be much smaller, nonlinear distortion will become significant faster. The difference between the achievable SINR of both precoders will constitute another mean to evaluate the actual benefits of CE precoder.

Tabla 4.15: CE SINR

Relative Transmit Power (dB)	**0**	**3**	**6**	**9**	**12**	**15**
SINR (dB)	-0.98	2.01	5.01	8.01	10.98	13.31
Δ	0	2.99	3	3	2.97	2.33

For low transmission powers, an increase of 3 dB in the transmission power corresponds to an increase of 3 dB in the SINR. For 15 dB of relative transmission power, the corresponding back-off value is 1.5 dB, the nonlinear distortion becomes significant and the improvement in the SINR reduces.

In the following figure the performance of the ZF precoder is shown.

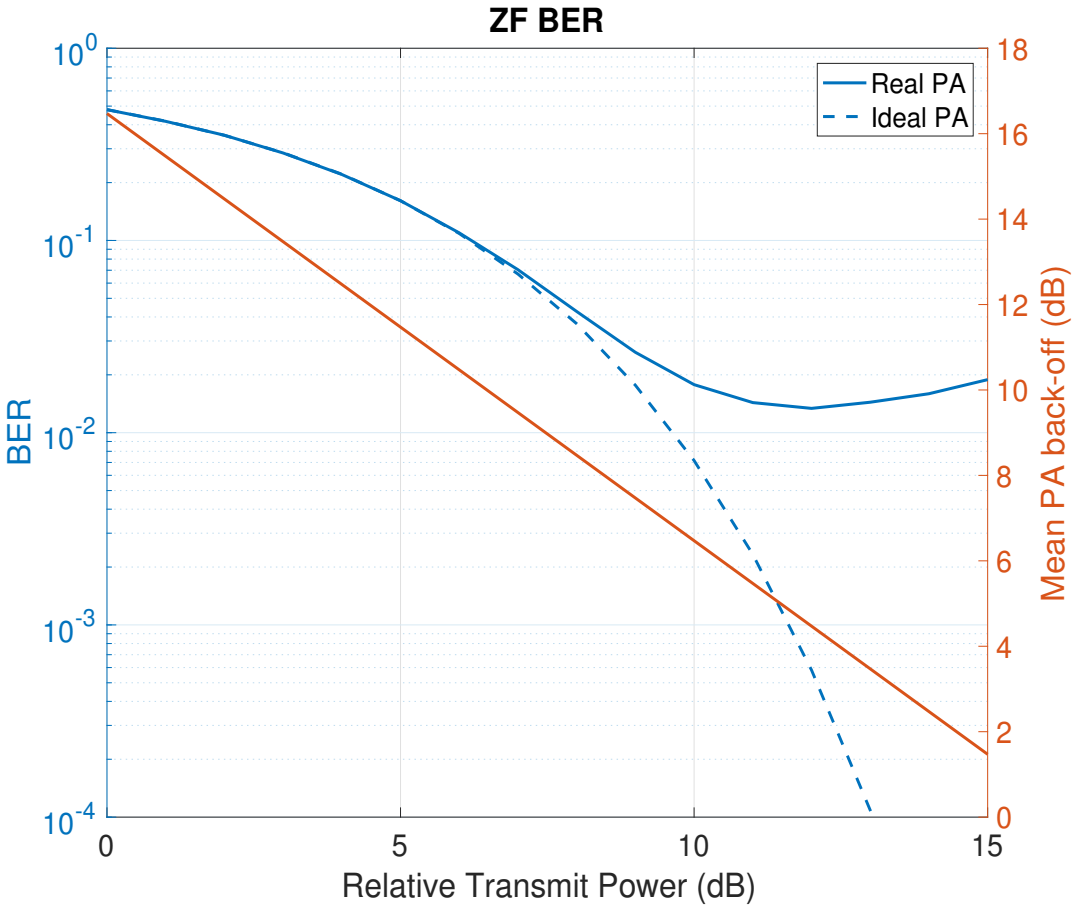

Figure 4.17: ZF BER. Transmit power scaled down to equal the EIRP of CE precoder

For low transmission powers, the behavior of ZF is basically the same as that of CE. In the linear regime, increasing transmit power maps into an increase of the same amount in the SINR, however, when transmit power is sufficiently high such that back-off is not large enough to hold the signal amplitude in the linear range, the effect of nonlinear distortion starts to be non-negligible. This fact takes place considerably

earlier than in the previous case. For high transmit powers, the nonlinear distortion is already so high, that the SINR starts to actually decrease instead of increasing with growing transmit power.

Now, the BER performance will be represented together with the estimated SINR at the receiver side, instead of with the back-off value.

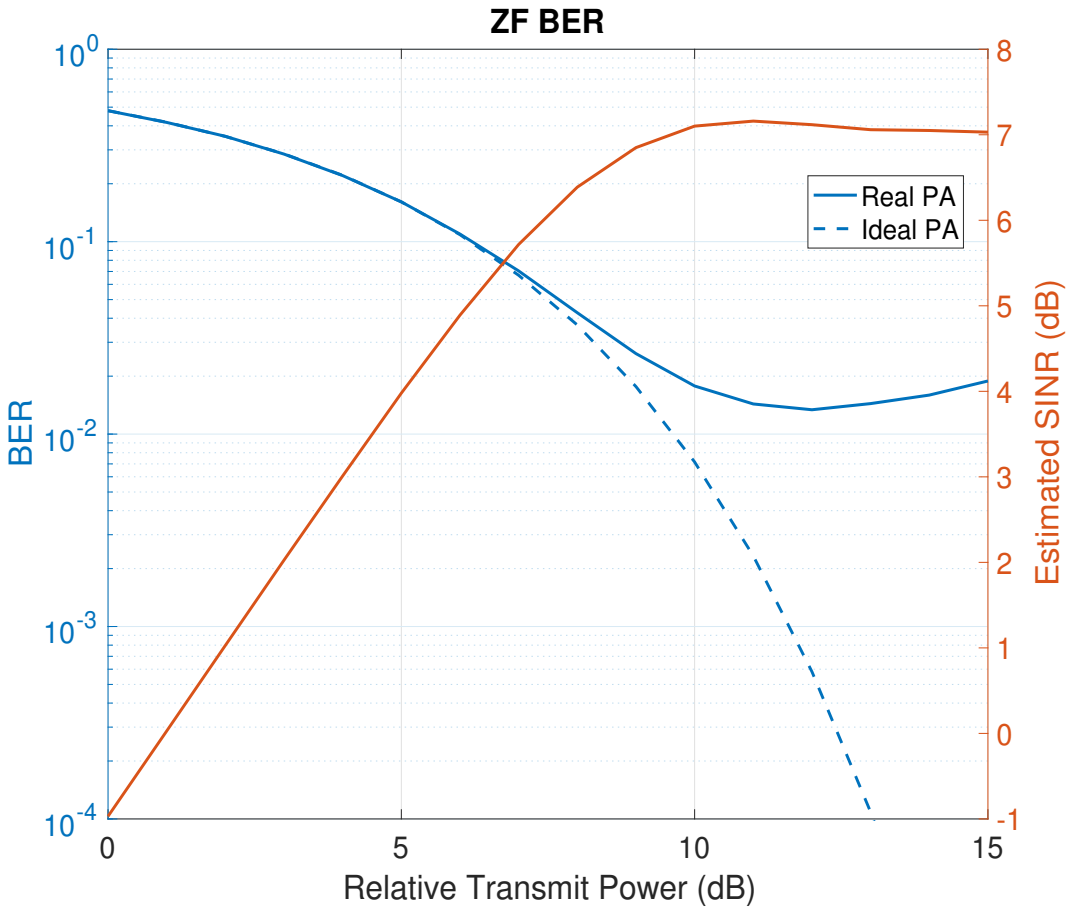

Figure 4.18: ZF BER and estimated SINR. Transmit power scaled down to equal the EIRP of CE precoder

The SINR basically follows the same shape as that of power amplifiers transfer function. For low relative transmit power, the SINR increases linearly (1 dB stepwise) as it could be expected. However, when nonlinear distortion becomes significant compared to the noise level, the SINR starts improving to a lesser extent until it saturates.

Tabla 4.16: ZF SINR

Relative Transmit Power (dB)	**0**	**3**	**6**	**9**	**12**	**15**
SINR (dB)	-0.98	2.02	4.89	6.85	7.12	7.03
Δ	0	3	2.87	1.96	0.27	-0.09

The high PAPR of the resulting waveform allows small room for increasing the transmission power before the distortion becomes very significant.

If we compare the results in tables 4.15 and 4.16 , the CE precoder allows to push the power amplifier at least 6 dB more (there is still some margin for improving the SINR).

With an eye to better comparing both schemes, in the figure below the performance of both precoders is represented. For the case of same EIRP, both of them are expected to show the same performance in the linear regime, since same EIRP maps into same SINR at the receiver side. On the other hand, in the case of same transmit powers, as the EIRP is different, ZF is expected to perform slightly better due to the extra beamforming gain (before nonlinear distortion becomes meaningful).

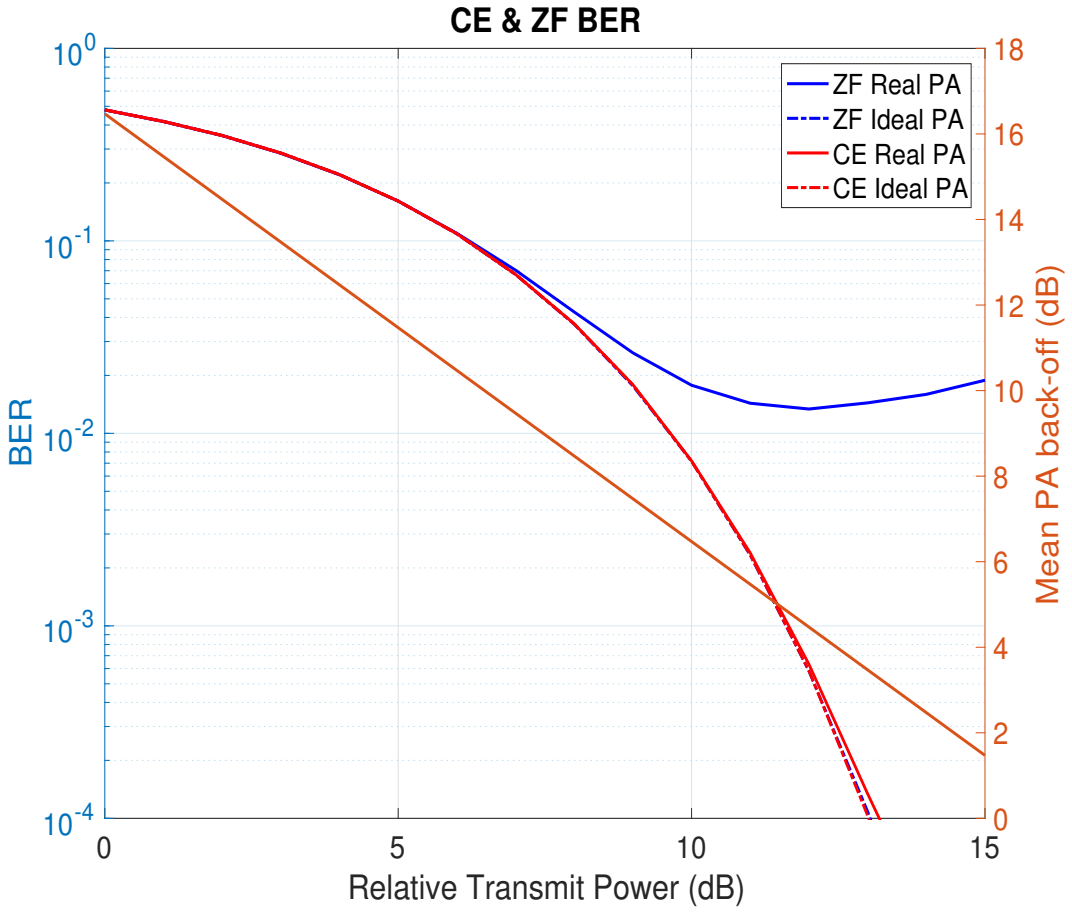

Figure 4.19: CE and ZF BER. ZF transmit power is scaled down to equal the EIRP pf CE precoder

As it was expected, both precoders perform the same way in the linear region, as well as if we consider ideal power amplifiers. This is mainly because in both schemes, the predominant source of interference are the noise for low transmission powers, and the nonlinear distortion for high transmission powers. Multi-user interference

is negligible. When ideal power amplifiers are considered, it is important to realize that if the transmit power keeps increasing, we will get to the point in which the multi-user interference (20 dB of supression) is above the noise level. From this points onwards, the ZF ideal curve outperforms CE precoder.

Recall that ZF transmit power was scaled in order to equal the same EIRP than that of CE precoder, there is still some room for improvement for ZF precoder which is analyzed in the following section.

Same Transmit Power

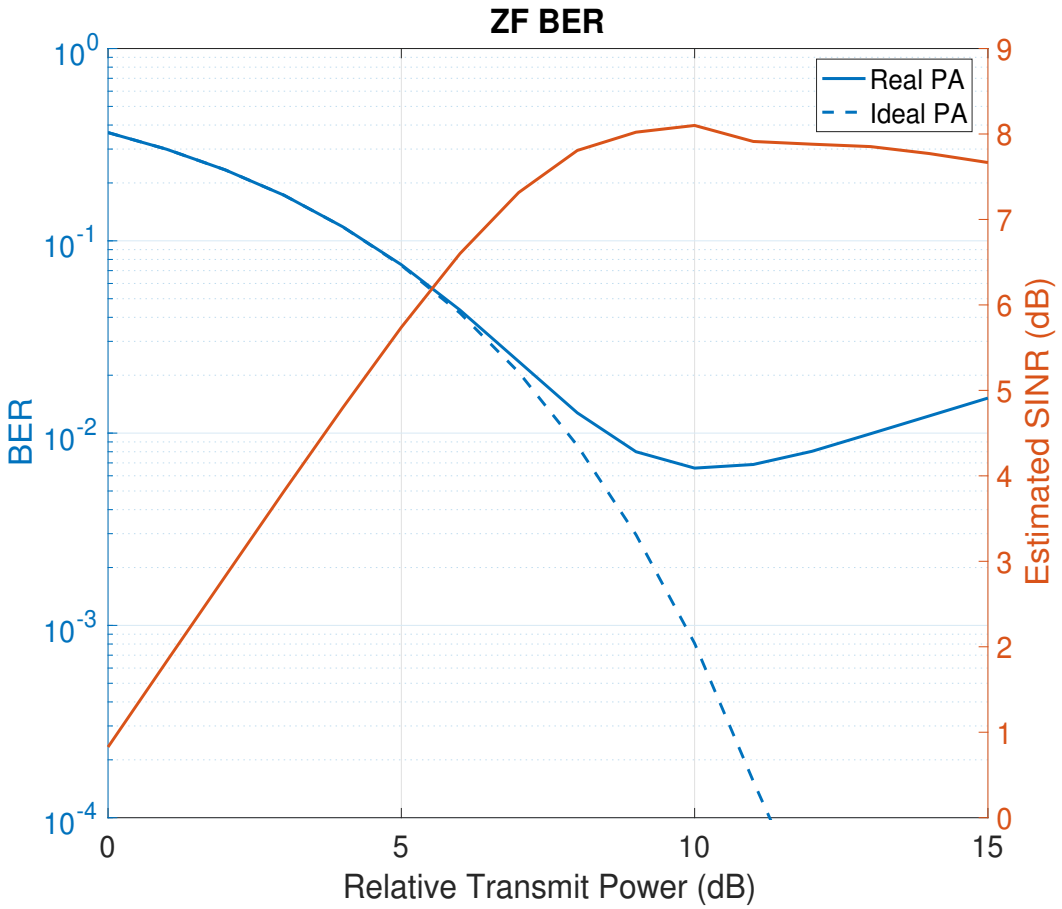

Figure 4.20: ZF BER. Transmit power is not scaled anymore.

When both schemes utilize the same transmit power, the EIRP is not the same, since the antenna gain in the link direction is higher for the ZF due to the extra beamforming gain. The results here are basically the same than those shown in Figure (4.19), but the ZF curves are slightly displaced a couple of dB towards the right.

Tabla 4.17: ZF SINR with extra beamforming gain

Relative Transmit Power (dB)	**0**	**3**	**6**	**9**	**12**	**15**
SINR (dB)	0.82	3.82	6.6	8.02	7.88	7.66
Δ	0	3	2.78	1.42	-0.14	-0.22

the extra beamforming gain of ZF precoder is more significant in the noise-limited scenario, since noise level is less significant compared to the signal strength, the effect of nonlinear distortion can be noticed earlier.

Note that the performance of the constant envelope precoder is the same than the one shown in 4.15.

The effect of the beamforming gain can be visualized in the figure below:

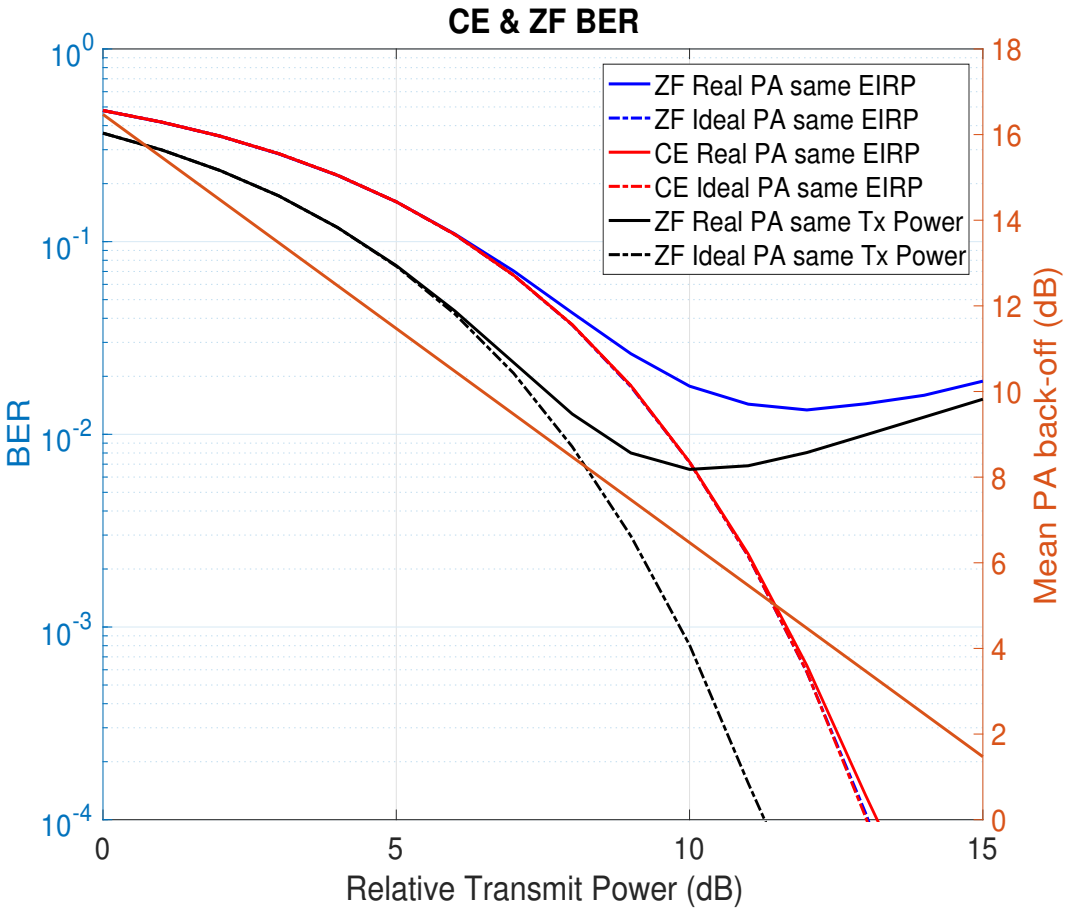

Figure 4.21: ZF and CE BER for the same transmit power

ZF beamforming gain is approximately 1.9 dB higher than that of CE precoder. Because of this reason, ZF scheme outperforms CE for low transmission powers (noise-limited scenario), when the transmit power is being increased, the nonlinear distortion starts to soon limit the ZF precoder based system, and thus, the actual

benefit of CE precoder is very clear. CE precoder allows to push the power amplifier many more dB before the link performance saturates. Despite the CE precoder provides less beamforming gain, the fact that it allows to push the power amplifier closer to the 1 dB compression point makes the actual required transmission power be less than that of ZF. Considering the results shown in Figure (4.21), CE envelope power gain is given by:

$$\Delta P = \Delta_{Backoff} - \Delta_{Beamforming} \ \ (dB) \tag{4.6}$$

where $\Delta_{Backoff}$ denotes the extra back-off required by the ZF precoder compared to CE precoder for a given nonlinear distortion, while $\Delta_{Beamforming}$ denotes the beamforming gain difference between both precoders. The actual gain of constant envelope can also be computed with the following expression:

$$\Delta P = \Delta_{SINR} \ \ (dB) = 13.31 - 8.2 = 5.11 \tag{4.7}$$

which is the difference between the maximum achievable SINR of both precoders. ΔP basically refers to how larger CE precoder useful received signal is compared to that of ZF precoder.

Constant envelope precoder allows to obtain 5 dB of power gain thanks to being able to utilize the power amplifier more efficiently, which is a very significant improvement with regards traditional precoders.

To summarize:

- CE precoder is able to generate a discrete-time constant envelope signal.
- After pulse shaping, the resulting waveform of CE precoder has about 9 dB lower PAPR than that of ZF precoder.
- The multi-user interference of constant envelope precoder can be made arbitrarily low when the number of transmit antennas is large enough.
- The beamforming gain of constant envelope precoder is linear dependent upon the number of antennas.
- In general, the beamforming gain provided by constant envelope precoder is lower than that of ZF. For mild constraints on the multi-user interference, the resulting beamforming gain can be higher.
- CE precoder allows to push the power amplifier around 7 dB more than ZF, allowing thus, a more efficient utilization.
- Taking into account the different beamforming gains, the total gain provided by the CE precoder is around 5 dB higher than thar of ZF precoder.

Chapter 5

Conclusions and Future Work

5.1 Conclusions

In this Master Thesis the performance of a constant envelope precoder has been evaluated and compared to that of classical zero-forcing precoder. The analysis has been carried out for a large-scale multi-user MIMO scenario, which is commonly assumed to be a typical scheme in future mobile networks like 5G. The constant envelope precoder shows substantial benefits compared to ZF. First, it allows to significantly reduce the PAPR of the continuous-time waveform, allowing to push the power amplifier of every antenna branch several dB more, which in turns allows to increase the energy efficiency of the base stations. Second, it has been observed that CE precoder provides somewhat less beamforming gain than ZF precoder (1-2 dB), however, since it is possible to push the power amplifier harsher, the overall power gain, from the useful received signal point of view, when taking these two effects into account is still very significant, around 5 dB, making CE precoder to be a very viable approach. It has been shown that the multi-user interference can be made arbitrarily small, when sufficiently large antenna arrays are used. In order to obtain beamforming gain together with interference cancellation, the available degrees of freedom need to be shared between these two purposes, thus, for a given targeted MUI, the higher the needed beamforming is, the more antennas will be required to meet both requirements.

In general, CE precoder constitutes a new way of addressing the need of higher spectral efficiency and lower power consumption, showing promising results in these two regards. Its benefits compared to traditional precoders are quite significant. CE can definitely play an important role in future system specifications.

5.2 Future Work

CE precoding is intended to reduce the PAPR of the signal waveform. This technique could be implemented together with power amplifiers linearization techniques, such as digital predistortion, in order to obtain a superior performance. The evaluation of the precoders has been carried out for single carrier waveforms for simplicity. Modern wireless communication systems utilize multicarrier waveforms like OFDM. Thus, as future work, it would be interesting to extend the model to multicarrier waveforms. Another approach should however be considered, since the complexity would be increased proportionally to the number of subcarriers.

In this Master Thesis, the main emphasis was on evaluating the performance of the considered CE precoder and comparing it to the corresponding performance of more ordinary ZF precoding based system. Algorithms that address practical matters are of interest. For example, multi-user interference and bramforming gain need to be traded-off, so algorithms that would allow to determine the maximum allowed MUI in the system such that the individual link performances are not deteriorated because of the interference would be of interest.

Bibliography

[1] *"5GPP vision of 5G"* https://5g-ppp.eu/wp-content/uploads/2015/02/5G-Vision-Brochure-v1.pdf

[2] F. Rusek et al., *"Scaling Up MIMO: Opportunities and Challenges with Very Large Arrays," in IEEE Signal Processing Magazine, vol. 30, no. 1, pp. 40-60, Jan. 2013.*

[3] M. Olsson, C. Cavdar, P. Frenger, S. Tombaz, D. Sabella and R. Jantti, *"5GrEEn: Towards Green 5G mobile networks,"* 2013 IEEE 9th International Conference on Wireless and Mobile Computing, Networking and Communications (WiMob), Lyon, 2013, pp. 212-216.

[4] H.Q.Ngo, E.G.Larsson, and T.L.Marzetta,*"Energy and spectral efficiency of very large multiuser MIMO systems", IEEE Trans. Commun., vol. 61, no. 4, pp. 1436, 1449, Apr. 2013*

[5] V. Mancuso and S. Alouf, *"Reducing costs and pollution in cellular networks," in IEEE Communications Magazine, vol. 49, no. 8, pp. 63-71, August 2011.*

[6] Seung Hee Han and Jae Hong Lee, *"An overview of peak-to-average power ratio reduction techniques for multicarrier transmission," in IEEE Wireless Communications, vol. 12, no. 2, pp. 56-65, April 2005.*

[7] C. Paredes Paredes and M. Julia Fenandez-Getino Garcia "The Problem of Peak-to-Average Power Ratio in OFDM Systems Martha" Department of Signal Theory and Communications Universidad Carlos III de Madrid, Madrid, Spain

[8] A. Zhu, P. J. Draxler, J. J. Yan, T. J. Brazil, D. F. Kimball and P. M. Asbeck, *"Open-Loop Digital Predistorter for RF Power Amplifiers Using Dynamic Deviation Reduction-Based Volterra Series,"* in IEEE Transactions on Microwave Theory and Techniques, vol. 56, no. 7, pp. 1524-1534, July 2008.

[9] S. K. Mohammed and E. G. Larsson, *"Per-Antenna Constant Envelope Precoding for Large Multi-User MIMO Systems," in IEEE Transactions on Communications, vol. 61, no. 3, pp. 1059-1071, March 2013.*

[10] S. K. Mohammed and E. G. Larsson, "Per-Antenna Constant Envelope Precoding for Large Multi-User MIMO Systems," *in IEEE Transactions on Communications, vol. 61, no. 3, pp. 1059-1071, March 2013.*

[11] S. K. Mohammed and E. G. Larsson, *"Constant-Envelope Multi-User Precoding for Frequency-Selective Massive MIMO Systems," in IEEE Wireless Communications Letters, vol. 2, no. 5, pp. 547-550, October 2013.*

[12] Mikko Valkama, *"Advanced Course in Digital Transmission" lecture notes, Tampere University of Technology.*

[13] Mariano García, Santiago Zazo, Miguel Ángel García, *"Signal Analysis for Communications" lecture notes Escuela Técnica Superior de Ingenieros de Telecomunicación, Universidad Politécnica de Madrid.*

[14] Jack Rowley, *"Mobile Communication Networks: Energy Efficiency and Green Power"* https://www.itu.int/dms_pub/itu-t/oth/3C/02/T3C020000330001PDFE.pdf

[15] *"5G Energy Performance, Ericsson White Paper"* https://www.ericsson.com/assets/local/publications/white-papers/wp-5g-energy-performance.pdf

[16] R. L. G. Cavalcante, S. Stanczak, M. Schubert, A. Eisenblaetter and U. Tuerke, *"Toward Energy-Efficient 5G Wireless Communications Technologies: Tools for decoupling the scaling of networks from the growth of operating power," in IEEE Signal Processing Magazine, vol. 31, no. 6, pp. 24-34, Nov. 2014.*

[17] A. Checko et al., *"Cloud RAN for Mobile Networks?A Technology Overview," in IEEE Communications Surveys and Tutorials, vol. 17, no. 1, pp. 405-426, Firstquarter 2015.*

[18] Mikko Valkama, Markku Renfors, *"Radio Architectures and Signal Processing" lecture notes, Tampere University of Technology.*

[19] *"Evaluating Power Amplifier Performance for LTE and 802.11 ac Designs", LitePoint White Paper*

[20] T. Jiang and Y. Wu, *"An Overview: Peak-to-Average Power Ratio Reduction Techniques for OFDM Signals," in IEEE Transactions on Broadcasting, vol. 54, no. 2, pp. 257-268, June 2008.*

[21] Mikko Valkama, Markku Renfors, *"Multicarrier and Multiantenna Techniques" lecture notes, Tampere University of Technology.*

[22] M. Isaksson, D. Wisell and D. Ronnow, *"A comparative analysis of behavioral models for RF power amplifiers," in IEEE Transactions on Microwave Theory and Techniques, vol. 54, no. 1, pp. 348-359, Jan. 2006.*

[23] *RRC filters* http://www.navipedia.net/index.php/Square-Root_Raised_Cosine_Signals_(SRRC)

[24] H.Q.Ngo, E.G.Larsson, and T.L.Marzetta, *"Energy and spectral efficiency of very large multiuser MIMO systems"*, IEEE Trans. Commun., vol. 61, no. 4, pp. 1436,1449, Apr. 2013.